UC San Diego

UC San Diego Electronic Theses and Dissertations

Title

Protein-RNA networks regulated by normal and ALS-associated mutant HNRNPA2B1 in the nervous system

Permalink

https://escholarship.org/uc/item/70w6712q

Author

Martinez, Fernando

Publication Date

2016

Supplemental Material

https://escholarship.org/uc/item/70w6712q#supplemental

Peer reviewed|Thesis/dissertation

eScholarship.org Powered by the California Digital Library
University of California

UNIVERSITY OF CALIFORNIA, SAN DIEGO

Protein-RNA networks regulated by normal and ALS-associated mutant HNRNPA2B1 in the nervous system

A dissertation submitted in partial satisfaction of the requirements for the degree Doctor of Philosophy

in

Biomedical Sciences

by

Fernando J. Martinez

Committee in Charge:

Professor Eugene Yeo, Chair
Professor Lawrence Goldstein
Professor Jens Lykke-Andersen
Professor Alysson Muotri
Professor Amy Pasquinelli

2016

The Dissertation of Fernando J. Martinez is approved, and it is acceptable in quality and form for publication on microfilm and electronically:

_____

_____

_____

_____

_____

Chair

University of California, San Diego

2016

DEDICATION

This dissertation is dedicated to all of the doctoral students who
have been told "the Ph.D. is not for you;"
and to the wise men who told them so.

"Professing themselves to be wise, they became fools."

Romans 1:22

EPIGRAPH

Skill to do comes of doing;
knowledge comes by eyes always open, and working hands;
and there is no knowledge that is not power.

Ralph Waldo Emerson

TABLE OF CONTENTS

Signature Page iii

Dedication iv

Epigraph v

Table of Contents vi

List of Supplemental Files x

List of Figures xii

Acknowledgements xiv

Vita xvi

Publications xvi

Abstract of the Dissertation xvii

Introduction 1

Chapter 1: Results 4

1.1 Discovery of hnRNP A2/B1 RNA binding sites in mouse spinal cord and human iPSC-MNs. 4

1.2 HnRNP A2/B1 depletion in vivo results in limited changes in gene expression 10

1.3 HnRNP A2/B1 depletion in vivo and in vitro has minimal effect on mature microRNA levels 13

1.4 HnRNP A2/B1 regulates alternative 3' cleavage choice in vivo 16

1.5 Hundreds of alternative splicing events depend on hnRNP A2/B1 protein level 16

1.6 HnRNP A2/B1 interacts with RNA components of the spliceosome. 19

1.7 HnRNP A2/B1-dependent splicing in the D-amino acid oxidase gene results in reduced expression and enzymatic activity 21

1.8 HnRNP A2/B1 D290V mutation results in splicing defects in human fibroblasts 26

1.9 Altered hnRNP A2/B1-dependent alternative splicing in human iPSC-MNs 29

1.10 hnRNP A2/B1-mutant neurons display increased risk of death during long-term culture 38

1.11 hnRNP A2/B1-mutant iPSC-MNs exhibit excess hnRNP A2/B1 in stress granules 38

1.12 hnRNP A2/B1-mutant iPSC-MNs exhibit exacerbated gene expression and AS changes in response to stress 41

Chapter 2: Discussion 49

Chapter 3: Experimental Procedures 54

3.1 RNA Bind-n-Seq (RBNS) 54

3.1.1 RBNS experimental procedure 54

3.1.2 RBNS Computational Analysis 54

3.2 CLIP analysis of mouse and human samples 55

3.2.1 iCLIP experimental procedure 55

3.2.2 eCLIP experimental procedure 55

3.2.3 iCLIP computational analysis 56

3.2.4 eCLIP computational analysis 57

3.2.5 Distance away from motif 57

3.2.6 De novo motif analysis 58

3.3 Cell culture 58

3.3.1 Human fibroblasts 58

3.3.2 Human iPSC generation 58

3.3.3 iPSC and ESC culture 59

3.3.4 Differentiation of human motor neurons from PSCs 59

3.3.5 Multi-electrode array recordings 60

3.3.6 FLP-In-293 (HEK293-FRT) stable cell line generation 60

3.3.7 U-251 MG cell culture and shRNA transfection 61

3.4 Antisense oligonucleotide (ASO) based depletion of hnRNP A2/B1 62

3.4.1 Stereotactic injections of ASOs in mouse 62

3.4.2 ASO depletion of hnRNP A2/B1 in human fibroblasts 62

3.4.3 ASO depletion of hnRNP A2/B1 in human PSC derived motor neurons 63

3.5 Western blotting 63

3.6 Expression analysis by RNA-seq 64

3.6.1 Library preparation, sequencing, and analysis 64

3.6.2 Small RNA Sequencing 64

3.6.3 miRNA expression analysis 64

3.6.4 Quantitative (qPCR) analysis 65

3.7 Alternative splicing analysis by microarray 66

3.7.1 Splicing analysis in mouse spinal cord samples and human PSC derived motor neurons (Figure 8) 66

3.7.2 Splicing analysis in human fibroblasts 66

3.7.3 Splicing analysis in human PSC derived motor neurons (Figure 6) 67

3.7.4 RT-PCR analysis of splicing changes 67

3.7.5 Alternative Polyadenylation 68

3.8 Northern blotting and RNA immunoprecipitation (RIP) northern blotting 68

3.9 Measurements of alternative isoforms of Dao 69

3.9.1 RT-PCR of human DAO transcript 69

3.9.2 Constructs 69

3.9.3 Tertiary structure prediction 70

3.9.4 Proteasome assay 71

3.9.5 Cell based activity assay 71

3.9.6 Cell-free activity assay 72

3.10 Stress granule assays 72

3.10.1 Treatment of cells 72

3.10.2 Immunofluorescence and imaging 73

3.10.3 Image analysis 73

3.10.4 Nuclear / cytoplasmic and Detergent soluble / insoluble fractionation 73

3.11 Long Term Imaging Experiments 75

3.11.1 Differentiation and Cell Culture 75

3.11.2 Imaging and analysis. 75

Appendix 77

References 79

LIST OF SUPPLEMENTAL FILES

Data S1. Supplemental data and inventory of oligonucleotides, antibodies and other materials related to Figures 1-8, Figures S1-S8 and supplemental experimental procedures. martinez_datas1.xlsx

(A) iCLIP clusters in mouse spinal cord.

(B) Cell lines used. hFibs = human fibroblasts. GBM = glioblastoma multiforme.

(C) eCLIP peaks in human iPSC-MNs. Fold change refers to IP sample over the matching input sample.

(D) RNA-seq data from mouse spinal cord treated with ASO against hnRNP A2/B1.

(E) Gene expression data from microarray analysis of mouse spinal cord treated with ASO against hnRNP A2/B1. Fold change refers to ASO depleted over control.

(F) microRNA expression data from small RNA-seq in mouse spinal cord. Fold change refers to ASO depleted over control.

(G) microRNA expression data from small RNA-seq in human iPSC-MNs. Fold change refers to ASO depleted over control.

(H) Alternative polyadenylation events in mouse spinal cord.

(I) AS data from microarray analysis of mouse spinal cord treated with ASO against hnRNP A2/B1.

(J) AS data from microarray analysis of human fibroblasts from hnRNP A2/B1 D290V patients and controls. Columns are sepscore for pairwise comparison of the various samples.

(K) AS data from microarray analysis of iPSC-MNs from CTRL.JCV (unaffected individual) treated with ASO against hnRNP A2/B1 vs. nontargetting control ASO.

(L) AS data from microarray analysis of iPSC-MNs from D290V-2.1 (MSP individual, hnRNP A2/B1 D290V) treated with ASO against hnRNP A2/B1 vs. nontargetting control ASO.

(M) AS data from microarray analysis of iPSC-MNs from CTRL.JCV (unaffected individual) vs. D290V-2.1 (MSP individual, hnRNP A2/B1 D290V).

(N) Gene expression data from microarray analysis of puromycin-treated PSC-MNs. Columns indicate fold change calculated for each of the various samples and it's matching unstressed control.

(O) AS data from microarray analysis of puromycin-treated PSC-MNs. Columns indicate sepscore calculated for each of the various samples and it's matching unstressed control.

(P) Antibodies used. The lot number is mentioned for antibodies that were lot controlled. The applications column lists the application and the dilution used. WB = western blot; IF = immunofluorescence; IP = immunoprecipitation.

(Q) Oligonucleotide sequences.

LIST OF FIGURES

Figure 1. HnRNP A2/B1 predominantly binds 3' untranslated regions (3'UTRs) and recognizes a UAGG motif. 5

Figure S1. Supplemental data related to iCLIP, eCLIP and RNA Bind-N-Seq (Figure 1). ... 8

Figure 2. HnRNP A2/B1 depletion results in alternative polyadenylation changes. 11

Figure S2. Supplemental data related to gene expression changes upon hnRNP A2/B1 depletion (Figure 2)..... 14

Figure 3. HnRNP A2/B1 depletion in mouse spinal cord affects alternative splicing..... 17

Figure S3. Supplemental data related to AS changes induced upon hnRNP A2/B1 depletion (Figure 3). 20

Figure 4. hnRNP A2/B1-dependent AS in the D-amino acid oxidase (DAO) gene results in reduced DAO protein expression and enzymatic activity. 22

Figure S4. Supplemental data related to exon skipping in the ***Dao*** gene after hnRNP A2/B1 depletion in mouse spinal cord (Figure 4). 25

Figure 5. Fibroblasts from patients with mutations in HNRNPA2B1 and VCP exhibit widespread splicing defects not found when hnRNP A2/B1 is depleted. 27

Figure S5. Supplemental data related to the characterization of human iPSC and ESC lines used in Figures 6 and 7. 30

Figure 6. iPSC-MNs from patients with mutations in HNRNPA2B1 exhibit splicing defects. 33

Figure S6. Supplemental data related to the characterization of human PSC derived motor neurons used in Figures 6 and 7. 36

Figure 7. hnRNP A2/B1 D290V motor neurons exhibit increased risk of death and accumulate excess hnRNP A2/B1 in stress granules. 39

Figure S7. Supplemental data related to stress granule formation and nuclear aggregation in iPSC-MNs (Figure 7). 42

Figure 8. iPSC-MNs from affected patients display an exaggerated response to stress. 45

Figure S8. Supplemental data related to splicing and expression changes resulting from puromycin-induced stress in iPSC-MNs from hnRNP A2/B1 D290V patients and the VCP R155H patient (Figure 8). 47

ACKNOWLEDGEMENTS

First and foremost, I would like to thank my family for sticking with me and supporting me through my long and winding path through graduate school. I would especially like to thank my mom Esther, my dad Fernando, my stepdad Rob, and my sisters Christina, Jenna, and Elena. Thanks for believing in me. I could not have done it without you.

Many thanks are also owed to my advisor, Gene Yeo, for always being positive, always supporting me, and for putting up with my various eccentricities. I know it wasn't always easy.

I would also like to thank the great crew in they Yeo lab without whom this endeavor would have been impossible. You guys eat more candy than anyone I know. Special thanks to Katannya, and Julia for eating froyo, carving pumpkins, building gingerbread houses, and generally being the best friends anyone could ask for. Thanks also to my brilliant mentees, Harrison and Layla. You are stars.

Finally, I would like to thank Arshad Desai and the other members of 2011 admissions committee. After I failed once to complete the Ph.D., it would have been easy to say no. Thanks for taking a chance on me.

The introduction is a modified adaptation of the material as it appears in: Protein-RNA networks regulated by normal and ALS-associated mutant HNRNPA2B1 in the nervous system. Fernando J. Martinez, Gabriel A. Pratt, Eric Van Nostrand, Ron Batra, Stephanie C. Huelga, Katannya Kapeli, Mark Fang, Peter Freese, Seung J. Chun, Chelsea Gelboin-Burkhart, Layla Fijany, Harrison Wang, Hong-joo Kim, Rea Lardelli, Shibing Tang, Balaji Sundararaman, John P. Donohue, Jens Lykke-Andersen, Sheng Ding, Shuo-Chien Ling, Frank Bennett, Manuel Ares Jr., Christopher B. Burge, J. Paul Taylor, Frank Rigo, Gene W. Yeo. Neuron. 2016 Nov. The dissertation author was the primary investigator and author of this paper.

Chapter 1 is a modified adaptation of the material as it appears in: Protein-RNA networks regulated by normal and ALS-associated mutant HNRNPA2B1 in the nervous system. Fernando J. Martinez, Gabriel A. Pratt, Eric Van Nostrand, Ron Batra, Stephanie C. Huelga, Katannya Kapeli, Mark Fang, Peter Freese, Seung J. Chun, Chelsea Gelboin-Burkhart, Layla Fijany, Harrison Wang, Hong-joo Kim, Rea Lardelli, Shibing Tang, Balaji Sundararaman, John P. Donohue, Jens Lykke-Andersen, Sheng Ding, Shuo-Chien Ling, Frank Bennett, Manuel Ares Jr., Christopher B. Burge, J. Paul Taylor, Frank Rigo, Gene W. Yeo. Neuron. 2016 Nov. The dissertation author was the primary investigator and author of this paper.

Chapter 2 is a modified adaptation of the material as it appears in: Protein-RNA networks regulated by normal and ALS-associated mutant HNRNPA2B1 in the nervous system. Fernando J. Martinez, Gabriel A. Pratt, Eric Van Nostrand, Ron Batra, Stephanie C. Huelga, Katannya Kapeli, Mark Fang, Peter Freese, Seung J. Chun, Chelsea Gelboin-Burkhart, Layla Fijany, Harrison Wang, Hong-joo Kim, Rea Lardelli, Shibing Tang, Balaji Sundararaman, John P. Donohue, Jens Lykke-Andersen, Sheng Ding, Shuo-Chien Ling, Frank Bennett, Manuel Ares Jr., Christopher B. Burge, J. Paul Taylor, Frank Rigo, Gene W. Yeo. Neuron. 2016 Nov. The dissertation author was the primary investigator and author of this paper.

Chapter 3 is a modified adaptation of the material as it appears in: Protein-RNA networks regulated by normal and ALS-associated mutant HNRNPA2B1 in the nervous system. Fernando J. Martinez, Gabriel A. Pratt, Eric Van Nostrand, Ron Batra, Stephanie C. Huelga, Katannya Kapeli, Mark Fang, Peter Freese, Seung J. Chun, Chelsea Gelboin-Burkhart, Layla Fijany, Harrison Wang, Hong-joo Kim, Rea Lardelli, Shibing Tang, Balaji Sundararaman, John P. Donohue, Jens Lykke-Andersen, Sheng Ding, Shuo-Chien Ling, Frank Bennett, Manuel Ares Jr., Christopher B. Burge, J. Paul Taylor, Frank Rigo, Gene W. Yeo. Neuron. 2016 Nov. The dissertation author was the primary investigator and author of this paper.

VITA

2005	Bachelor of Arts, in physics, Princeton University
2008	Master of Science, in biophysics, Stanford University
2016	Doctor of Philosphy, University of California, San Diego

PUBLICATIONS

Protein-RNA networks regulated by normal and ALS-associated mutant HNRNPA2B1 in the nervous system. **Fernando J. Martinez**, Gabriel A. Pratt, Eric Van Nostrand, Ron Batra, Stephanie C. Huelga, Katannya Kapeli, Mark Fang, Peter Freese, Seung J. Chun, Chelsea Gelboin-Burkhart, Layla Fijany, Harrison Wang, Hong-joo Kim, Rea Lardelli, Shibing Tang, Balaji Sundararaman, John P. Donohue, Jens Lykke-Andersen, Sheng Ding, Shuo-Chien Ling, Frank Bennett, Manuel Ares Jr., Christopher B. Burge, J. Paul Taylor, Frank Rigo, Gene W. Yeo. **Neuron**. In press.

Distinct and shared molecular targets and functions of ALS-associated TDP-43, FUS, and TAF15 revealed by comprehensive multi-system integrative analyses. Katannya Kapeli, Gabriel A. Pratt, Anthony Q. Vu, Kasey R. Hutt, **Fernando J. Martinez**, Balaji Sundararaman, Ranjan Batra, Peter Freese, Nicole J. Lambert, Stephanie C. Huelga, Seung Chun, Tiffany Y. Liang, Jeremy Chang, John P. Donohue, Lily Shiue, Jiayu Zhang, Haining Zhu, Franca Cambi, Edward Kasarskis, Manuel Ares Jr., Christopher B. Burge, John Ravits, Frank Rigo, Gene W. Yeo. **Nature Communications**. 2016 July.

Target Discrimination in Nonsense-Mediated mRNA Decay Requires Upf1 ATPase Activity. Lee SR, Pratt GA, **Martinez FJ**, Yeo GW, Lykke-Andersen J. **Molecular Cell**. 2015 August.

The presenilin-1 ΔE9 mutation results in reduced γ-secretase activity, but not total loss of PS1 function, in isogenic human stem cells. Woodruff G, Young JE, **Martinez FJ**, Buen F, Gore A, Kinaga J, Li Z, Yuan SH, Zhang K, Goldstein LS. **Cell Reports**. 2013 November.

A cellular model for sporadic ALS using patient-derived induced pluripotent stem cells. Burkhardt MF*, **Martinez FJ***, Wright S, Ramos C, Volfson D, Mason M, Garnes J, Dang V, Lievers J, Shoukat-Mumtaz U, Martinez R, Gai H, Blake R, Vaisberg E, Grskovic M, Johnson C, Irion S, Bright J, Cooper B, Nguyen L, Griswold-Prenner I, Javaherian A. **Molecular and Cellular Neuroscience**. 2013 September.

Whole exome sequencing identifies a splicing mutation in NSUN2 as a cause of a Dubowitz-like syndrome. **Martinez FJ***, Lee JH*, Lee JE, Blanco S, Nickerson E, Gabriel S, Frye M, Al-Gazali L, Gleeson JG. **Journal of Medical Genetics**. 2012 May.

Enhanced Caenorhabditis elegans Locomotion in a Structured Microfluidic Environment Park S, Hwang H, Nam SW, **Martinez F**, Austin RH, Ryu WS.. **PLoS One**. 2008 Jun 25.

* Denotes equal contribution

ABSTRACT OF THE DISSERTATION

Protein-RNA networks regulated by normal and ALS-associated mutant HNRNPA2B1 in the nervous system

by

Fernando J. Martinez

Doctor of Philosophy in Biomedical Sciences

University of California , San Diego 2016

Professor Eugene Yeo, Chair

HnRNPA2B1 encodes an RNA binding protein associated with neurodegeneration. However, its function in the nervous system is unclear. Transcriptome-wide cross-linking and immunoprecipitation in mouse spinal cord discover UAGG motifs enriched within ~2,500 hnRNP A2/B1 binding sites and an unexpected role for hnRNP A2/B1 in alternative polyadenylation. HnRNP A2/B1 loss results in alternative splicing (AS), including skipping of an exon in amyotrophic lateral sclerosis (ALS)-associated D-amino acid oxidase

(DAO) that reduces D-serine metabolism. ALS-associated hnRNP A2/B1 D290V mutant patient fibroblasts and motor neurons differentiated from induced pluripotent stem cells (iPSC-MNs) demonstrate abnormal splicing changes, likely due to increased nuclear-insoluble hnRNP A2/B1. Mutant iPSC-MNs display decreased survival in long-term culture, and exhibit hnRNP A2/B1 localization to cytoplasmic granules as well as exacerbated changes in gene expression and splicing upon cellular stress. Our findings provide a cellular resource and reveal RNA networks relevant to neurodegeneration, regulated by normal and mutant hnRNP A2/B1.

INTRODUCTION

Altered levels or mutations within RNA binding proteins (RBPs) are increasingly associated with neurological diseases, including Spinal Muscular Atrophy, Fragile X Syndrome, Amyotrophic Lateral Sclerosis (ALS), Frontotemporal Dementia (FTLD) (Mohagheghi et al., 2016) and Alzheimer's disease (AD) (Belzil et al., 2013; Gallo et al., 2005; Ling et al., 2013; Modic et al., 2013; Nussbacher et al., 2015; Polymenidou et al., 2012). ALS is a fatal, neurodegenerative disorder characterized by progressive loss of upper and lower motor neurons. The causes of ALS remain largely unknown, with 90% of cases being sporadic. The remaining 10% have a hereditary component (Pasinelli and Brown, 2006). Mutations in RBPs, including TAR DNA Binding Protein (TDP-43), Fused in Sarcoma (FUS) and TAF15 (Couthouis et al., 2011; Kabashi et al., 2008; Van Deerlin et al., 2008; Vance et al., 2009) have been identified as familial causes of ALS. Both familial and sporadic cases of ALS are characterized by TDP-43 or FUS positive aggregates or amyloid-like fibrils, even when neither gene is mutated (Mackenzie et al., 2007; Neumann et al., 2006; Sreedharan et al., 2008).

FUS/TLS and TDP-43 are both members of the heterogeneous nuclear ribonucleoprotein particle protein (hnRNP) family of RBPs. Another prominent member is the hnRNP A2/B1 gene, implicated in neurological diseases. HnRNP A2/B1 is thought to be sequestered by multiple CGG repeats in FMR1 and, in a Drosophila Fragile X-associated tremor/ataxia syndrome (FXTAS) model, hnRNP A2/B1 over-expression rescued the neurodegenerative phenotype (Sofola et al., 2007). In Alzheimer's disease, hnRNP A2/B1 is depleted in patient brains and this loss is mediated by the death of cholinergic neurons (Berson et al., 2012). Multisystem proteinopathy (MSP) is an autosomal dominant disorder characterized by muscle weakness and skeletal abnormalities. Mutations in the gene encoding Valosin Containing Protein (VCP) have been shown to cause MSP with motor neuron degeneration (Johnson et al., 2010; Watts et al., 2004). Excitingly, whole exome sequencing of a multiplex

MSP family recently revealed a p.D290V mutation in the HNRNPA2B1 gene (Kim et al., 2013), and muscle samples from affected patients exhibit hnRNP A2/B1 mislocalization.

Although hnRNP A2/B1 is believed to have numerous functions, its role in the central nervous system (CNS) is poorly understood. HnRNP A2/B1 exists in two distinct isoforms, A2 (341aa) and B1 (353aa), both transcribed from the HNRNPA2B1 gene. The putative functions of hnRNP A2/B1 include pre-mRNA splicing (Clower et al., 2010; Hutchison et al., 2002), mRNA trafficking (Gao et al., 2008; Raju et al., 2011; Shan et al., 2003), transcript stability (Fahling et al., 2006; Goodarzi et al., 2012), and translational control (Kosturko et al., 2006). Like TDP-43, hnRNP A2/B1 contains two RNA recognition motifs (RRMs) and has a glycine-rich domain (GRD) near the C-terminal end. HnRNP A2/B1 is primarily localized in the nucleus; however, nuclear-cytoplasmic trafficking does occur and is controlled in part by a nuclear localization signal in the GRD (Siomi et al., 1997). It is notable that the pathogenic D290V mutation occurs within the GRD of hnRNP A2/B1. This is akin to TDP-43 where most ALS-causing mutations also occur in its GRD (Lagier-Tourenne et al., 2010).

While we and others have previously characterized the function of hnRNP A2/B1 in human cell-lines (Huelga et al., 2012), the role that hnRNP A2/B1 plays in vivo in CNS tissues and disease-relevant cell-types is largely unknown. Furthermore, the effects of pathogenic mutations in hnRNP A2/B1 on RNA metabolism are not understood. Here, we map the endogenous binding sites of hnRNP A2/B1 in mouse spinal cord and human induced pluripotent stem cell (iPSC)-derived motor neurons (MNs). We identify alternative splicing (AS) and unexpectedly, alternative polyadenylation events affected by depletion of hnRNP A2/B1 in vivo. Surprisingly, we identify an alternative cassette exon within the D-amino acid oxidase (Dao) gene that is affected by hnRNP A2/B1 loss. Skipping of this exon leads to a shorter DAO isoform that is unstable and enzymatically inactive. Since loss of DAO activity and elevated levels of D-serine have been proposed to cause ALS (Sasabe et

al., 2007), this unexpected link between splicing and amino acid metabolism provides new insights into the importance of maintaining hnRNP A2/B1 levels in the nervous system. In addition to assessing the normal function of hnRNP A2/B1 in the CNS, we generated iPSC models with mutant (D290V) hnRNP A2/B1 that exhibited AS defects far in excess of what was anticipated from simple loss of hnRNP A2/B1. Longitudinal image analysis revealed a decreased survival rate of mutant hnRNP A2/B1 neurons. Upon stress, hnRNP A2/B1 D290V iPSC-MNs showed a propensity to accumulate hnRNP A2/B1 protein in cytoplasmic aggregates, further cementing the utility of these cells as an in vitro model for ALS/MSP. Finally, we show that iPSC-MNs generated from patients with MSP exhibit excessive changes in gene expression and AS after chemical stress.

The introduction is a modified adaptation of the material as it appears in: Protein-RNA networks regulated by normal and ALS-associated mutant HNRNPA2B1 in the nervous system. Fernando J. Martinez, Gabriel A. Pratt, Eric Van Nostrand, Ron Batra, Stephanie C. Huelga, Katannya Kapeli, Mark Fang, Peter Freese, Seung J. Chun, Chelsea Gelboin-Burkhart, Layla Fijany, Harrison Wang, Hong-joo Kim, Rea Lardelli, Shibing Tang, Balaji Sundararaman, John P. Donohue, Jens Lykke-Andersen, Sheng Ding, Shuo-Chien Ling, Frank Bennett, Manuel Ares Jr., Christopher B. Burge, J. Paul Taylor, Frank Rigo, Gene W. Yeo. Neuron. 2016 Nov. The dissertation author was the primary investigator and author of this paper.

CHAPTER 1: RESULTS

1.1 Discovery of hnRNP A2/B1 RNA binding sites in mouse spinal cord and human iPSC-MNs.

We constructed transcriptome-wide maps of hnRNP A2/B1 protein-RNA binding sites from UV-irradiated 8-week old mouse spinal cord. Protein-RNA complexes were immunoprecipitated using hnRNP A2/B1-specific antibodies (Figure 1A (left); Figures S1A and S1B). Using the individual-nucleotide CLIP (iCLIP) protocol, 2,394 clusters representing hnRNP A2/B1 binding sites in 564 genes (Fig. 1B; Data S1A) were identified by the CLIPper algorithm (Lovci et al., 2013). Gene ontology (GO) analyses of hnRNP A2/B1 RNA targets revealed statistically significantly enriched ($p<10\text{-}5$) categories, including protein binding, myelination, axon and neural projection. Most binding sites were within 3' untranslated regions (3'UTRs) of protein-coding genes (Figure 1B) and motif analysis revealed a statistically significantly enriched UAG[A/G] sequence within these clusters (Figure 1C) that resembled the previously identified binding sequence of hnRNP A2/B1 protein (Huelga et al., 2012). To further characterize the sequence specificity of hnRNP A2/B1, we applied RNA Bind-N-Seq (RBNS) (Lambert et al., 2014). Recombinantly expressed and purified hnRNP A2/B1 containing both RNA recognition domains was used for RBNS at five concentrations with an RNA pool consisting of random 20-mer RNAs (Figure 1A, right). The tagged hnRNP A2/B1 protein was then affinity-purified along with bound RNAs, which were subjected to RT-PCR, library preparation and high-throughput sequencing. We applied motif analysis on k-mers of lengths 4 to 6, calculating their enrichment in the hnRNP A2/B1 pull-down libraries compared to the input random-mers (enrichment is computed by dividing the frequency in pull-down with that in the input library). We found that hexamers containing the UAGG core sequence were not only shifted significantly towards higher hnRNP A2/B1 RBNS enrichments, but they also showed stron-

Figure 1. HnRNP A2/B1 predominantly binds 3′ untranslated regions (3′UTRs) and recognizes a UAGG motif.

(A) Schematic of experimental approaches. Individual nucleotide crosslinking followed by immunoprecipitation (iCLIP) in mouse spinal cord was used to identify hnRNP A2/B1 protein-RNA binding sites in vivo (left). RNA binding followed by sequencing (RNA bind-n-seq, RBNS) using the recombinantly expressed and purified RNA binding domain of hnRNP A2/B1 was employed to identify high affinity RNA nucleotides in vitro motifs (right). Motifs enriched by both methods were compared.

(B) hnRNP A2/B1 iCLIP-derived clusters are enriched in 3'UTRs of protein coding genes (left) when compared to the expected distribution of gene regions (5' and 3'UTRs, exons, and exon-proximal and distal portions of introns; right). Proximal intron regions are defined as extending up to 2 kb from an exon-intron junction (bottom).

(C) The UAGG motif is statistically significantly enriched in clusters from all regions (top) and those restricted to 3'UTRs (bottom). p-values were determined by the HOMER algorithm.

(D) Hexamers from RNA sequences found by RBNS and iCLIP that contain UAGG are significantly enriched (red dots) compared to those that did not contain UAGG (black dots). p values were calculated by a Kolmogorov-Smirnov test on the distributions represented by UAGG (red) and other k-mers (black).

(E–J) Genome browser views of CLIP reads (green, plotted in the positive direction of the y axis) and clusters (maroon) mapped to selected genes characteristic of the spinal cord (blue). y axes are scaled to the read numbers indicated to the right of each plot. In (H), alternative transcript isoforms are indicated in light blue. Reads from strand-specific RNA-seq analyses are plotted in mauve in the negative direction of the y axis in (F), (H) and (I). (E) – (I) show iCLIP analyses from mouse spinal cord; (J) shows eCLIP analysis from human iPSC-derived motor neurons, represented as log2 ratio of antibody-enriched immunoprecipitate (IP) over size-matched input. The dark green track is eCLIP reads enriched in IP. The light green track is eCLIP reads enriched in input.

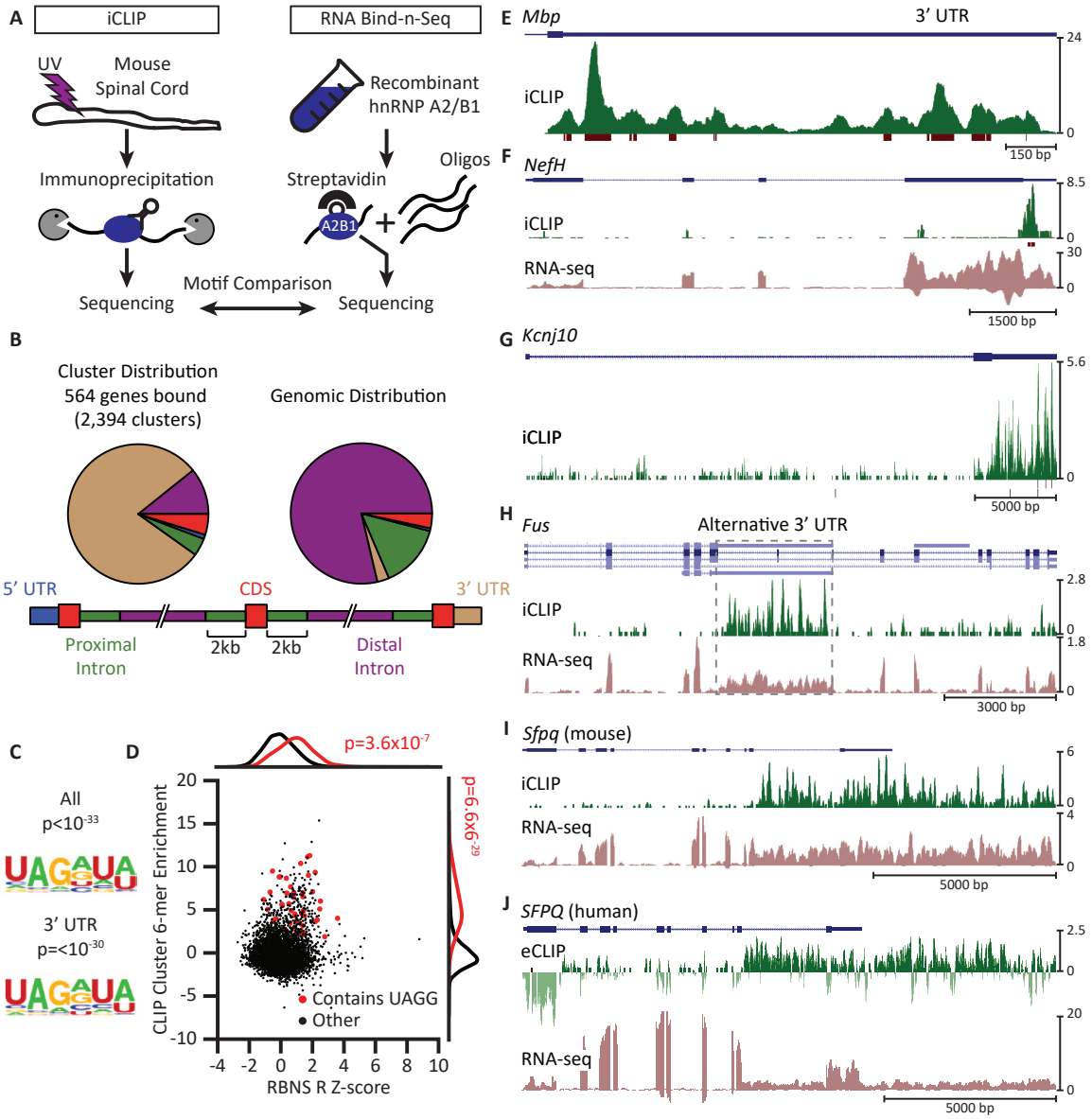
A
iCLIP
RNA Bind-n-Seq
UV
Mouse
Spinal Cord
Recombinant
hnRNP A2/B1
Immunoprecipitation
Streptavidin
Oligos
A2B1
Sequencing
Motif Comparison
Sequencing
B
Cluster Distribution
564 genes bound
(2,394 clusters)
Genomic Distribution
5′ UTR
CDS
3′ UTR
Proximal
Intron
2kb
2kb
Distal
Intron
C
All
p<10-33
3′ UTR
p=<10-30
D
p=3.6x10-7
p=6.6x10-29
CLIP Cluster 6-mer Enrichment
RBNS R Z-score
Contains UAGG
Other
E
Mbp
3′ UTR
iCLIP
150 bp
F
NefH
iCLIP
RNA-seq
1500 bp
G
Kcnj10
iCLIP
5000 bp
H
Fus
Alternative 3′ UTR
iCLIP
RNA-seq
3000 bp
I
Sfpq (mouse)
iCLIP
RNA-seq
5000 bp
J
SFPQ (human)
eCLIP
RNA-seq
5000 bp

ger enrichments among hnRNP A2/B1 CLIP binding sites than other hexamers (Figure 1D; Figure S1C). This result is in agreement with a UAGGG motif identified by RNAcompete (Ray et al., 2013). Thus we conclude that hnRNP A2/B1 binds to UAGG motifs within RNAs in mouse spinal cord tissue without requiring co-factor associations.

Next we investigated if hnRNP A2/B1 binds to genes specifically expressed in the major cell-types in the spinal cord. We observed abundant 3'UTR binding in the myelin basic protein (Mbp) gene, a known hnRNP A2/B1 RNA substrate (Ainger et al., 1997) (Figure 1E) the neurofilament heavy chain gene (Nefh) (Figure 1F) and the astroglial inward rectifying potassium channel gene Kcnj10 (Figure 1G). Thus, hnRNP A2/B1 binds transcripts characteristic of oligodendrocytes (Mbp), neurons (Nefh) and astroglia (Kcnj10). We also evaluated if hnRNP A2/B1 protein interacts with RNA encoded by ALS-associated genes. We found seven genes, of which five exhibited hnRNP A2/B1 binding within 3'UTRs, including Hnrnpa2b1 itself, the glial glutamate transporter Slc1a2, and Ubqln2 (Figure S1D). FUS/TLS contained hnRNP A2/B1 binding sites within an intronic region that may be processed as an alternative 3'UTR (Figure 1H). HnRNP A2/B1 binding was also found within long, unannotated 3'UTRs, as illustrated by the murine splicing factor proline/glutamine-rich (Sfpq) gene (Figure 1I) and its human ortholog expressed in iPSC-MNs (Figure 1J). The bound region in the SFPQ gene illustrates an intronic region that may be retained to lengthen the 3'UTR. We conclude that hnRNP A2/B1 binds to 3'UTRs within CNS transcripts, including ALS-associated genes.

To characterize the RNA binding properties of hnRNP A2/B1 in human cells, we differentiated human iPSCs to motor neurons (iPSC-MNs; Figure S6A; see Data S1B for a list of cell lines) and employed enhanced CLIP (eCLIP; (Van Nostrand et al., 2016); Figure S1E). Compared to iCLIP, eCLIP uses improved ligation strategies that increase recovery of RNA fragments and efficiency of library generation and features a size-matched input control to decrease false-positive rates (Van Nostrand et al., 2016), and is useful for limited

Figure S1. Supplemental data related to iCLIP, eCLIP and RNA Bind-N-Seq (Figure 1).

(A) Efficient immunoprecipitation of hnRNP A2/B1 complexes used for iCLIP. Western blot of mouse spinal cord lysate immunoprecipitated with either hnRNP A2/B1 specific antibody or rabbit IgG (Rb. IgG) and used for iCLIP. Input (In.), Supernatant (Sup.), Immunoprecipitate (IP).

(B) Autoradiogram of ^{32}P-labeled protein-RNA complexes fractionated by PAGE. White box indicates the area cut and used for iCLIP library preparation.

(C) RNA sequences found in 3'UTRs by iCLIP contain k-mers that are significantly enriched for UAGG (red dots) in RBNS data compared to all other k-mers (black dots). *p*-values were calculated by HOMER.

(D) Table of significantly bound iCLIP target genes that have been previously implicated in ALS.

(E) Efficient immunoprecipitation of hnRNP A2/B1 complexes used for eCLIP. Western blot of iPSC-MN lysate immunoprecipitated with either hnRNP A2/B1 specific antibody or rabbit IgG (Rb. IgG) and used for eCLIP. Input (In.), Supernatant (Sup.), Immunoprecipitate (IP). Black bars denote serial dilution of RNase I used for RNA fragmentation. White box indicates the area cut and used for eCLIP library preparation.

(F) hnRNP A2/B1 eCLIP-derived clusters are enriched in 3'UTRs of protein coding genes (left) when compared to the expected distribution of gene regions (5' and 3'UTRs, exons, and exon-proximal and -distal portions of introns; right). Proximal intron regions are defined as extending up to 2 kb from an exon-intron junction (bottom).

(G) Fold-enrichment of UAGG motifs in the genome plotted as a function of their distance to the center of the actual eCLIP peaks vs a shuffled control set.

(H) Venn diagram showing the overlap between the sets of hnRNP A2/B1-bound target genes from eCLIP and iCLIP in human motor neurons and mouse spinal cord, respectively.

(I) Table of the 35 hnRNP A2/B1-bound genes from (G) overlapping in both CLIP datasets. The 12 genes in yellow are RBPs. The 3 genes in green are motor proteins (2 kinesins and 1 dynein).

(J-K) Genome browser tracks of hnRNP A2/B1 iCLIP (mouse spinal cord) and eCLIP (human iPSC-MNs) targets. The binding pattern for both species is similar for the *Pnisr* / *PNISR* (J) and *Leng8* / *LENG8* (K) genes.

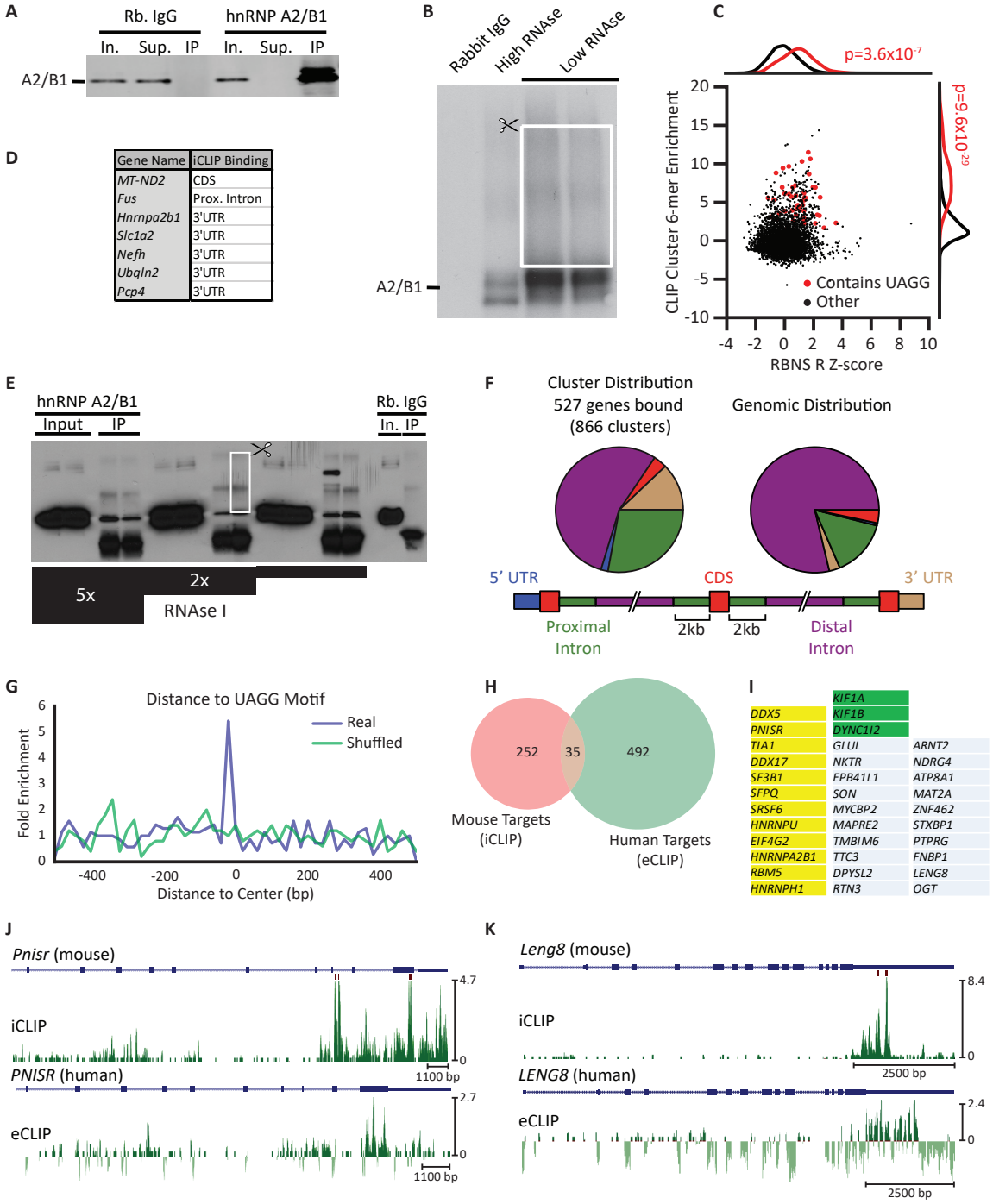
A
Rb. IgG
hnRNP A2/B1
In. Sup. IP In. Sup. IP
A2/B1
B
Rabbit IgG
High RNAse
Low RNAse
A2/B1
C
p=3.6x10-7
p=9.6x10-6
CLIP Cluster 6-mer Enrichment
RBNS R Z-score
Contains UAGG
Other
D
Gene Name | iCLIP Binding
MT-ND2 | CDS
Fus | Prox. Intron
Hnrnpa2b1 | 3'UTR
Slc1a2 | 3'UTR
Nefh | 3'UTR
Ubqln2 | 3'UTR
Pcp4 | 3'UTR
E
hnRNP A2/B1
Input IP
Rb. IgG
In. IP
5x
2x
RNAse I
F
Cluster Distribution
527 genes bound
(866 clusters)
Genomic Distribution
5' UTR
CDS
3' UTR
Proximal Intron
2kb
2kb
Distal Intron
G
Distance to UAGG Motif
Real
Shuffled
Fold Enrichment
Distance to Center (bp)
H
252
35
492
Mouse Targets (iCLIP)
Human Targets (eCLIP)
I
KIF1A
KIF1B
DDX5 DYNC1I2
PNISR
TIA1 GLUL ARNT2
DDX17 NKTR NDRG4
SF3B1 EPB41L1 ATP8A1
SFPQ SON MAT2A
SRSF6 MYCBP2 ZNF462
HNRNPU MAPRE2 STXBP1
EIF4G2 TMBIM6 PTPRG
HNRNPA2B1 TTC3 FNBP1
RBM5 DPYSL2 LENG8
HNRNPH1 RTN3 OGT
J
Pnisr (mouse)
iCLIP
PNISR (human)
eCLIP
1100 bp
K
Leng8 (mouse)
iCLIP
LENG8 (human)
eCLIP
2500 bp

cell numbers. eCLIP cluster identification in iPSC-MNs revealed 866 clusters in 527 genes enriched above input (Figure S1E; Data S1C). Compared to mouse spinal cord, the regional distribution of hnRNP A2/B1 binding did not concentrate as heavily in 3'UTRs. Nevertheless, 3'UTR binding was still highly enriched above expectation (Figure S1F). The UAGG motif, previously identified by iCLIP and RBNS, was significantly enriched near the center of eCLIP clusters (Figure S1G). Despite differences in heterogeneity and maturity of cell-types, the 35 target transcripts conserved between both adult mouse spinal cord and human iPSC-MNs (Fig. S1H) included a surprising number of RBPs (yellow) and motor proteins (green) (Figure S1I), often with similar binding patterns across transcripts of homologous genes, including those encoding PNISR and LENG8 (Figures S1J-S1K). We conclude that hnRNP A2/B1 binds similar regions in mouse spinal cord and human iPSC-MNs and harbors a conserved propensity to bind transcripts encoding RBPs.

1.2 HnRNP A2/B1 depletion in vivo results in limited changes in gene expression

To gain insights into the molecular pathways controlled by hnRNP A2/B1 in vivo, antisense oligonucleotides (ASOs) targeting Hnrnpa2b1 or saline controls, were injected into the lateral ventricle of adult mice (Figure 2A). After 28 days, the spinal cords were harvested and examined for hnRNP A2/B1 expression. HnRNP A2/B1 protein was reproducibly depleted by ~75% (Figure 2B). Surprisingly, we detected only a small number of gene expression changes either by RNA-seq (Figure 2C; Data S1D) or microarray analysis (Figure 2D; Data S1E). Specifically, we identified only 10 significantly down-regulated genes, which included Hnrnpa2b1 itself, indicating successful ASO targeting of Hnrnpa2b1 RNA. Interestingly, of the similar numbers of upregulated genes, we detected reproducible increases in mRNA levels of splicing factors such as Hnrnpa1, Hnrnph1, and Srsf7, which were validated by quantitative RT-PCR (Figure 2E; Figures S2A-S2C). We observed increased protein levels of hnRNP A1 and SRSF7 upon hnRNP A2/B1 depletion compared to non-targeting

Figure 2. HnRNP A2/B1 depletion results in alternative polyadenylation changes.

(A) Experimental approach. An antisense oligonucleotide (ASO) targeting the Hnrnpa2b1 transcript, or a vehicle control (saline) solution, was injected into the lateral ventricles of mice (n=4 mice per treatment) and RNA was isolated from spinal cords 28 days later.

(B) Western blotting shows that ASO treatment leads to a ~75% reduction in hnRNP A2/B1 protein levels compared to saline controls. A non-specific band was used a loading control.

(C–D) Statistically significant changes in transcript levels were identified for 17 and 27 genes when analyzed by RNA-seq (C) and microarray (D) analyses, respectively. Down- and upregulated genes are indicated in black and white, respectively. Significance was defined using a false-discovery rate threshold of 0.05 of Benjamini-Hochberg corrected values for multiple hypothesis testing.

(E) Quantitative RT-PCR validation of the results from (C) and (D) confirmed increased transcript levels for nine of ten genes, including Srsf7, Hnrnpa1, Hnrnph and Hnrnpf (left), and decreased transcript levels for all ten genes, including Hnrbpa2b1 itself (right), upon ASO-mediated depletion of hnRNP A2/B1. Tbp was used as a reference gene

(F) DaPars analysis of RNA-seq data from the mouse spinal cord samples reveals that depletion of hnRNP A2/B1 leads to changes in poly(A) site (PAS) utilization. The scatterplot of distal PAS (dPAS) usage indexes (PDUIs) in control and hnRNP A2/B1 depletion samples is shown. Significantly (FDR < 0.05, $|\Delta PDUI| \geq 0.2$, and $|dPDUI| \geq 0.2$) shortened and lengthened transcripts are colored in red and blue, respectively. Gray dots indicate transcripts that did not pass the significance threshold.

(G) Upon hnRNP A2/B1 depletion, 3'UTR shortening and lengthening was observed for 20 and 61 transcripts, respectively.

(H) Of the 81 transcripts displaying differential PAS utilization, 40 contained significant hnRNP A2/B1 occupancy in their 3'UTRs, as identified by iCLIP.

(I–J) Examples of genes with differential PAS utilization that are bound by hnRNP A2/B1 in their 3'UTRs. Regions of alternative usage are highlighted in blue (control) and red (ASO treated) in the corresponding RNA-seq track.

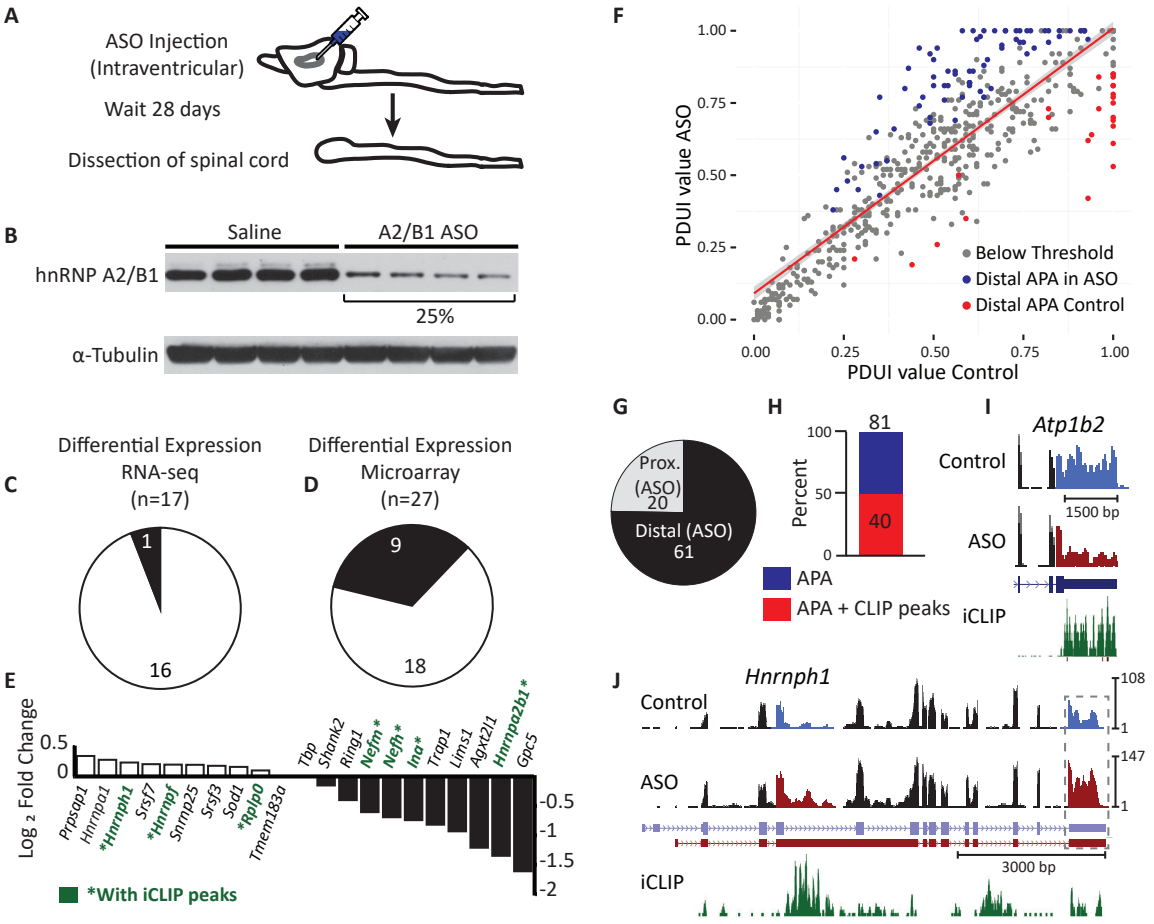
A
ASO Injection
(Intraventricular)
Wait 28 days
Dissection of spinal cord
B
Saline
A2/B1 ASO
hnRNP A2/B1
25%
α-Tubulin
C
Differential Expression
RNA-seq
(n=17)
1
16
D
Differential Expression
Microarray
(n=27)
9
18
E
Log 2 Fold Change
0.5
0
-0.5
-1
-1.5
-2
Prpsap1
Hnrnpa1
*Hnrnph1
Srsf7
*Hnrnpf
Snrnp25
Srsf3
Sod1
*Rplp0
Tmem183a
Tbp
Shank2
Ring1
Nefm*
Nefh*
Ina*
Trop1
Lims1
Agxt2l1
Hnrnpa2b1*
Gpc5
*With iCLIP peaks
F
PDUI value ASO
PDUI value Control
0.00
0.25
0.50
0.75
1.00
Below Threshold
Distal APA in ASO
Distal APA Control
G
Prox.
(ASO)
20
Distal (ASO)
61
H
Percent
100
50
0
81
40
APA
APA + CLIP peaks
I
Atp1b2
Control
ASO
iCLIP
1500 bp
J
Hnrnph1
Control
ASO
iCLIP
108
1
147
1
3000 bp

control ASO treatment (Figure S2D). This upregulation of hnRNP A1 is consistent with our previous report of cross-regulation among hnRNP A2/B1 and other RNA binding proteins (Huelga et al., 2012). We did not, however, find altered protein levels for hnRNP H1, M or U (Fig. S2D). We conclude that loss of hnRNP A2/B1 does not lead to widespread changes in transcript levels in the nervous system, in contrast to other ALS-associated RBPs such as TDP-43, FUS/TLS and TAF15 evaluated in mouse brain (Kapeli et al., 2016; Lagier-Tourenne et al., 2012; Polymenidou et al., 2011; Rogelj et al., 2012; Tollervey et al., 2011).

1.3 HnRNP A2/B1 depletion in vivo and in vitro has minimal effect on mature microRNA levels

A previous study reported a role for hnRNP A2/B1 in microRNA biogenesis, with 61 microRNAs decreased in expression by more than 50% upon hnRNP A2/B1 depletion in HEK293 human embryonic kidney cells (Alarcon et al., 2015). We sought to recapitulate these findings in mouse spinal cords and human iPSC-MNs that had been treated with ASOs targeting hnRNP A2/B1 or non-targeting controls in triplicate (Figure 2B; Figures 6E and 6F). Small RNA sequencing detected about 500 distinct mature microRNAs per sample. However, differential expression analysis indicated only minimal changes in microRNA levels, with no microRNAs passing a 0.05 adjusted p-value cutoff in the human iPSC-MN samples. Similarly, only a single microRNA (miR-146a) was differentially expressed (upregulated by two-fold) upon hnRNP A2/B1 depletion in mouse spinal cord (Figure S2E; Data S1F and S1G). We conclude that hnRNP A2/B1 does not play a major role in regulating the steady-state levels of microRNAs in the CNS.

Figure S2. Supplemental data related to gene expression changes upon hnRNP A2/B1 depletion (Figure 2).

(A) Correlation of $\log_2$ fold change in hnRNP A2/B1 ASO treated mouse spinal cord compared to saline treated spinal cord for 32 genes with the highest fold-change as judged by RNA-seq or microarray. Fold change is determined by qPCR (x-axis) and RNA-seq (y-axis). Dotted line is the least-squares linear regression.

(B) Correlation of $\log_2$ fold change in hnRNP A2/B1 ASO treated mouse spinal cord vs. saline treated spinal cord (X-axis) and hnRNP A2/B1 ASO treated spinal cord, vs. NTC ASO (y-axis), for the same 32 genes. Dotted line is the least squares linear regression.

(C) Table of the 32 most highly differentially expressed upon hnRNP A2/B1 depletion in mouse spinal cord. Differential expression was determined by RNA-seq and microarray and then confirmed by qPCR. Genes marked in green contain iCLIP enrichment.

(D) Western blotting showing upregulation, upon hnRNP A2/B1 depletion, of the levels of hnRNP A1 and SRSF7, but not of the other splicing factors indicated. Tubulin served as a loading control. Each lane represents lysate prepared from one spinal cord.

(E) Summary of small RNA sequencing results from mouse spinal cords and human iPSC-MNs in which hnRNP A2/B1 was depleted by ASO treatment, compared to control treatment (n=3 replicates per treatment and cell/tissue type, for a total of 12 samples). The data show that among 578 and 460 microRNAs detected in mouse spinal cords and human iPSC-MNs, respectively, only one microRNA (miR-146a) was significantly differentially expressed in mouse spinal cords, while none were found to be affected by hnRNP A2/B1 depletion in human iPSC-MNs.

(F) Validation of alternative poly-A site usage upon knockdown of hnRNP A2/B1 of events in Figures 2I and 2J. qPCR was performed for each gene with primer sets detecting the proximal and distal cleavage sites. The ratio is displayed on the y-axis. Error bars are SEM calculated with three replicates per condition.

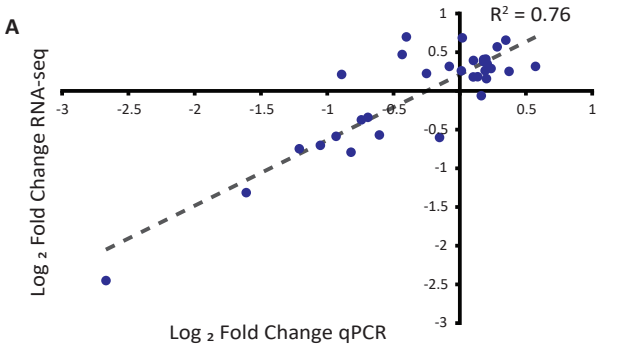

C

	Log 2 Fold Change		
Gene Name	RNA-seq (vs. saline)	qPCR (vs. saline)	qPCR (vs. NT ASO)
Agxt2l1	-0.748	-1.231	-1.099
Ctnna3	-0.704	-1.072	-0.896
Fam178a	0.317	0.262	0.094
Fam63b	0.394	0.057	0.069
Gpc5	-1.315	-1.531	-1.219
HnRNP A1	0.569	0.298	0.424
HnRNP A2/B1	-2.450	-3.276	-2.354
HnRNP H1	0.289	0.246	0.247
HnRNP Pf	0.159	0.146	0.203
Ina	-0.373	-0.604	-0.236
Lims1	-0.588	-0.864	-0.539
Nefh	-0.341	-0.663	-0.552
Nefm	-0.568	-0.620	-0.483
Nrxn3	-0.989	-0.749	-0.467
Prpf4b	0.263	0.148	0.112
Prpsap1	0.655	0.349	0.515
Ptrf	0.315	-0.136	0.307
Ralgapa1	0.226	-0.312	0.342
Ring1	0.697	-0.348	0.391
RplP0	0.182	0.037	0.568
Shank2	-0.602	-0.276	-0.141
Slc39a12	0.260	-0.041	0.271
SnRNP 25	0.410	0.200	0.240
Sod1	-0.094	0.047	0.198
Srsf3	0.377	0.163	0.060
Srsf7	0.349	0.218	0.113
Stom	0.469	-0.089	0.534
Sv2A	0.214	-0.144	-0.469
Tcf20	0.404	0.140	-0.128
Trap 1	-0.793	-0.845	-0.418
Ube2d3	0.252	0.322	-0.121
Upp2	-0.279	-1.193	-1.465

With iCLIP peaks

D

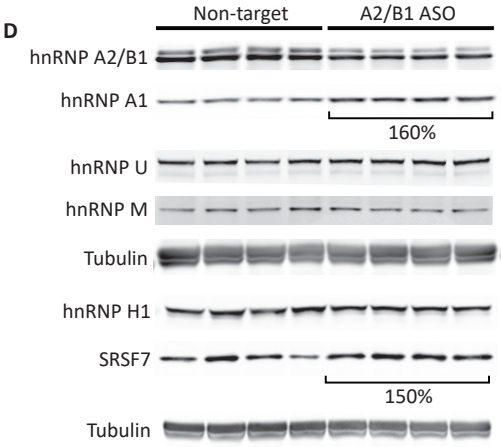

E

Summary: Small RNA Sequencing			
Tissue Type	Treatment	miRNAs Detected	Differentially Expressed
Mouse Spinal Cord	*Hnmpa2b1* ASO	578	miR-146a (+2.15 fold)
Human iPSC MNs	*HNRNPA2B1* ASO	460	none

F

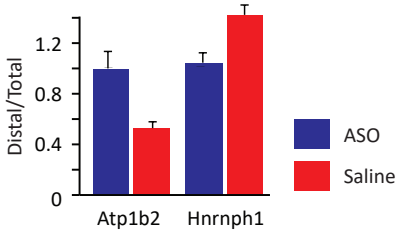

1.4 HnRNP A2/B1 regulates alternative 3' cleavage choice in vivo

As hnRNP A2/B1 binds within 3'UTRs, we next evaluated whether hnRNP A2/B1 affects alternative polyadenylation. To identify alternative 3' cleavage sites, we utilized the DaPars algorithm (Xia et al., 2014) to analyze the RNA-seq data obtained from the ASO-treated mouse spinal cords. We identified 81 alternative polyA site (PAS) shifts (Figure 2F; Data S1H), of which 61 (~80%) resulted in distal polyA site usage to generate a longer 3'UTR upon depletion of hnRNP A2/B1, with the remainder exhibiting 3'UTR shortening (proximal polyA usage; Figure 2G). Strikingly, half (40) of the 81 APA changes contained hnRNPA2/B1 binding sites within the 3'UTR (Figure 2H). To illustrate, we identified a shortening of the 3'UTR in the ATPase, Na+/K+ Transporting, Beta 2 polypeptide (Atp1b2) gene (Figure 2I), and a lengthening of the 3'UTR in Hnrnph1 (Figure 2J). Quantitative RT-PCR successfully validated PAS shifts within these genes (Figure S2F). We conclude that hnRNP A2/B1 binding within 3'UTRs is associated with hnRNP A2/B1-dependent alternative polyadenylation choice.

1.5 Hundreds of alternative splicing events depend on hnRNP A2/B1 protein level

We identified 276 AS changes from our splicing-sensitive microarray data (Figure 3A, Data S1I). The largest differences were observed in the class of AS events known as alternative cassette exons, which were more frequently skipped (repressed) upon depletion of hnRNP A2/B1 than included (activated) (Figure 3B). Interestingly, while only 12% (17) of cassette events harbored hnRNP A2/B1 binding sites in flanking intronic regions (Figure 3C), we did observe that 5 of the top 20 cassette events featured hnRNP A2/B1 binding proximal to the exon (genes marked in green in Figure 3D). RT-PCR validation of AS events confirmed the microarray data using both saline (vehicle) as well as non-targeting ASO as controls (Figure 3E; Figure S3A). Intriguingly, we identified an alternative cassette

Figure 3. HnRNP A2/B1 depletion in mouse spinal cord affects alternative splicing.

(A) Pie chart shows the classification of 276 significantly changing (q value < 0.05, sepscore > 0.5) splicing events identified by splicing-sensitive microarray. The legend illustrates the types of splicing events represented on the array.

(B) 137 alternative cassette events are altered upon loss of hnRNP A2/B1. 85 events were repressed upon knockdown and 52 were activated.

(C) Of the 137 transcripts displaying differential inclusion of cassette exons, 17 contained significant hnRNP A2/B1 occupancy, as identified by iCLIP

(D) Ranked list of the 30 alternative cassette events with the largest absolute fold change. Activated cassettes are in red. Repressed cassettes are in blue. Gene names shown in green have significant hnRNP A2/B1 occupancy, as identified by iCLIP.

(E) RT-PCR validation of 6 alternative cassette events. Samples from control mice (white bars) are normalized to 1. Samples from ASO treated mice are shown in red (activated) and blue (repressed). Of the four samples from each treatment group used to generate the bar graphs, three are shown in the gel images that were used to generate the bar graphs. Error bars are SEM computed with 4 replicates per condition.

(F) The alternative exon (dashed box) regulated by hnRNP A2/B1 within its own 3'UTR has nearby iCLIP clusters. Color coding of the browser tracks is as in (1E-J). The red browser track shows the position of PCR primers used for validation. Inset: RT-PCR validation of the event. Bars are as in 3E.

(G) An example of alternative 3'UTR usage (grey box) regulated by hnRNP A2/B1, in the Rsrp1 gene with nearby iCLIP clusters. Color coding of the browser tracks is as in (1E-J). The red, grey and green lines above the gene models indicate the position of primers used for qPCR validation. Colors correspond to the bar graph in the inset. Inset: qPCR validation of alternative 3'UTR usage. Tbp was used as the reference gene. Error bars are SEM computed with 3 replicates per condition.

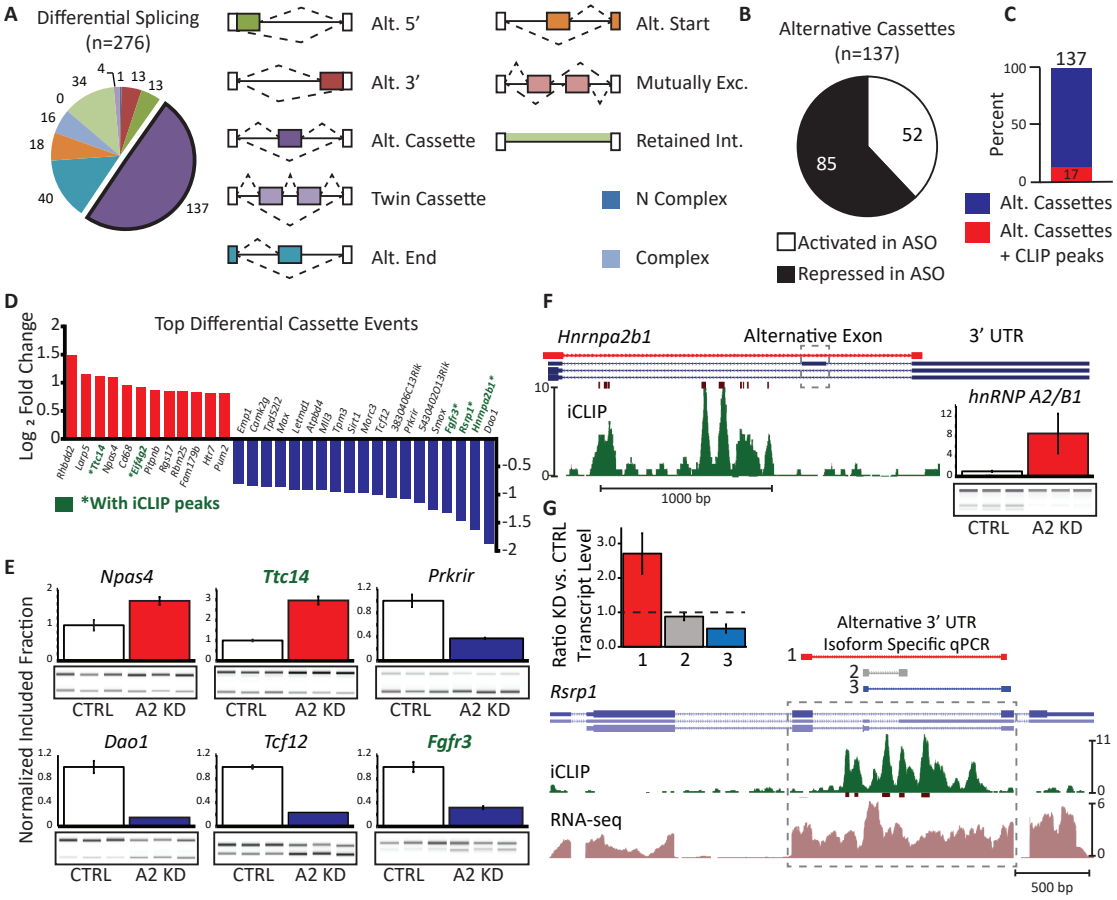
A
Differential Splicing
(n=276)
Alt. 5'
Alt. 3'
Alt. Cassette
Twin Cassette
Alt. End
Alt. Start
Mutually Exc.
Retained Int.
N Complex
Complex
B
Alternative Cassettes
(n=137)
52
85
Activated in ASO
Repressed in ASO
C
137
Percent
Alt. Cassettes
Alt. Cassettes
+ CLIP peaks
D
Top Differential Cassette Events
Log 2 Fold Change
*With iCLIP peaks
E
Normalized Included Fraction
Npas4
Ttc14
Prkrir
Dao1
Tcf12
Fgfr3
CTRL
A2 KD
F
Hnrnpa2b1
Alternative Exon
3' UTR
iCLIP
1000 bp
hnRNP A2/B1
G
Ratio KD vs. CTRL
Transcript Level
Alternative 3' UTR
Isoform Specific qPCR
Rsrp1
iCLIP
RNA-seq
500 bp

exon within the 3'UTR of the Hnrnpa2b1 gene itself (Figure 3F). iCLIP data indicated that hnRNP A2/B1 binds upstream of the exon to enhance its use, resulting in an isoform that is expected to be subjected to nonsense-mediated decay (McGlincy et al., 2010). This mode of autoregulation is consistent with our and others' reports of splicing factors controlling their own levels (Huelga et al., 2012; McGlincy et al., 2010). We also observed AS events within 3'UTRs of other genes. For example, hnRNP A2/B1 binding is observed in a region that alternatively encodes either an intron or a 3'UTR for a shorter isoform in the Arginine/serine-rich protein 1 (Rsrp1) gene (Figure 3G). Depletion of hnRNP A2/B1 results in removal of the intron that generates a longer isoform (Figure 3G). We also found that decreased levels of hnRNP A2/B1 affect the AS of cassette exons within other ALS-associated genes, namely D-amino acid oxidase (Dao), Ataxin-2 (Atxn2) and inositol triphosphate receptor, type 2 (Itpr2) (Figure S3B). We conclude that loss of hnRNP A2/B1 affects hundreds of AS events in vivo, including an exon within its own 3'UTR.

1.6 HnRNP A2/B1 interacts with RNA components of the spliceosome.

To evaluate if hnRNP A2/B1 interacts with components of the splicing machinery, we performed isotonic lysis of mouse spinal cord samples and RNA immunoprecipitation followed by Northern blotting with probes interrogating the snRNA family. We confirmed specific enrichment of U2, U4, U5, and U6 snRNA with immunoprecipitation of hnRNP A2/B1, but not U1 snRNA (Figure S3C). Using Northern blotting, we measured total snRNA levels in saline treated and hnRNP A2/B1 depleted mouse spinal cords. We did not observe significant changes in overall snRNA levels (Figure S3D). From these data, we conclude that hnRNP A2/B1 interacts with snRNAs but loss of hnRNP A2/B1 does not affect snRNA levels.

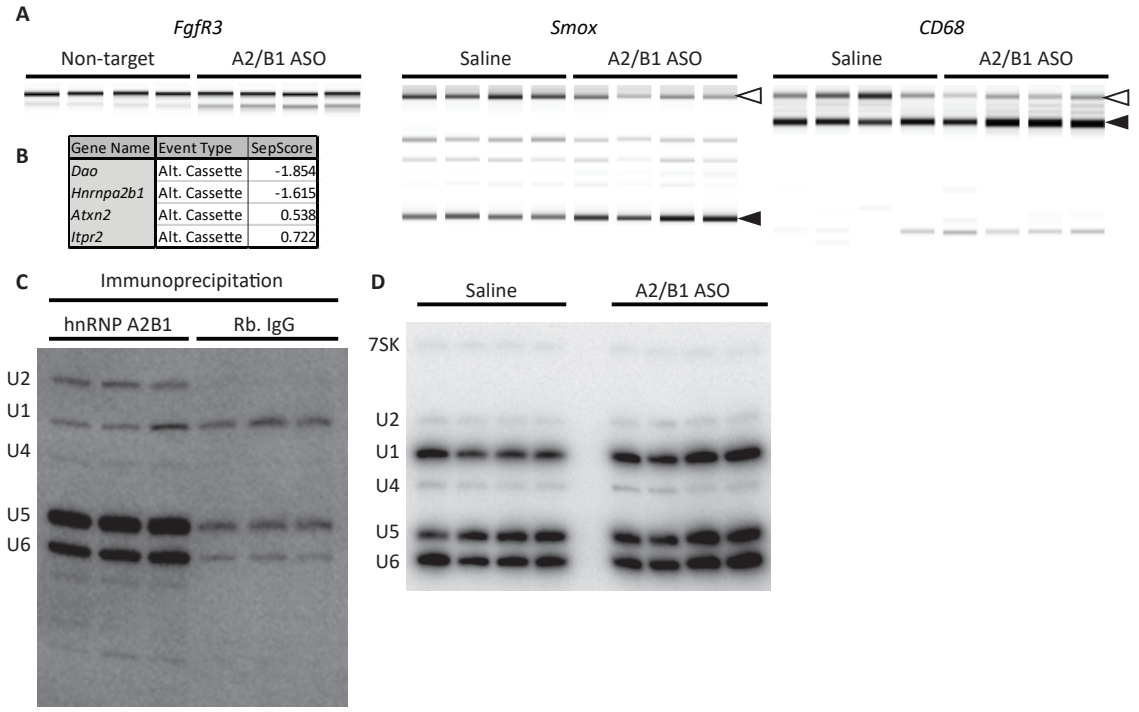

Figure S3. Supplemental data related to AS changes induced upon hnRNP A2/B1 depletion (Figure 3).

(A) Three additional splicing changes detected in ASO treated mouse spinal cords validated by RT-PCR and capillary electrophoresis. Arrows point to the transcripts produced by alternative cassette events.

(**B**) Table of significantly changed splicing events, altered upon depletion of hnRNP A2/B1 in mouse spinal cord, that overlap with previously published ALS related genes.

(C) Enrichment of hnRNP A2/B1 on RNA components of the spliceosome. hnRNP A2/B1 was immunoprecipitated from mouse spinal cord lysates. The bound RNA was recovered and detected by northern blot against five snRNAs.

(D) Northern blot against five snRNAs from mouse spinal cord total RNA. There is no consistent difference in snRNA levels after hnRNP A2/B1 depletion.

1.7 HnRNP A2/B1-dependent splicing in the D-amino acid oxidase gene results in reduced expression and enzymatic activity

The AS event that harbored the largest magnitude change in our splicing microarray analysis is a 118 nucleotide cassette exon (exon 9) in the Dao gene (Figure 4A). This event is prominent because of previous studies implicating Dao in ALS (Kosuge et al., 2009; Sasabe et al., 2007). Dao codes for an enzyme important in the metabolism of D-serine and is largely expressed in the brainstem and spinal cord. D-serine is a known agonist of the NMDA receptor, and reports have suggested that increased D-serine levels contribute to excito-toxicity in ALS (Sasabe et al., 2007). Upon depletion of hnRNP A2/B1 protein, overall Dao mRNA expression is unaltered (Figure 4B), but RT-PCR validation of the microarray-predicted exon skipping event shows a substantial increase in the abundance of the shorter isoform, relative to the longer isoform (Figure 4C). This alteration is predicted to cause a shift in reading frame and early termination of the protein, but the location of the premature termination codon is not predicted to lead to nonsense-mediated decay.

Upon hnRNP A2/B1 knockdown, we observed a 30% reduction in protein levels of the long isoform (Figure 4D). The predicted structure of the short isoform lacks two alpha helices and three beta sheets, which are present in the structure of the full-length isoform (Figure 4E). This suggests that the short isoform may have defects in enzymatic activity. To test if the shorter mRNA isoform is translated and retains enzymatic activity, we stably expressed both the long and short isoforms in human 293 FRT cell lines (Figure 4F). We found that while both isoforms were similarly expressed at the mRNA level (Figure 4G), the protein level of the short isoform was significantly reduced (Figure 4F), suggesting that the shorter isoform is subjected to reduced translation or protein stability. To determine the mechanism for reduced protein levels of the short isoform, we treated cell lines stably expressing each isoform with the proteasome inhibitor MG-132. We performed immunoblotting over 24 hours and found that cell lines expressing the short isoform of Dao accumu-

Figure 4. hnRNP A2/B1-dependent AS in the D-amino acid oxidase (DAO) gene results in reduced DAO protein expression and enzymatic activity.

(A) Gene models of the long and short mRNA isoforms produced by AS of the hnRNP A2/B1-dependent cassette exon (in white) in the Dao pre-mRNA. Unaffected exons are shown as black boxes. Introns and UTRs are shown as thin boxes and lines, respectively. The lengths of the predicted protein products are indicated. Amino acid (AA).

(B) The transcript levels of Dao mRNA in control and hnRNP A2/B1 depleted mouse spinal cord (n=4 mice per group) determined by qPCR. Tbp is used as reference. Error bars are SEM computed with 4 replicates. The mean transcript level for the control mice is normalized to one.

(C) Gel-like image of AS of the Dao cassette exon in mice, determined by RT-PCR, shows exon exclusion upon hnRNP A2/B1 depletion.

(D) Western blotting shows a reduction in DAO protein levels to ~70% of non-target control levels in mice treated with hnRNP A2/B1 targeting ASO.

(E) X-ray crystallography structure of human DAO (left; Protein Database ID 2E48, Kawazoe et al. (2006)) and the predicted structure of the short isoform (right). The circles denote 2 alpha helices and 3 beta sheets that are absent in the predicted shorter isoform.

(F) Schematic of constructs used to express DAO long and short isoforms in stable cell lines. Western blotting shows reduced protein levels in clones expressing the short isoform.

(G) No difference in transcript level of Dao mRNA from the clones shown in (F) determined by qPCR. Tbp was used as a reference gene. Error bars are SEM computed with 4 replicates per condition.

(H) D-amino acid oxidase activity in the clones shown in (F). Bars represent the ratio of substrate to non-substrate dependent activity. Error bars are SEM computed with 4 replicates per condition.

(I) Western blotting of DAO protein translated in rabbit reticulocyte lysate reveals similar levels in cells expressing either isoform.

(J) D-amino acid oxidase activity in the lysates shown in (J). The wedge below the bars denotes serial 2 fold dilutions of the lysates.

(K) Depletion of hnRNP A2/B1 in the human U251 glioblastoma cell line. Three different targeting shRNAs and one non-targeting control shRNA plasmids were used in triplicates. Splicing-sensitive RT-PCR (top) for DAO shows that under conditions where the short DAO isoform cannot be detected in the NTC-shRNA treated samples, the short DAO isoform was consistently detected in samples treated with the two most effective shRNA constructs. hnRNP A2/B1 depletion was verified by western blotting (bottom). Tubulin was the loading control.

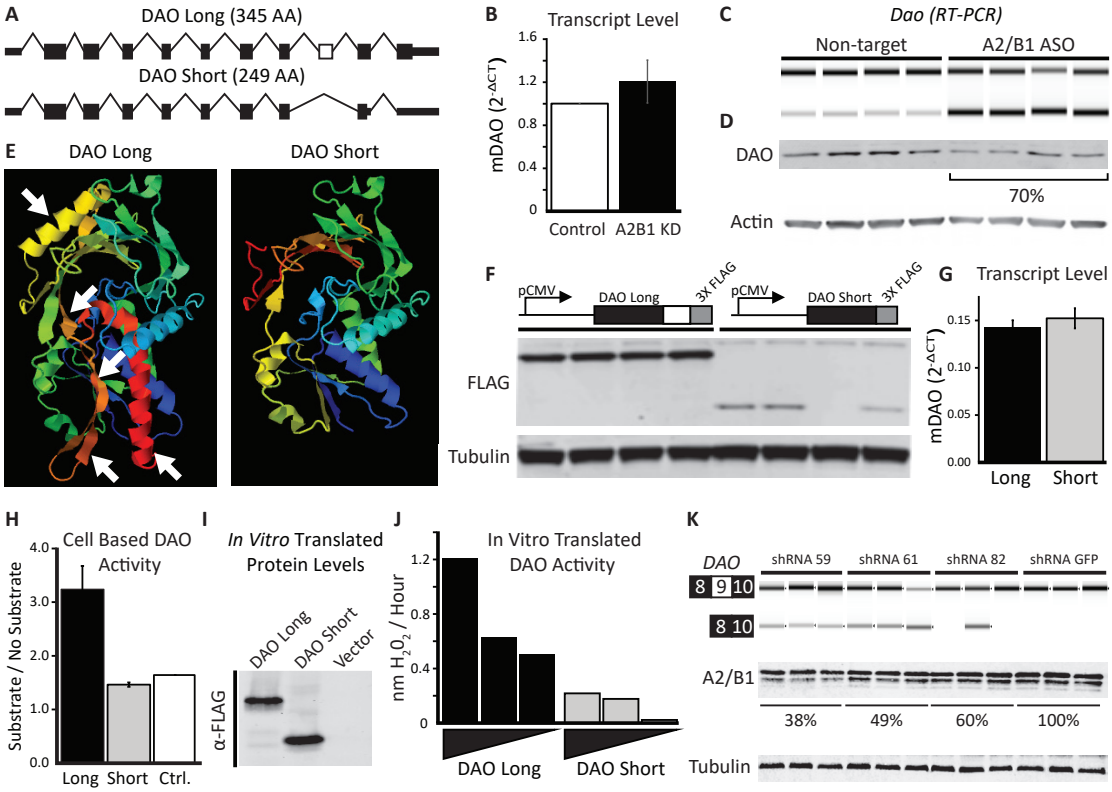
A
DAO Long (345 AA)
DAO Short (249 AA)
B
Transcript Level
mDAO (2-ΔCT)
1.6
1.2
0.8
0.4
0
Control
A2B1 KD
C
Dao (RT-PCR)
Non-target
A2/B1 ASO
D
DAO
70%
Actin
E
DAO Long
DAO Short
F
pCMV
DAO Long
3X FLAG
pCMV
DAO Short
3X FLAG
FLAG
Tubulin
G
Transcript Level
mDAO (2-ΔCT)
0.15
0.10
0.05
0.00
Long
Short
H
Cell Based DAO Activity
Substrate / No Substrate
4.0
3.0
2.0
1.0
0.0
Long
Short
Ctrl.
I
In Vitro Translated Protein Levels
DAO Long
DAO Short
Vector
α-FLAG
J
In Vitro Translated DAO Activity
nm H2O2 / Hour
1.2
0.8
0.4
0
DAO Long
DAO Short
K
DAO
shRNA 59
shRNA 61
shRNA 82
shRNA GFP
8 9 10
8 10
A2/B1
38%
49%
60%
100%
Tubulin

lated the protein (Figures S4A and S4B). Conversely, cell lines expressing the long isoform had stable levels of protein expression. To measure enzymatic activity, we subjected the transgenic cell lines expressing each isoform to a cell-based assay that measures the release of H2O2 during DAO activity (Figure S4C). Cell lines expressing the long isoform showed significant DAO activity, while cell lines expressing the short isoform had no DAO activity above background level (Figure 4H). To distinguish effects due to protein expression from effects due to reduced enzymatic activity, we translated the long and short isoforms of Dao in vitro using rabbit reticulocyte lysate (Figure 4I). We measured the activity of the in vitro translated long and short protein and found that the short isoform has an 85% reduction in enzymatic activity (Figure 4J). Taken together, we conclude that hnRNP A2/B1 depletion leads to production of a shorter isoform of Dao, which is subject to proteasomal degradation and exhibits ~six-fold reduction in enzymatic activity.

To determine if AS of Dao is evolutionarily conserved, we inspected the orthologous 118bp exon in human DAO, which has high amino acid conservation to the murine exon. However, the exon is not annotated as being alternatively spliced. We designed RT-PCR primers in the adjacent constitutive exons and checked for multiple isoforms in human PSC-MNs. Unfortunately, we observed no expression of DAO mRNA in these samples (data not shown). As expression of DAO is thought to be region and cell-type specific (Horiike et al., 1994), we consulted the Brain RNA-seq database (Zhang et al., 2014), which comprises expression data for a variety of cell types obtained from mouse and human cerebral cortices. Little to no expression of DAO in any of the samples in this database was reported (Figures S4D and S4E). Finally, we obtained a panel of human CNS RNA samples. We observed DAO mRNA expression only in astrocytes from human cerebellum and spinal cord (Figure S4F top). Sanger sequencing of the bands from RT-PCR analysis confirmed a longer isoform as human mRNA containing exons 8, 9, and 10 and a shorter isoform as lacking exon 9 (Figure S4F bottom). We conclude that DAO mRNA is expressed primarily

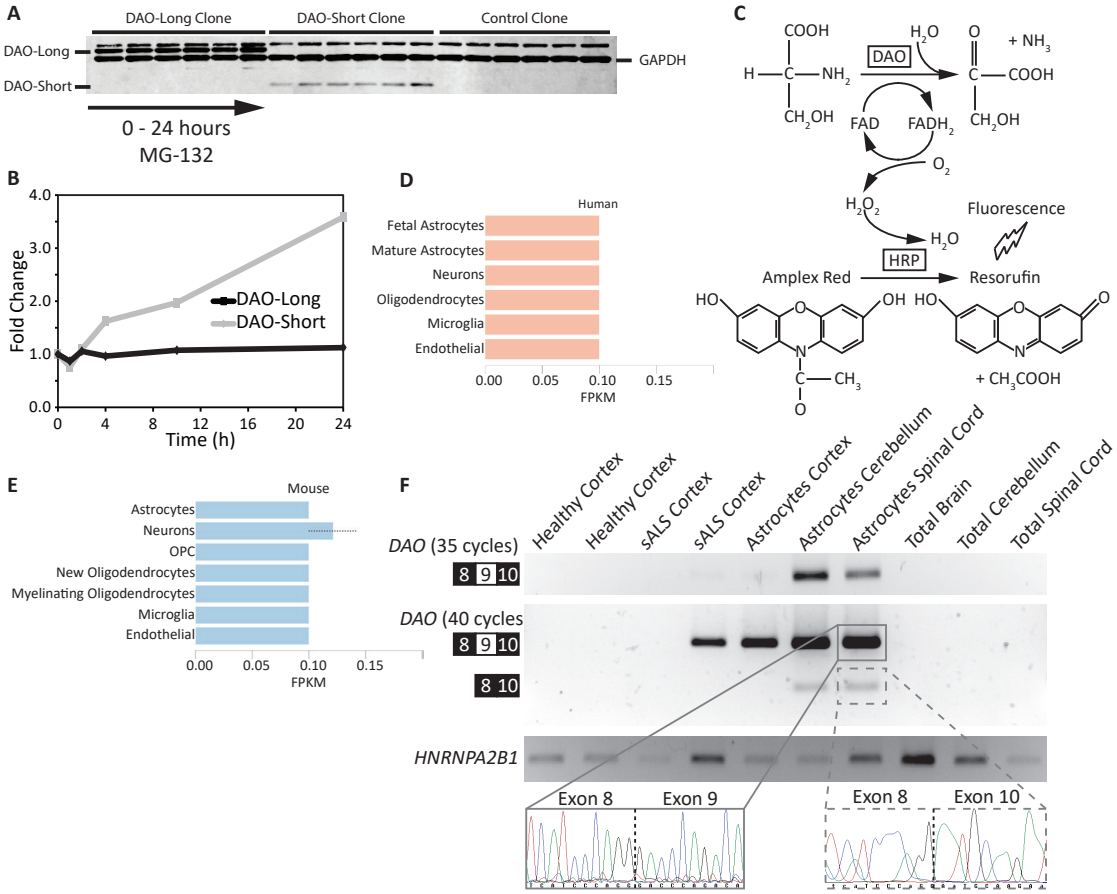

Figure S4. Supplemental data related to exon skipping in the *Dao* gene after hnRNP A2/B1 depletion in mouse spinal cord (Figure 4).

(A) Western blot of DAO in transgenic cell lines expressing the long or short isoforms of the protein. Cells were treated with MG-132 and harvested 1h, 2h, 4h, 10h and 24 later. GAPDH served as a loading control. These data were used to generate the graph in Figure 4H. The top band is an unspecific band.

(B) Relative fold change in DAO protein after treatment with MG-132 determined by Western blotting. The zero time point for each line is normalized to 1.

(C) A schematic representation showing how the Amplex Red assay is coupled to DAO and used to read out the activity level by fluorescence emission.

(D-E) Expression data from the Brain RNA-Seq project. FPKM values for *DAO*/*Dao* are at the noise level for all samples in both human (D) and mouse (E).

(F) RT-PCR analysis of the long and short *DAO* transcript isoforms in a panel of RNA from h isolated from healthy cortex and sALS primary motor cortex obtained from deceased individuals, primary human astrocytes (ScienCell) and total brain, cerebellum and spinal cord (Clontech). The isoforms detected and the PCR amplification cycle numbers used are depicted to the left of the agarose gel image. Sanger sequencing from the indicated gel-extracted PCR amplicons (Insets) confirmed the identity of the PCR products (bottom).

in human astrocytes of the cerebellum and spinal cord and that its AS is conserved in mouse spinal cord. Importantly, shRNA-mediated depletion of hnRNP A2/B1 in a human U-251 cell line derived from human glioblastoma multiforme revealed an increase in the shorter isoform, consistent with exon 9 skipping (Figure 4K). This result confirms conservation of hnRNP A2/B1-dependent splicing of DAO exon 9 in mice and humans. Thus, an unanticipated hnRNP A2/B1-dependent AS of an exon in Dao dramatically reduces D-serine metabolism, implicating lower levels of hnRNP A2/B1 with DAO-mediated pathogenicity observed in disease.

1.8 HnRNP A2/B1 D290V mutation results in splicing defects in human fibroblasts

As mutations within the hnRNP A2/B1 gene are associated with MSP and ALS (Kim et al., 2013), we next examined if the D290V mutation affects AS. RNA isolated from fibroblasts harboring wildtype hnRNP A2/B1 and disease-associated hnRNP A2/B1 D290V mutations (two affected individuals) were subjected to splicing array analysis (Figure 5A; Data S1J). To evaluate if splicing changes could be attributed to a mutant-dependent loss of normal splicing, we introduced non-targeting (control) and ASOs targeting human hnRNP A2/B1 in fibroblasts from unaffected control individuals to deplete hnRNP A2/B1 (Figures 5B and 5C). For splicing-sensitive array analysis, hnRNP A2/B1 mutant and depletion samples were compared to two unrelated, unaffected control samples. For hnRNP A2/B1 D290V mutants, we found that ~4,000 splicing events were altered relative to controls (Figure 5D). This is in contrast to fibroblasts depleted of hnRNP A2/B1, where only 875 events registered as significantly different (Figure 5D). Interestingly, when RNA from fibroblasts harboring a mutation in the only other known gene related to MSP, the VCP R155H mutation, was subjected to the same analysis, 703 AS events were altered (Figure 5D). We compared the overlap of significantly changing alternative cassette events between the different groups of samples (Figures 5E and 5F). For the VCP R155H mutant fibroblasts, we found that 465

Figure 5. Fibroblasts from patients with mutations in HNRNPA2B1 and VCP exhibit widespread splicing defects not found when hnRNP A2/B1 is depleted.

(A) A multiplex family affected by MSP, where affected (filled in black) individuals harbor p.D290V mutations in the HNRNPA2B1 gene. Fibroblasts and iPSCs used in experiments in Figures 5-7 were obtained from the indicated individuals.

(B) Depletion of HNRNPA2B1 mRNA in fibroblasts from an unaffected individual by treatment with ASOs, as measured by qPCR using GAPDH as the reference gene. Error bars are SEM computed with 3 replicates per condition. The control transcript level is normalized to one. The error for the control samples is added to the error for the other conditions by error propagation.

(C) Western blot analysis showing successful depletion of hnRNP A2/B1 protein. GAPDH was used as the loading control.

(D) Splicing-sensitive microarrays detected splicing changes in fibroblasts obtained from individuals with the indicated genotype. hnRNP A2/B1 depletion is from samples in 5B and 5C. Significant splicing changes are determined by comparing to two different unrelated control samples. Color coding and splicing event categories are as in Figure 3A.

(E) Quantification of alternative cassette events detected in the various samples. Colors indicate the direction of the splicing change. Excluded refers to excluded in the depleted or affected sample. Included refers to included in the depleted or affected sample.

(F) Venn diagrams illustrating overlapping splicing events between the indicated groups. Overlapping events refers to identical splicing events flagged as significant in two or more samples, regardless of the directionality of the changes.

(G) Heat map of 32 splicing changes that were flagged as significant in all four groups. Red changes are activated compared to controls. Green changes are repressed. Color mapping is performed according to the column wise Z-score.

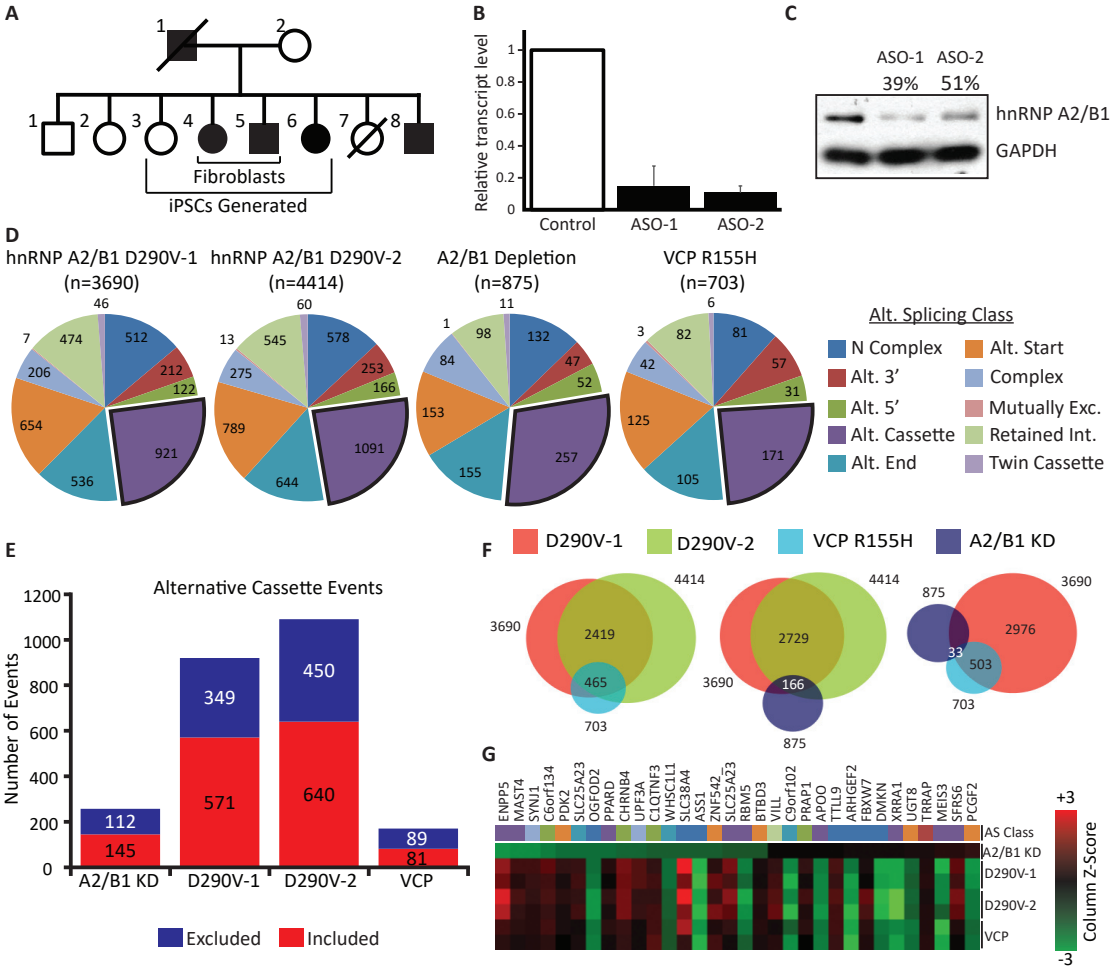
A
1
2
1
2
3
4
5
6
7
8
Fibroblasts
iPSCs Generated
B
Relative transcript level
1
0.8
0.6
0.4
0.2
0
Control
ASO-1
ASO-2
C
ASO-1 ASO-2
39% 51%
hnRNP A2/B1
GAPDH
D
hnRNP A2/B1 D290V-1 (n=3690)
hnRNP A2/B1 D290V-2 (n=4414)
A2/B1 Depletion (n=875)
VCP R155H (n=703)
46
512
212
122
921
536
654
206
474
7
60
578
253
166
1091
644
789
275
545
13
11
132
47
52
257
155
153
84
98
1
6
81
57
31
171
105
125
42
82
3
Alt. Splicing Class
N Complex
Alt. 3'
Alt. 5'
Alt. Cassette
Alt. End
Alt. Start
Complex
Mutually Exc.
Retained Int.
Twin Cassette
E
Alternative Cassette Events
Number of Events
1200
1000
800
600
400
200
0
112
145
349
571
450
640
89
81
A2/B1 KD
D290V-1
D290V-2
VCP
Excluded
Included
F
D290V-1
D290V-2
VCP R155H
A2/B1 KD
3690
2419
465
4414
703
4414
2729
166
3690
875
875
2976
33
503
703
3690
G
ENPP5
MAST4
SYNJ1
C6orf134
PDK2
SLC25A23
OGFOD2
PPARD
CHRNB4
UPF3A
C1QTNF3
WHSC1L1
SLC38A4
ASS1
ZNF542
SLC25A23
RBM5
BTBD3
VILL
C9orf102
PRAP1
APOO
TTLL9
ARHGEF2
FBXW7
DMKN
XRRA1
UGT8
TRRAP
MEI53
SFR56
PCGF2
AS Class
A2/B1 KD
D290V-1
D290V-2
VCP
+3
Column Z-Score
-3

(129 are alternative cassette events) out of 703 (171 are alternative cassettes) AS events were shared between both of the hnRNP A2/B1 mutant samples. This indicates a very strong and statistically significant ($p<10\text{-}25$) overlap between the splicing signatures of these two disease-causing variants (Figure 5F). However, each of the hnRNP A2/B1 D290V samples had about 1,000 alternative cassette events that were not in common with the VCP mutant samples, indicating potentially divergent molecular processes (Figure 5F). In contrast, hnRNP A2/B1 knockdown samples had only a small, statistically insignificant overlap in cassette events with hnRNP A2/B1 D290V or VCP R155H mutant samples ($p=0.21$ and $p=0.11$, respectively). To further investigate the difference between hnRNP A2/B1 depletion and the D290V mutation, we analyzed the 32 splicing events that were significantly different in all four comparisons tested. Interestingly, we observed that the direction of splicing changes in the three mutant samples was usually anti-correlated with the knockdown sample (Figure 5G). We conclude that disease-causing mutations in hnRNP A2/B1 result in thousands of splicing changes that are detectable in fibroblasts, the majority of which were not observed when hnRNP A2/B1 was depleted. Furthermore, we find a remarkable (66%) overlap in significant splicing changes in patient samples with mutations in the only two genes known to cause MSP (hnRNP A2/B1 and VCP).

1.9 Altered hnRNP A2/B1-dependent alternative splicing in human iPSC-MNs

To evaluate if RNA processing was altered in iPSC-MNs harboring hnRNP A2/B1 mutations, we generated iPSCs from the affected and non-affected fibroblasts above (Figure 5A, and Figure S5A). Normal ploidy was confirmed by array CGH (Figure S5A) and expression of pluripotency markers was confirmed by immunofluorescence in the iPSC lines (Figure S5B). PSCs were differentiated to motor neurons using a modified dual-SMAD inhibition protocol (Burkhardt et al., 2013; Chambers et al., 2009) (Fig. S6A). Differentiation was allowed to proceed for 53 days, at which point cells abundantly expressed pan-neuronal

Figure S5. Supplemental data related to the characterization of human iPSC and ESC lines used in Figures 6 and 7.

(A) Summary of PSCs used in Figures 6 and 7 and associated patient information where applicable.

(B) Immunofluorescence staining of selected iPSC lines demonstrating the expression of pluripotency markers.

A

Designation	Cell Type	Gender	Disease Status	Genotype	Karyotype
Ctrl. JCV	hiPSC	Male	Unaffected	WT	46 XY
H1	hESC	Male	N/A	WT	46 XY
H7	hESC	Fermale	N/A	WT	46 XX
H9	hESC	Fermale	N/A	WT	46 XX
VCP R155H-1.1	hiPSC	Male	MSP	VCP R155H	46 XY
VCP R155H-1.2	hiPSC	Male	MSP	VCP R155H	46 XY
A2B1 D290V-1	hiPSC	Fermale	MSP	hnRNP A2/B1 D290V	46 XX
A2B1 D290V-2	hiPSC	Fermale	MSP	hnRNP A2/B1 D290V	46 XX
A2B1 D290V-3	hiPSC	Male	MSP	hnRNP A2/B1 D290V	46 XY

B

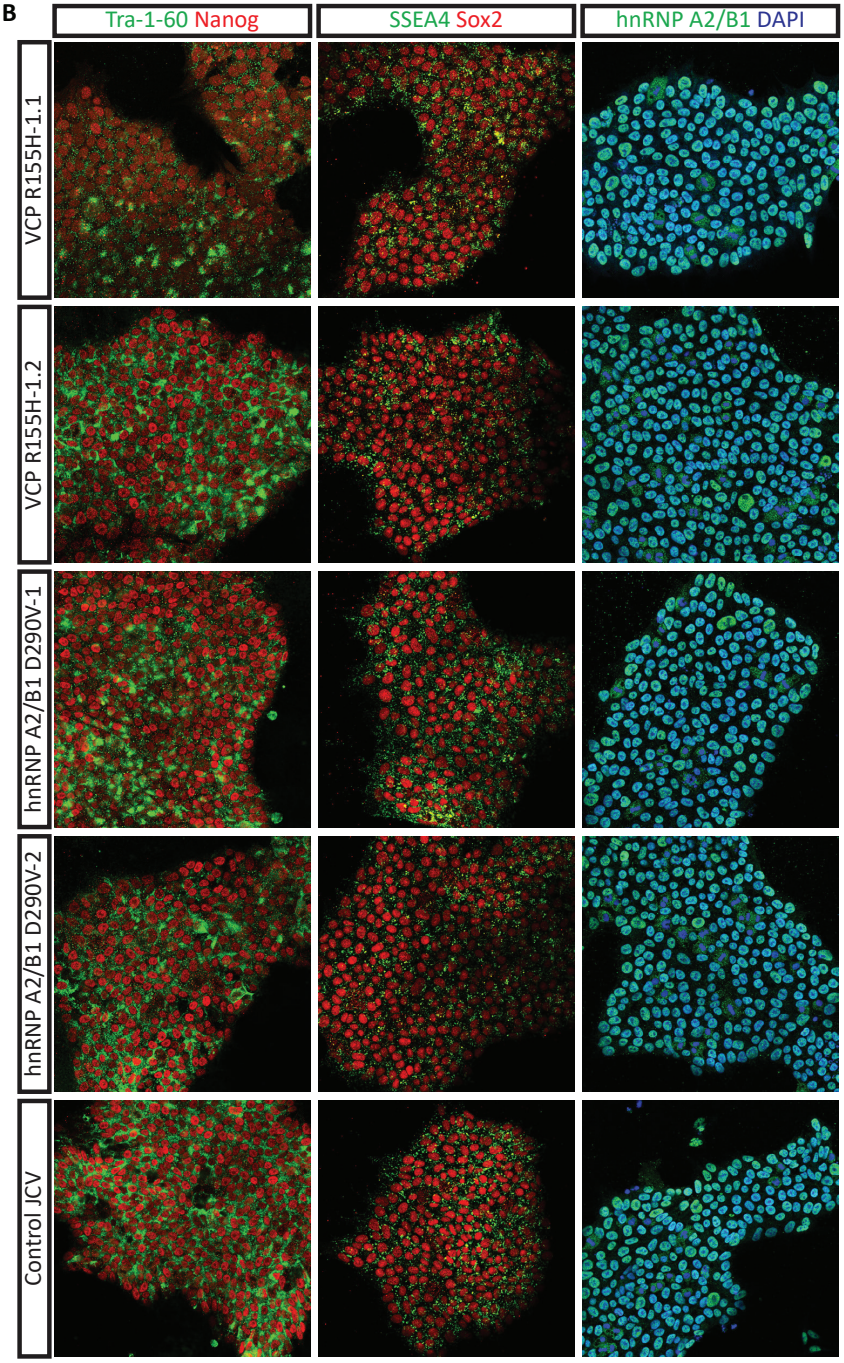

markers such as MAP2 and phosphorylated Neurofilament (SMI31). We also observed robust expression of the motor neuron-specific markers ISLET1, HB9 and cholinergic marker CHT1 (Figure S6B). Using multi-electrode arrays, we observed high frequency action potentials and synchronous firing (Figures S6C-S6G). These results demonstrate that we generated mature and active motor neuron networks.

To identify AS events affected by depletion of hnRNP A2/B1 in normal iPSC-MNs and to study if these events are similarly affected in the D290V mutant lines, iPSC-MNs differentiated from one non-affected and one D290V mutant iPSC line were incubated with non-targeting control (NTC) and hnRNP A2/B1 targeting ASOs (Figure 6A). HnRNP A2/B1 protein was successfully reduced in normal and D290V mutant human iPSC-MNs (Figure 6B) and RNA extracted from these cells was subjected to splicing-sensitive microarrays (Data S1K-S1M). To limit the confounding effects of genetic variation between samples, we conservatively limited our analysis to splicing events that were sensitive to hnRNP A2/B1 depletion. We first identified cassette exons sensitive to hnRNP A2/B1 depletion in normal iPSC-MNs. Next we identified cassette exons sensitive to hnRNP A2/B1 depletion in hnRNP A2/B1 D290V iPSC-MNs. We then compared the sets of alternative exons identified in each genotype. Splicing events that were altered only in the unaffected sample are characteristic of mutant-dependent loss-of-function. Splicing events altered only in the affected sample are characteristic of mutant-dependent gain-of-function. Splicing events that were changed in both samples are characteristic of events unaffected by the mutation status of hnRNP A2/B1. We found 67 differentially altered splicing events that were indicative of loss of normal hnRNP A2/B1 function, 512 events that were mutant-dependent gain-of-function and 223 mutant-dependent loss-of-function events (Figures 6C and 6D). Notably, nearly two-thirds of all splicing events are grouped into the mutant-dependent gain-of-function category, corroborating our findings in patient fibroblasts (Figure 5).

Figure 6. iPSC-MNs from patients with mutations in HNRNPA2B1 exhibit splicing defects.

(A) Schematic of experimental design. Fibroblasts expressing wildtype and hnRNP A2/B1 D290V were reprogrammed to iPSCs. iPSCs were differentiated to motor neurons. Motor neurons were treated with ASO against HNRNPA2B1 or non-targeting control (NTC). ASO treated and NTC treated RNA from both individuals was subjected to splicing sensitive microarray analysis.

(B) Depletion of hnRNP A2/B1 protein by ASO in motor neurons confirmed by Western blotting. Tubulin was the loading control. Tubulin (Tub.).

(C) Classification of 802 alternative cassette splicing changes into loss of function, gain of function, or normal function based on whether the event was detected in one genotype only, or both.

(D) Scatterplots comparing the sepscore (ASO vs. NTC) for WT HNRNPA2B1 vs. HNRNPA2B1 p.D290V. Dotted line is the least squares linear regression. The colors denote events detected in the WT sample only (blue), the mutant sample (green), or both samples (red). See the supplemental experimental procedures for a definition of sepscore.

(E) Western blotting for hnRNP A2/B1, hnRNP A1, hnRNP H1 and SRSF7 after ASO-mediated hnRNP A2/B1 depletion, or non-targeting control (NTC) ASO, in iPSC-MNs from an unaffected individual. Tubulin served as a loading control. Each lane represents a technical replicate of ASO treatment.

(F) Densitometry quantitation of the blot in (E) shows efficient depletion of hnRNP A2/B1, a small decrease in levels of hnRNP H1 and a modest increase in levels of SRSF7. Averages are plotted with error bars representing SEM. Three replicates per condition.

(G) Western blots of hnRNP A2/B1, hnRNP A1, hnRNP H1 and SRSF7 in iPSC-MNs from three unaffected and three affected individuals. Tubulin served as a loading control. Each lane contains lysate from a separate tissue culture well.

(H) Densitometry quantitation of the blot in (G). Dots represent band intensities normalized to tubulin loading control, color-coded according to the individual. Lines represent the median levels across all nine samples for each indicated protein. A two sample, two tailed, homoscedastic t-test was performed with n=9 to generate the relevant p values.

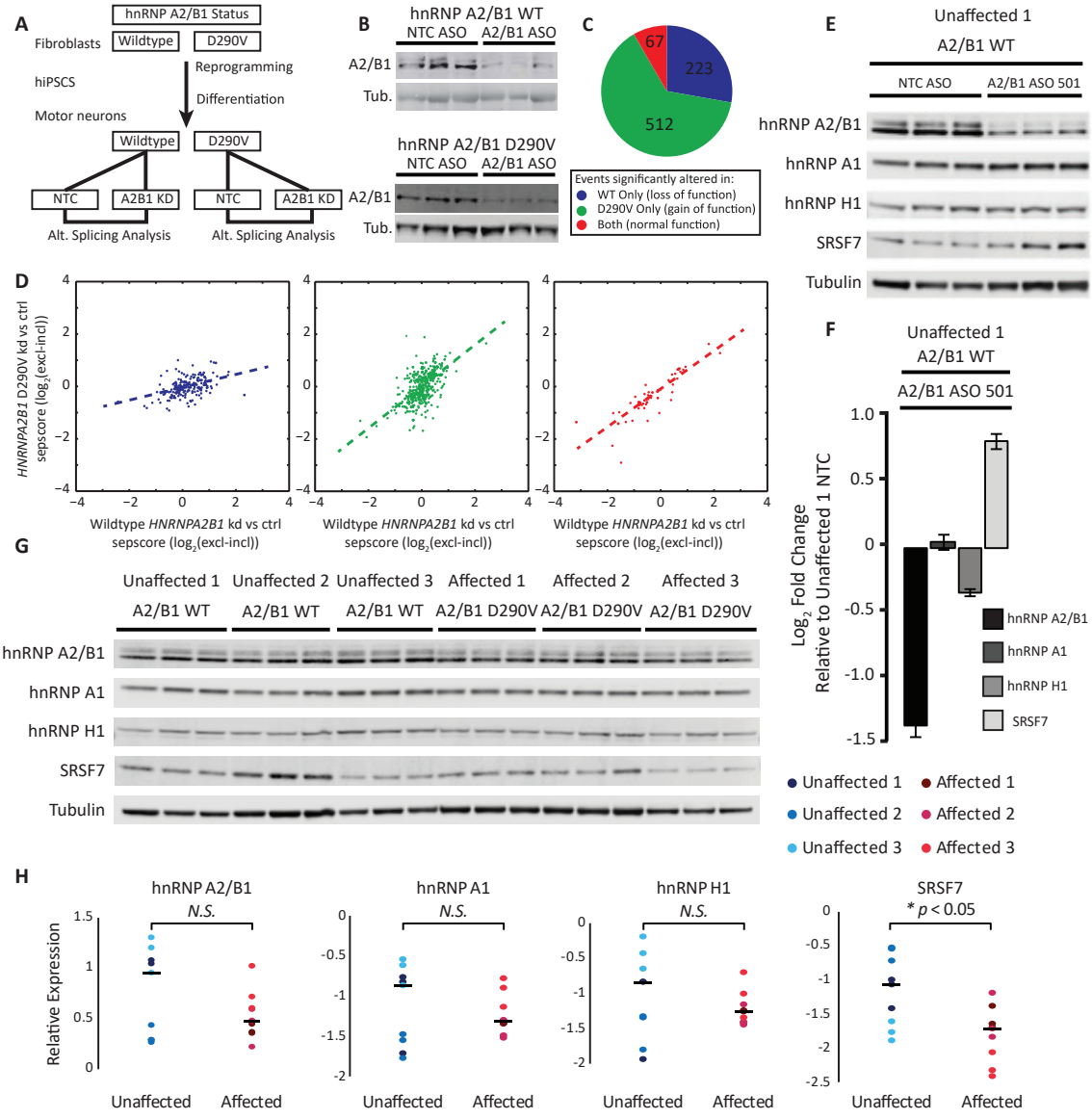
A
hnRNP A2/B1 Status
Fibroblasts
Wildtype
D290V
Reprogramming
hiPSCS
Differentiation
Motor neurons
Wildtype
D290V
NTC
A2B1 KD
NTC
A2B1 KD
Alt. Splicing Analysis
Alt. Splicing Analysis
B
hnRNP A2/B1 WT
NTC ASO
A2/B1 ASO
A2/B1
Tub.
hnRNP A2/B1 D290V
NTC ASO
A2/B1 ASO
A2/B1
Tub.
C
67
223
512
Events significantly altered in:
WT Only (loss of function)
D290V Only (gain of function)
Both (normal function)
E
Unaffected 1
A2/B1 WT
NTC ASO
A2/B1 ASO 501
hnRNP A2/B1
hnRNP A1
hnRNP H1
SRSF7
Tubulin
D
HNRNPA2B1 D290V kd vs ctrl sepscore (log2(excl-incl))
Wildtype HNRNPA2B1 kd vs ctrl sepscore (log2(excl-incl))
Wildtype HNRNPA2B1 kd vs ctrl sepscore (log2(excl-incl))
Wildtype HNRNPA2B1 kd vs ctrl sepscore (log2(excl-incl))
F
Unaffected 1
A2/B1 WT
A2/B1 ASO 501
Log2 Fold Change Relative to Unaffected 1 NTC
hnRNP A2/B1
hnRNP A1
hnRNP H1
SRSF7
G
Unaffected 1 A2/B1 WT
Unaffected 2 A2/B1 WT
Unaffected 3 A2/B1 WT
Affected 1 A2/B1 D290V
Affected 2 A2/B1 D290V
Affected 3 A2/B1 D290V
hnRNP A2/B1
hnRNP A1
hnRNP H1
SRSF7
Tubulin
Unaffected 1
Unaffected 2
Unaffected 3
Affected 1
Affected 2
Affected 3
H
hnRNP A2/B1
N.S.
hnRNP A1
N.S.
hnRNP H1
N.S.
SRSF7
* p < 0.05
Relative Expression
Unaffected
Affected
Unaffected
Affected
Unaffected
Affected
Unaffected
Affected

We hypothesize that hnRNP A2/B1 D290V mutant protein may be aggregating in the nucleus thus causing widespread splicing changes. Indeed, previous studies have reported nuclear TDP-43 aggregation in ALS patient samples and models of ALS (Burkhardt et al., 2013; Udan-Johns et al., 2014). We performed nuclear versus cytoplasmic separation followed by detergent soluble versus insoluble fractionation in PSC-MNs from unaffected and MSP patients. We observed increased levels of nuclear-insoluble hnRNP A2/B1 in samples from a VCP R155H patient and one of two hnRNP A2/B1 D290V patients (Figure S7A), suggesting that these mutant proteins are indeed more aggregation-prone than wildtype and may start to aggregate in the nucleus. This aggregation may also cause perturbations in expression of other RBPs. Thus, we measured the protein levels of SRSF7, as well as hnRNP A1 and hnRNP H1, shown previously to be subjected to cross-regulation by hnRNP A2/B1 (Huelga et al., 2012). In iPSC-MNs from one control individual, hnRNP A2/B1 depletion led to no change in hnRNP A1 or hnRNP H1 protein levels (Figures 6E and 6F). We did observe a significant increase in SRSF7 protein levels, consistent with our result observed in mouse spinal cord (Figure S2D). We next compared the protein levels of these four RNA binding proteins in PSC-MNs derived from three unaffected and three affected individuals. For hnRNP A2/B1, hnRNP A1, and hnRNP H1, we observed no consistent difference in protein levels between the two groups ($p > 0.05$), while SRSF7 levels were significantly lower in affected samples compared to unaffected samples ($p < 0.05$) (Figures 6G and 6H). Our findings indicate divergent regulation of SRSF7 at the protein level by mutant and wild-type hnRNP A2/B1. We conclude that alternative splicing is abnormal in iPSC-MNs from patient cells harboring MSP-causing mutations, potentially caused in part by increased nuclear insolubility of mutant hnRNP A2/B1.

Figure S6. Supplemental data related to the characterization of human PSC derived motor neurons used in Figures 6 and 7.

(A) A schematic of the differentiation and treatment of human PSC derived motor neurons. For stress granule experiments (Figure 7; Figure S7) cells were treated at day 28 and were not treated with aphidicolin. For ASO depletion experiments (Figure 6) cells were harvested at day 53 after aphidicolin treatment. For MEA experiments (Figure S6C-S6F), cells were recorded on the indicated day and were not treated with aphidicolin.

(B) Immunofluorescence staining of the indicated protein markers in iPSC-MNs derived from an unaffected individual. Cells were fixed at day 28 without aphidicolin treatment, and day 53 after aphidicolin treatment. Scale bare = 100 μm.

(C) Heat map of spontaneous electrophysiological activity on an multielectrode array (MEA) in four wells (64 electrodes per well) recorded at the indicated time points. MNs were derived from unaffected control hiPSCs.

(D) Six examples of spikes recorded by the MEA at the indicated time points.

(E) Raster plot of MEA activity across 64 electrodes (rows) in a single well over 30 seconds. Tick marks indicate single spikes. Blue ticks indicate bursting events closely spaced in time (5 spikes in less than 100 msec). Pink boxes denote spontaneous synchronous activity distributed over many electrodes (10 spikes in less than 100 msec).

(F–G) Quantification of firing rate (F) and mean number of bursts (G) over a 5 minute recording session in unaffected iPSC-MNs. Error bars are SEM calculated using four wells per condition.

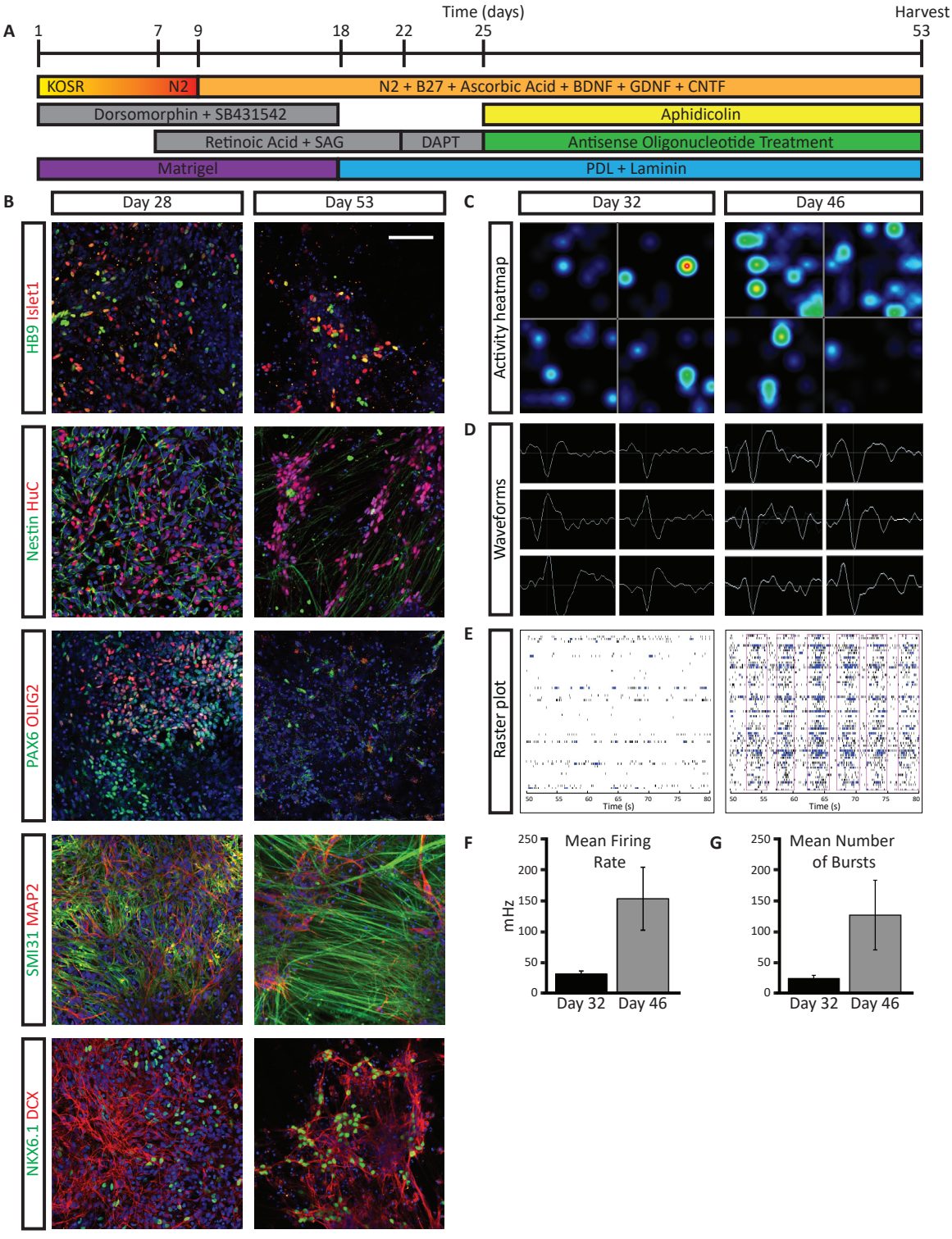
A
Time (days)
Harvest
1
7
9
18
22
25
53
KOSR
N2
N2 + B27 + Ascorbic Acid + BDNF + GDNF + CNTF
Dorsomorphin + SB431542
Aphidicolin
Retinoic Acid + SAG
DAPT
Antisense Oligonucleotide Treatment
Matrigel
PDL + Laminin
B
Day 28
Day 53
HB9 Islet1
Nestin HuC
PAX6 OLIG2
SMI31 MAP2
NKX6.1 DCX
C
Day 32
Day 46
Activity heatmap
D
Waveforms
E
Raster plot
Time (s)
F
Mean Firing Rate
mHz
Day 32
Day 46
G
Mean Number of Bursts
Day 32
Day 46

1.10 hnRNP A2/B1-mutant neurons display increased risk of death during long-term culture

We hypothesize that increased nuclear insolubility of hnRNP A2/B1 and abnormal RNA processing in mutant hnRNP A2/B1 MNs is likely to result in decreased survival over time. To recapitulate the progressive death of motor neurons, a defining characteristic of ALS, we tracked iPSC-MNs from affected and unaffected individuals longitudinally. iPSC-MNs were generated and transfected with a mApple reporter under the control of the synapsin promoter, a marker of neurons. mApple-positive cells were tracked over time using an automated microscope and analyzed for survival (Figure 7A) according to methods previously described (Skibinski and Finkbeiner, 2013). Interestingly, iPSC-MNs from two affected individuals had a significantly higher risk of death compared to two unrelated controls (Figures 7B and 7C). We conclude that our in vitro iPSC-MN model of hnRNP A2/B1 D290V proteinopathy exhibits progressive death.

1.11 hnRNP A2/B1-mutant iPSC-MNs exhibit excess hnRNP A2/B1 in stress granules

Another hallmark of ALS and other related proteinopathies is the accumulation of aggregates of mutant protein in the cytoplasm of affected cells (Mackenzie et al., 2007; Neumann et al., 2006; Van Deerlin et al., 2008). HnRNP A2/B1-positive aggregates were previously reported for patient muscle biopsy samples from individuals with hnRNP A2/B1 D290V mutations (Kim et al., 2013). However, this aggregation of hnRNP A2/B1 into RNA granules has not been observed in human neurons with endogenous expression of mutant RBPs. In unstressed PSC-MNs, we do not have biochemical evidence that there is more insoluble hnRNP A2/B1 in the cytoplasm (Figure 7D; Figures S7A-D). Indeed, by immunofluorescence, hnRNP A2/B1 was localized to the nucleus and dense cytoplasmic aggregates were not observed in either affected individuals or controls (Figures 7D 7E;

Figure 7. hnRNP A2/B1 D290V motor neurons exhibit increased risk of death and accumulate excess hnRNP A2/B1 in stress granules.

(A) Schematic of experimental design for long term imaging and survival analysis. iPSCs from affected and unaffected individuals were differentiated into MNs. MNs were transfected with Synapsin-mApple and plated in 96 well plates. Fluorescent cells were tracked over time using time lapse imaging. Survival of motor neurons was evaluated using Kaplan-Meier analysis

(B) Cumulative risk of death curves derived from Kaplan-Meier survival curves for iPSC-MNs differentiated from two affected (hnRNP A2/B1 D290V) and two unaffected individuals. Data was recorded over four days. Cells from both unaffected individuals are combined into a single line for analysis purposes.

(C) Summary of Cox proportional hazard analysis of survival data depicted in (B). Affected cells have a significantly higher hazard ratio compared to unaffected cells. A hazard ratio greater than 1.0 indicates increased risk of death as compared to the control lines from healthy individuals. See supplemental experimental procedures for a discussion of hazard ratio and p-value calculations.

(D) Immunofluorescence antibody staining of hnRNP A2/B1 and the stress granule marker G3BP1 in iPSC-MNs from an unaffected and an affected individual. iPSC-MNs from both individuals accumulate foci positive for G3BP1 when treated with puromycin, but not vehicle (PBS). iPSC-MNs derived from the affected individual also accumulate hnRNP A2/B1 in the foci. Scale bar = 10 μm.

(E) Quantification of images in (A). hnRNP A2/B1 positive granules per nucleus were counted. “n” refers to the number of individuals analyzed with each genotype. Error bars are SEM computed with the indicated sample size.

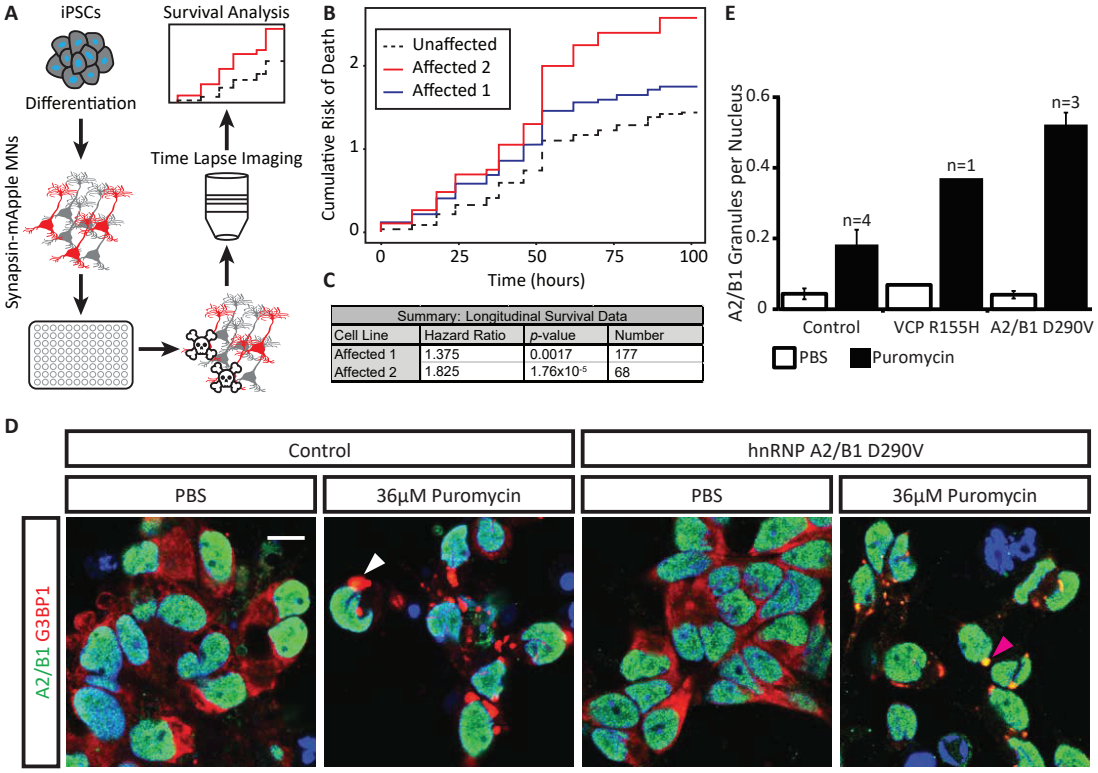
A
iPSCs
Differentiation
Synapsin-mApple MNs
Survival Analysis
Time Lapse Imaging
B
Unaffected
Affected 2
Affected 1
Cumulative Risk of Death
Time (hours)
C
Summary: Longitudinal Survival Data
Cell Line | Hazard Ratio | p-value | Number
Affected 1 | 1.375 | 0.0017 | 177
Affected 2 | 1.825 | 1.76x10-5 | 68
E
A2/B1 Granules per Nucleus
n=4
n=1
n=3
Control
VCP R155H
A2/B1 D290V
PBS
Puromycin
D
Control
hnRNP A2/B1 D290V
PBS
36μM Puromycin
PBS
36μM Puromycin
A2/B1 G3BP1

Figures S7B-D). To induce the formation of stress granules, we challenged PSC-MNs with puromycin (Kedersha et al., 2000; Liu-Yesucevitz et al., 2010). After 24 hours of puromycin treatment, PSC-MNs developed dense cytoplasmic aggregates positive for the stress granule markers G3BP1 (white arrows in Figure 7D), TIA1, PABP, and TDP43 (Figure S7B). In iPSC-MNs from patients with D290V mutations, these aggregates were positive for hnRNP A2/B1 (magenta arrows in Figure 7D; Figures S7B and S7C). In contrast, control samples rarely accumulated any cytoplasmic hnRNP A2/B1 even during puromycin treatment (Figures 7D and 7E). This result is consistent with previous data demonstrating increased aggregation and fibrillization of hnRNP A2/B1 D290V in in vitro biochemical experiments (Kim et al., 2013; Molliex et al., 2015). Interestingly, iPSC-MNs from a VCP R155H carrier also harbored an increase in hnRNP A2/B1-containing granules upon puromycin induction (Figure S7C). We conclude that iPSC-MNs from hnRNP A2/B1 D290V patients exhibit reproducible disease-relevant cellular attributes such as increased propensity for stress granule accumulation.

1.12 hnRNP A2/B1-mutant iPSC-MNs exhibit exacerbated gene expression and AS changes in response to stress

After observing robust and consistent accumulation of hnRNP A2/B1 in stress granules in cells carrying a D290V mutation, we wondered if the mutant genotype was also associated with unusual gene expression or splicing changes in response to chemical stress. We exposed PSC-MNs with various genotypes to puromycin treatment and measured the changes with splicing sensitive microarrays (Figure S8A; Data S1N and S1O). We used cells from three affected individuals carrying hnRNP A2/B1 D290V, one affected individual carrying VCP R155H, and three unaffected individuals with normal genotype. PSC-MNs were generated and treated with puromycin or saline for 24 hours in triplicate. We focused our splicing array analysis on stress related changes, employing an analysis strategy similar to

Figure S7. Supplemental data related to stress granule formation and nuclear aggregation in iPSC-MNs (Figure 7).

(A) Western blots showing results of nuclear / cytoplasmic (left / right) and detergent insoluble / soluble fractionation (top / bottom) in unaffected and MSP iPSC-MN. Histone H3 and β-Actin were used as nuclear and cytoplasmic loading controls, respectively. Quantification is shown for the hnRNP A2/B1 bands in the nuclear insoluble fraction. Quantification determined relative to the unaffected sample.

(B) Immunofluorescence staining for hnRNP A2/B1 (green) and PABP (red) (top row; see Figure S7C for unmerged channels), as well as the indicated additional stress granule markers (red) in iPSC-MNs from an unaffected individual and an hnRNP A2/B1 D290V patient (middle and bottom rows). The images of TIA1 staining in controls also serve as controls in Figure S7D. Scale bar = 10 μm. Magenta arrows indicate hnRNP A2/B1 localized to stress granules. White arrows indicate stress granules negative for hnRNP A2/B1 staining.

(C) Immunofluorescence staining for PABP and hnRNP A2/B1 in iPSC-MNs from an unaffected individual (control) and an hnRNP A2/B1 D290V patient, treated with puromycin or PBS (vehicle). Arrows indicate hnRNP A2/B1 located to stress granules. Scale bar = 10 μm.

(D) Immunofluorescence staining showing the localization of hnRNP A2/B1 (green) and TIA-1 (red) in control and VCP R155H iPSC-MNs. Nuclei are DAPI-stained (blue). Scale bar = 10 μm.

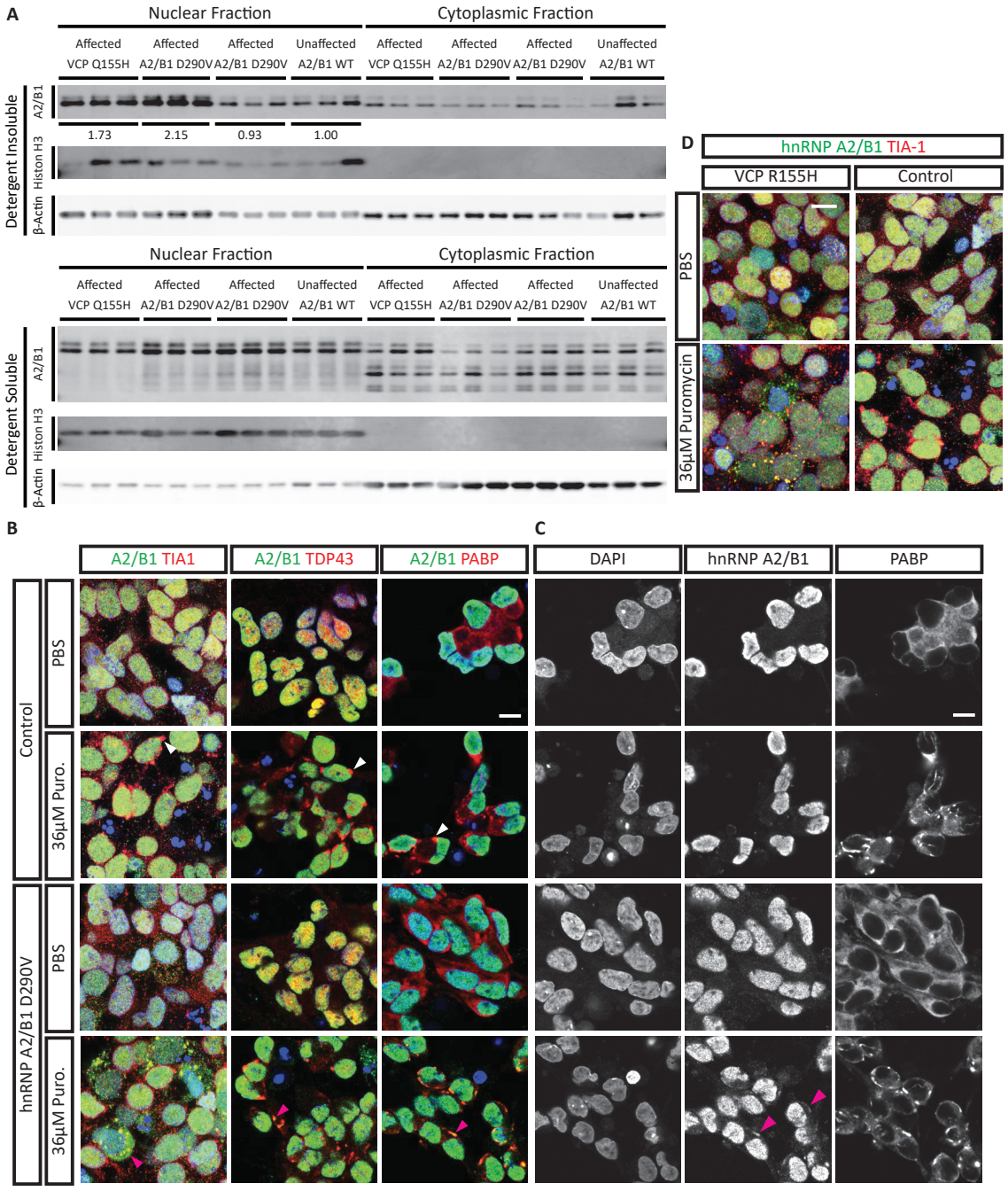
A
Nuclear Fraction
Cytoplasmic Fraction
Affected VCP Q155H
Affected A2/B1 D290V
Affected A2/B1 D290V
Unaffected A2/B1 WT
Detergent Insoluble
A2/B1
1.73
2.15
0.93
1.00
Histon H3
β-Actin
Detergent Soluble
D
hnRNP A2/B1 TIA-1
VCP R155H
Control
PBS
36μM Puromycin
B
A2/B1 TIA1
A2/B1 TDP43
A2/B1 PABP
C
DAPI
hnRNP A2/B1
PABP
Control
hnRNP A2/B1 D290V
36μM Puro.

that used in Figure 6. Significant expression or splicing changes were called for each of the seven pairs of treated and untreated samples. We then examined the resulting statistically significant changes to determine which changes were shared between all samples and which changes were associated with disease status. The majority of gene expression and AS changes upon stress were shared among all seven samples (Figures 8A and 8B). A large fraction of observed gene expression and splicing changes was observed only in affected samples (pink crescent in Figures 8A and 8B). A smaller fraction was observed only in control cells (green crescent in Figures 8A and 8B). Analysis of alternative cassette events showed a clear bias towards exon skipping upon stress in all sample types (Figure 8C). Hierarchical clustering of the raw intensity correlation from all arrays showed a clear delineation of stressed and unstressed samples (Figure S8B). As expected, we found significant upregulation of the Hsp70-like gene HSPA14, the chaperone DNAJC12 and early response genes JUN and FOS in all samples (Data S1N). We also observed significant AS changes in the transcription factor HSF2, the chaperones DNAJC12, DNAJB2, DNAJC120, DNAJC13, and DNAJC21 in all samples tested (Data S1O).

To understand stress-responsive, mutant-specific splicing and expression changes, we considered the 748 genes found to be changed in all samples. Hierarchical clustering using pairwise fold changes for these genes revealed two distinct clusters, one containing affected samples, and another containing the unaffected controls (Figure S8C). Clustering using pairwise AS differences for the 2333 shared splicing changes revealed a similar clustering pattern (Figure S8D). We next examined these shared changes to determine if there were systematic differences between affected and unaffected individuals. We constructed scatterplots of the shared expression and splicing changes, using the median fold change or AS difference, respectively, for each sample group. Regression analysis showed a highly significant slope value less than one (Figure 8D and 8E). This indicates a trend towards increased magnitude for expression and splicing changes in affected samples compared to

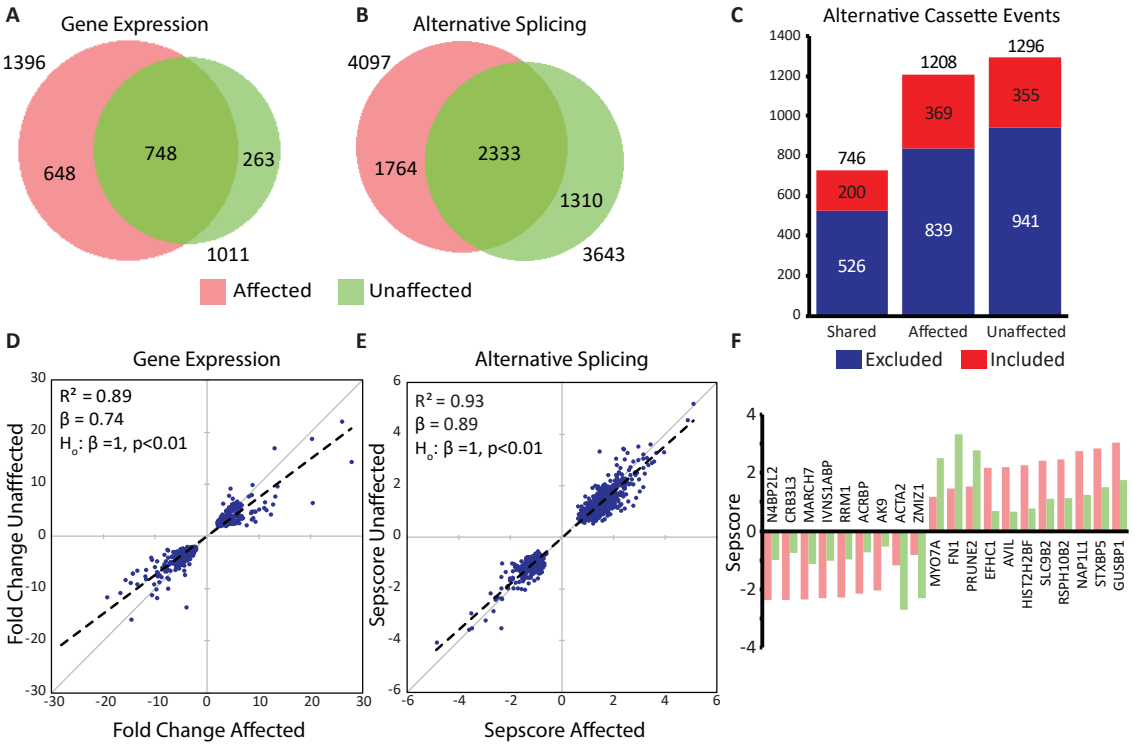

Figure 8. iPSC-MNs from affected patients display an exaggerated response to stress.

(A-B) Venn diagrams showing the overlap of stress-induced gene expression (A) and AS (B) changes between iPSC-MNs from four affected (pink) and three unaffected (green) individuals. For both analyses, a plurality of events is shared.

(C) For each group in (B), the type of alternative cassette exon events (excluded vs. included) were counted. Most stress-induced changes are exon-skipping in all groups.

(D-E) Scatterplots generated by calculating the median magnitude change from affected (X-axis) and unaffected (Y-axis) samples for each shared event shown in (A-B). Dashed lines represent the fit obtained by linear regression, with the coefficient of determination (R2) and slope (beta) indicated. A Student's t-test shows that the slopes are significantly different from unity ($p<0.01$) for both analyses, indicating that the magnitude of the stress-induced events are more pronounced in affected than in unaffected samples. See supplemental experimental procedures for a definition of sepscore.

(F) The 20 splicing changes with the largest difference in Sepscore between affected and unaffected samples are plotted along with the genes they are found in. While the direction (exclusion vs. inclusion) is the same regardless of disease status, for 15 of the 20 events the magnitudes of the stress-induced splicing changes were larger in affected samples than in unaffected samples.

controls upon stress. Plotting the top AS events ranked by their absolute difference between the affected and unaffected samples showed that for 15 of these 20 events, the median splicing change was larger in magnitude for affected samples than unaffected samples (Figure 8F).

In summary, we find that stress treatment induces both shared and disease-specific changes in gene expression and AS. Most changes are shared between all sample groups. Nevertheless, we find that the magnitudes of gene expression and splicing changes are consistently larger in affected samples compared to controls. Thus iPSC-MNs derived from patients with MSP exhibit an exacerbated stress response compared to controls.

Chapter 1 is a modified adaptation of the material as it appears in: Protein-RNA networks regulated by normal and ALS-associated mutant HNRNPA2B1 in the nervous system. Fernando J. Martinez, Gabriel A. Pratt, Eric Van Nostrand, Ron Batra, Stephanie C. Huelga, Katannya Kapeli, Mark Fang, Peter Freese, Seung J. Chun, Chelsea Gelboin-Burkhart, Layla Fijany, Harrison Wang, Hong-joo Kim, Rea Lardelli, Shibing Tang, Balaji Sundararaman, John P. Donohue, Jens Lykke-Andersen, Sheng Ding, Shuo-Chien Ling, Frank Bennett, Manuel Ares Jr., Christopher B. Burge, J. Paul Taylor, Frank Rigo, Gene W. Yeo. Neuron. 2016 Nov. The dissertation author was the primary investigator and author of this paper.

Figure S8. Supplemental data related to splicing and expression changes resulting from puromycin-induced stress in iPSC-MNs from hnRNP A2/B1 D290V patients and the VCP R155H patient (Figure 8).

(A) Schematic of the experimental design.

(B) Heat map of the correlation of the raw intensities of the 42 splicing-sensitive microarrays used in this experiment. Hierarchical clustering shows clear separation of puromycin- and vehicle (PBS)-treated samples.

(C-D) Heat maps of fold-changes in gene expression (C) and AS (SepScore; D) in those gene that are changed upon stress in all samples. Hierarchical clustering shows clear separation of affected and unaffected control samples. Color mapping is by Z-score computed for each row.

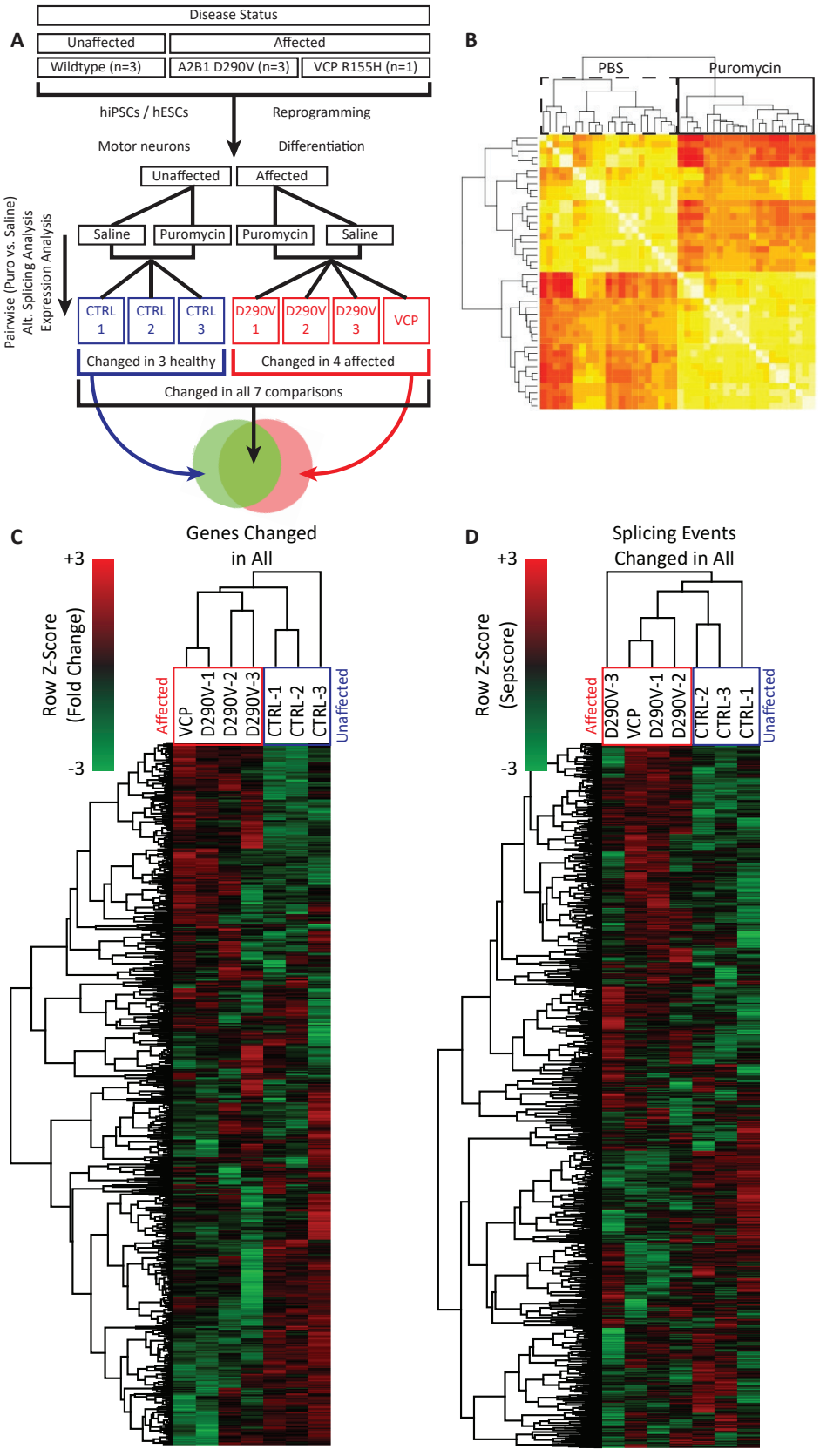
A
Disease Status
Unaffected
Affected
Wildtype (n=3)
A2B1 D290V (n=3)
VCP R155H (n=1)
hiPSCs / hESCs
Reprogramming
Motor neurons
Differentiation
Unaffected
Affected
Saline
Puromycin
Puromycin
Saline
Pairwise (Puro vs. Saline)
Alt. Splicing Analysis
Expression Analysis
CTRL 1
CTRL 2
CTRL 3
D290V 1
D290V 2
D290V 3
VCP
Changed in 3 healthy
Changed in 4 affected
Changed in all 7 comparisons
B
PBS
Puromycin
C
Genes Changed in All
+3
Row Z-Score (Fold Change)
-3
Affected
VCP
D290V-1
D290V-2
D290V-3
CTRL-1
CTRL-2
CTRL-3
Unaffected
D
Splicing Events Changed in All
+3
Row Z-Score (Sepscore)
-3
Affected
D290V-3
VCP
D290V-1
D290V-2
CTRL-2
CTRL-3
CTRL-1
Unaffected

CHAPTER 2: DISCUSSION

Our study provides the first transcriptome-wide analysis of hnRNP A2/B1 binding and function in the nervous system. We identified thousands of binding sites on hundreds of distinct transcripts in both mouse spinal cord and human PSC-MNs. Interestingly, the binding pattern of hnRNP A2/B1 in vivo adult nervous system is largely distinct from the binding modes observed for other ALS associated RNA binding proteins. FUS/TLS, TDP43 and TAF15 were previously found to bind mostly in intronic regions, especially within genes with exceptionally long introns. In the case of hnRNP A2/B1, we found intronic binding to be relatively infrequent (359 intronic binding sites in mouse). Instead, the majority of binding sites were found in 3'UTRs. While FUS and TDP43 (Lagier-Tourenne et al., 2012; Polymenidou et al., 2011; Rogelj et al., 2012; Tollervey et al., 2011) were each found to bind thousands of transcripts, hnRNP A2/B1 bound a much more modest number of genes. These qualitative differences in binding indicate distinct roles in RNA processing for hnRNP A2/B1 compared to FUS/TLS and TDP43 in vivo. Previous data has shown that FUS/TLS associates with PolII complexes and may be deposited in a co-transcriptional manner (Kwon et al., 2013; Schwartz et al., 2012). Similarly, TDP43 may be involved in transcriptional elongation and PolII pausing (Lalmansingh et al., 2011). However, the presence of hnRNP A2/B1 in 3'UTR regions and not "coating" introns indicates that hnRNP A2/B1 proteins are not deposited until the nascent mRNA is almost completely transcribed. These findings are consistent with our observation that very few genes (fewer than 30) exhibit significant expression changes after depletion of hnRNP A2/B1. When we examined microRNA levels, we also found a minimal effect on microRNA expression upon knockdown of hnRNP A2/B1.

When we compared AS changes induced by hnRNP A2/B1 depletion in vivo to hnRNP A2/B1 binding sites observed by iCLIP, we found that while the most significantly ranked splicing changes did harbor proximal binding sites, the vast majority of splicing changes did not. This is also in contrast to other ALS proteins (FUS/TLS, and TDP43), where binding sites are frequently observed proximal to AS events and depletion is associated with widespread gene expression changes (Lagier-Tourenne et al., 2012; Polymenidou et al., 2011; Rogelj et al., 2012; Tollervey et al., 2011). Aside from a strong intronic binding site downstream of an auto-regulated alternative exon in the 3'UTR of HNRNPA2B1, our data supports our conclusion that the majority of the splicing changes observed after depletion of hnRNP A2/B1 are not likely due to direct pre-mRNA binding of hnRNP A2/B1. Significant hnRNP A2/B1 association on the U2, U5 and U6 snRNAs suggests that hnRNP A2/B1 may play a role in spliceosome assembly or snRNA recycling and thereby affects AS without direct interaction with the affected transcripts. Another possible mechanism is indirect action through regulation of other splicing factors, such as SRSF7.

Aside from AS regulation we unexpectedly identified alternative polyadenylation events affected by loss of hnRNP A2/B1 in vivo. Importantly, half of these events exhibited hnRNP A2/B1 binding within the 3'UTRs. Two notable transcripts that encode splicing factors showed large differences in 3'UTR selection preference near hnRNP A2/B1 binding sites after depletion. These genes – RSRP1 and HNRNPH1 – could also be responsible for a large number of secondary splicing changes in other genes.

The most significant and robust splicing change observed after depletion of hnRNP A2/B1 in the mouse spinal cord is an exon within the gene encoding D-amino-acid-oxidase. Although low in abundance, D-amino acids are important receptor co-agonists in the CNS with disease implications (Paul and de Belleroche, 2014). D-serine is a known agonist for the NMDA receptor and has been implicated in schizophrenia and ALS (Burnet et al., 2008; Mitchell et al., 2010; Paul et al., 2014; Yang et al., 2013). Previous studies have

shown that D-serine metabolism is affected in the SOD1 transgenic mouse model of ALS (Thompson et al., 2012) and mutant mice that do not express DAO protein exhibit weakness, motor neuron loss, and other ALS-like symptoms (Lobsiger et al., 2007; Sasabe et al., 2012; Thompson et al., 2012). Recently, a large study of ALS patients found polymorphisms in the DAO gene to be associated with decreased survival (Cirulli et al., 2015). In our study, we observed exon skipping of an 118nt exon in the Dao transcript after depletion of hnRNP A2/B1. The resulting protein isoform is highly unstable and appears to be compromised in its enzymatic activity. We do not yet know if CNS tissue harboring hnRNP A2/B1 D290V mutations will recapitulate our findings involving D-amino acid metabolism in hnRNP A2/B1 depleted tissue.

Consistent with previous reports, we identified DAO expression only in astrocytes isolated from the adult cerebellum and spinal cord. We also demonstrated that AS is an evolutionarily conserved mode of regulation of DAO in human and mouse. Determining if D-serine metabolism is perturbed by mutations in hnRNP A2/B1 may require new transgenic mouse models or the analysis of post-mortem human tissue harboring HNRNPA2B1 mutations. We opine that this connection between AS and regulation of amino acid metabolism is relevant to neurodegeneration. Reduced levels of hnRNP A2/B1 have been associated with Alzheimer's disease and this depletion was specifically linked to loss of cholinergic neurons (Berson et al., 2012). Our unexpected findings link the levels of an RNA binding protein to a physiologically important enzyme.

Our data provides compelling hypotheses regarding how mutations in hnRNP A2/B1 may lead to neurodegeneration. We generated iPSC-MNs derived from patients with MSP mutations that feature reduced survival in long-term culture compared to controls, thereby recapitulating a defining characteristic of ALS i.e. progressive neuronal death. We also found a substantial number of differential splicing events in mutant cells that were not present after depletion. This indicates that at least by AS, the effects of hnRNP A2/B1

D290V mutations are not equivalent to a simple loss-of-function. Our observation is reminiscent of a recent study showing that an ALS-causing FUS mutation causes motor neuron degeneration in mice not by simple loss-of-function, but by a combination of loss and gain-of-function (Scekic-Zahirovic et al., 2016).

One possible mechanism underlying the abnormal splicing changes observed is suggested by an increase in the levels of nuclear, insoluble hnRNP A2/B1 protein in unstressed mutant motor neurons, compared to controls. This aberrant assembly of protein-RNA granules likely sequesters hnRNP A2/B1 protein, as well as other RBPs from their RNA substrates, leading to both loss and gain-of-function effects in RNA processing. As hnRNP A2/B1 also affects the levels of other RBPs, it is reasonable that the normal control of alternative splicing is impacted.

We expected that the propensity of hnRNP A2/B1 to form aggregates would also be reflected in an increase in insoluble hnRNP A2/B1 in the cytoplasm of unstressed motor neurons. However, chemical stress was required to induce hnRNP A2/B1 to move to cytoplasmic aggregates, called stress granules (Kim et al., 2013; Molliex et al., 2015; Xiang et al., 2015). Similar phenomena have been observed for other ALS RBPs including, TDP43, FUS/TLS, and EWSR1. It has been suggested that cytoplasmic aggregation of these proteins represents a loss-of-function and may be the cause of neurodegeneration in ALS (Iguchi et al., 2013; Sun et al., 2015; Wu et al., 2012; Yang et al., 2014). In light of our own data, we put forward an alternative interpretation. The RBPs mentioned above are also normally localized to the nucleus of cells. Although aggregation is typically described in the cytoplasm, nuclear aggregates of TDP43 have been reported (Burkhardt et al., 2013; Udan-Johns et al., 2014). In our view, cytoplasmic aggregation may represent an end stage symptom of dysfunction that begins in the nucleus. For instance, in the case of hnRNP A2/B1 D290V, we did not observe cytoplasmic aggregation until the cells had been severely stressed with puromycin for 24 hours.

Besides protein aggregation, we also found that cells derived from MSP patients respond abnormally to stress in other ways. Cells with hnRNP A2/B1 D290V mutations and VCP R155H mutations responded to stress with numerous changes in gene expression and AS. Some of these changes were unique to affected cells, however, most were also detected in controls. Surprisingly, when we examined these common changes we found that affected cells systematically responded with changes in the same genes but at greater magnitude than controls. In our view, we believe that hnRNP A2/B1 D290V mutant motor neurons respond to stress in largely the same way as controls, but their response is exacerbated. This may indicate that drugs that dampen the stress response or reduce the assembly of stress granules may be useful in treating ALS or other neurodegenerative diseases.

Chapter 2 is a modified adaptation of the material as it appears in: Protein-RNA networks regulated by normal and ALS-associated mutant HNRNPA2B1 in the nervous system. Fernando J. Martinez, Gabriel A. Pratt, Eric Van Nostrand, Ron Batra, Stephanie C. Huelga, Katannya Kapeli, Mark Fang, Peter Freese, Seung J. Chun, Chelsea Gelboin-Burkhart, Layla Fijany, Harrison Wang, Hong-joo Kim, Rea Lardelli, Shibing Tang, Balaji Sundararaman, John P. Donohue, Jens Lykke-Andersen, Sheng Ding, Shuo-Chien Ling, Frank Bennett, Manuel Ares Jr., Christopher B. Burge, J. Paul Taylor, Frank Rigo, Gene W. Yeo. Neuron. 2016 Nov. The dissertation author was the primary investigator and author of this paper.

CHAPTER 3: EXPERIMENTAL PROCEDURES

3.1 RNA Bind-n-Seq (RBNS)

3.1.1 RBNS experimental procedure

RBNS was performed as previously described (Lambert et al., 2014). Briefly, a truncated reading frame of HNRNPA2B1 (amino acids 1-197), which contains both RRMs, was cloned downstream of a tandem GST-SBP tag into a modified pGex6p-1 vector (GE). The truncated protein was recombinantly expressed, purified via the GST tag, and used for RBNS performed at 5 concentrations (5 nM, 20 nM, 80 nM, 320 nM, and 1300 nM) with a pool of randomized 20-mer RNAs flanked by short primers. Preparation of the randomized RNA pool and experimental conditions were described in (Lambert et al., 2014), with the modification that RBNS was performed at 4 degrees C rather than 37 degrees C.

3.1.2 RBNS Computational Analysis

Motif enrichment (R) values were calculated for 6-mers as the motif frequency in the RBP-selected pool over the frequency in the input RNA library. R values were considered significant if they had a Z-score ≥ 2 (mean and standard deviation calculated over all 6-mers). Values in Fig. 1D are for the protein concentration library with the highest overall enrichment (80 nM). For comparison with CLIP-seq data, RBNS enrichments were determined from the concentration with the largest enrichment. For enrichment in CLIP-seq 6-mers, FASTQ sequences were extracted from all clusters, and a matched number of random clusters from the same genomic region (5'-UTR, CDS, 3'-UTR, proximal introns, and distal introns. EMBOSS compseq was performed on the true and background set, and a delta between real and background k-mers was calculated with the equation:

$$\Delta\text{kmer} = \frac{\frac{f_{CLIP}}{N_{CLIP}} - \frac{f_{background}}{N_{background}}}{\sqrt{\left(\frac{1}{N_{CLIP}} + \frac{1}{N_{background}}\right) * g * (1-g)}}, \text{ for } g = \frac{f_{CLIP} + f_{background}}{N_{CLIP} + N_{background}}$$

where N is the number of times the motif occurs in the set and f is observed frequency of the motif. To plot enrichment, all 6-mers with the 4-mer of interest were highlighted and a KDE plot was created for all 6-mers. Statistical significance in differences between distributions was determined by the Kolmogorov–Smirnov 2-tailed test.

3.2 CLIP analysis of mouse and human samples

3.2.1 iCLIP experimental procedure

8-week old, female, C57/BL6J mice were obtained from Jackson Labs (Bar Harbor, ME). Mice were sacrificed and the spinal cords were removed, flash frozen in liquid nitrogen, and ground finely with a mortar and pestle. The frozen cords were UV crosslinked at λ=254nm with 400 mJ/cm2 of energy. iCLIP libraries were prepared as previously described (Huppertz et al., 2014) using rabbit polyclonal antibody GTX127928 (Genetex) (10 mg per sample) (Data S1P) (RRID: AB_2616069). Libraries were sequenced on the HISEQ 2500 platform in single end mode with a read length of 50 base pairs.

3.2.2 eCLIP experimental procedure

eCLIP was performed according to (Van Nostrand et al., 2016). Human iPSC-MNs were differentiated in culture for 28 days. Approximately 20 million cells were UV crosslinked at λ=254nm with 400 mJ/cm2 of energy. Crosslinked cell pellets were lysed and treated with RNAse I (Ambion). Lysate was immunoprecipitated using rabbit polyclonal antibody GTX127928 (Genetex) (10 μg per sample) and Dynabeads Protein G (Thermo Fisher Scientific). Immunoprecipitated samples were washed and dephosphorylated with Fast AP (Thermo Fisher Scientific) and T4 PNK (NEB). A 3' RNA adapter was ligated using

T4 RNA Ligase (NEB). Samples were run on PAGE gels and transferred to nitrocellulose membranes. A region of membrane spanning 75kDa above themolecular weight of hnRNP A2/B1 was cut and RNA was recovered using Proteinase K and phenol-chloroform. RNA was reverse transcribed using Affinityscript (Agilent Technologies) and treated with ExoSAP-IT (Affymetrix). A DNA adapter containing a 5nt randomer was then ligated to the 3' end (T4 RNA Ligase, NEB). Samples were purified using Dynabeads MyOne Silane (Thermo Fisher Scientific), quantified by qPCR, and then PCR amplified to the appropriate number of cycles. Amplified libraries were size selected with an agarose gel, quantified using the Agilent Tapestation, and sequenced on the Illumina HiSeq 2500 platform using paired end 50bp reads.

3.2.3 iCLIP computational analysis

Raw CLIP-seq reads were trimmed of polyA tails, adapters and low quality ends using Cutadapt with parameters:

--match-read-wildcards --times 2 -e 0 -O 5 --quality-cutoff' 6 -m 18 -b TCGTAT GCCGTCTTCTGCTTG -b ATCTCGTATGCCGTCTTCTGCTTG -b CGACAG GTTCAGAGTTCTACAGTCCGACGATC -b TGGAATTCTCGGGTGCCAAGG -b AAAAAAAAAAAAAAAAAAAAAAAAAAAAAAAAAAAAAAAAAAAAAA -b TTTTTTTTTTTTTTTTTTTTTTTTTTTTTTTTTTTTTTTTTTTTTT

Trimmed reads were mapped against a database of repetitive elements derived from RepBase (version 18.05) using Bowtie (version 1.0.0) with parameters (Langmead et al., 2009):

-S -q -p 16 -e 100 -l 20

Reads not mapped to repetitive elements were mapped to the mm9 mouse genome (UCSC assembly) using STAR (version 2.3.03) with parameters (Dobin et al., 2013):

--outSAMunmapped Within –outFilterMultimapNmax 1 –outFilterMultimap ScoreRange 1

Reads having the same 5' mapping position were collapsed to a single read to eliminate PCR duplication. CLIPseq peaks were identified as previously described (Zisoulis et al., 2010).

3.2.4 eCLIP computational analysis

Reads were demultiplexed using custom scripts and the randomer was appended to the read name. Reads were trimmed, filtered for repetitive elements, and mapped to human genome assembly hg19 as described in iCLIP computational analysis. PCR duplicated reads were removed based on the start positions of read1, read2, and the sequence of the randomer. eCLIP peaks were identified using CLIPPER with parameters (Lovci et al., 2013):

–s hg19 –o –bonferroni –superlocal --threshold-method binomial --save-pickle

Peak strength was then normalized against a size matched input by calculating fold enrichment of number of reads in IP versus number of reads in size matched input. Peaks were called significant if the number of reads in IP was greater than the number of reads in input and the peaks a Bonferroni corrected Fisher exact p-value of less than .05.

3.2.5 Distance away from motif

All significant peaks were used to compute distance of motifs away from peaks. Distance was calculated using the HOMER command:

annotatePeaks.pl <peaks> hg19 -m <motif file> -hist 20 -size 1000 -noann.

Peaks were then shuffled with the number of peaks binding in each region (5'UTR, 3'UTR, CDS, proximal and distal introns) in the transcriptome being preserved and a background distribution was computed.

3.2.6 De novo motif analysis

Motif analysis was performed using the findMotifs program in the HOMER software package with parameters (Lovci et al., 2013): -p 4 -rna -S 10 -len 5,6,7,8,9 (REF)
A background set was obtained using random clusters in the same genic regions as CLIPPER-identified hnRNP A2/B1 clusters.

3.3 Cell culture

All cell cultures were kept humidified at 37°C and 5% CO2.

3.3.1 Human fibroblasts

Human fibroblasts were grown on Poly-L-Lysine coated plates in DMEM (High Glucose) supplemented with 10% FBS, 1% NEAA, and 1% L-glutamine (Thermo Fisher Scientific). Cells were passaged using TrypLE select (Thermo Fisher Scientific). Cell line information is detailed in Data S1B.

3.3.2 Human iPSC generation

Human fibroblasts were reprogrammed using the CytoTune iPS Sendai Reprogramming kit, according to the manufacturer's instructions (Thermo Fisher Scientific). Nascent colonies were manually passaged onto Matrigel coated dishes (Becton Dickenson) for several passages and then expanded using Accutase (Innovative Cell Technologies). In some cases, previously generated iPSC lines from individual J. Craig Venter were used (Gore et al., 2011). Cell line information is detailed in Data S1B.

3.3.3 iPSC and ESC culture

All human pluripotent cells (PSCs) were grown on Matrigel coated dishes (Becton Dickenson), in mTesR1 media (Stem Cell Technologies) and passaged manually or with Accutase (Innovative Cell Technologies). During all passaging or thawing steps, the ROCK inhibitor Y27632 (Tocris) was used at a concentration of 10μM for 24 hours.

3.3.4 Differentiation of human motor neurons from PSCs

Human iPSCs and ESCs were differentiated according to a modified version of (Burkhardt et al., 2013; Chambers et al., 2009). Confluent dishes of feeder free PSCs were placed in hEB Media: Knockout D-MEM + 10% Knockout Serum Replacement (Thermo Fisher Scientific) + 10% Plasmanate (Biocare) + GLUTAMAX + NEAA (Thermo Fisher Scientific) and supplemented with 10 uM SB431542, 10 uM Dorsomorphin dihydrochloride, and 4 μM CHIR99021 (Tocris). SB431542 and Dorsomorphin were maintained in all cultures until day 18 of differentiation CHIR99021 was maintained until day 6 of differentiation. On days 4, 5 and 6 of differentiation, hEB media was mixed with N2 Base media: D-MEM/F12 + GLUTAMAX, 1% N-2 Supplement + 4.5 mM D-Glucose, 0.05 mM Ascorbic Acid (Sigma-Aldrich) at a ratio of 70:30, 50:50, and 50:50, respectively. On days 7 and 8 of differentiation, cells were maintained in a 50:50 combination of hEB media and Maturation Media: D-MEM/F12 + GLUTAMAX, 2% N-2 Supplement, 4% B-27 Serum-Free Supplement (Thermo Fisher Scientific), 9.0 mM D-Glucose, 0.1 mM Ascorbic Acid (Sigma-Aldrich) in addition to 2 ng/mL each of Ciliary Neurotrophic Factor (CNTF), Brain-Derived Neurotrophic Factor (BDNF), and Glial Cell-Derived Neurotrophic Factor (GDNF) (Peprotech). Beginning on day 7, the neurons were patterned with 200 nM Smoothened Agonist (EMD Biosciences) and 1.5uM Retinoic Acid (Sigma-Aldrich). These compounds were maintained until day 22. After 18 days of differentiation, cells were dissociated using Accutase,

and transferred to Poly-D-Lysine (Sigma-Aldrich) + Laminin (Thermo Fisher Scientific) coated dishes and maintained in Maturation Media with Retinoic Acid and Smoothened Agonist. On day 22, RA and SAG were withdrawn and the cells were maintained in Maturation Media containing 2 μM DAPT (Tocris) for a period of 3 days. After this time, cells were maintained in Maturation Media only. Throughout the protocol media was changed daily. We analyzed PSC-MNs for neuronal markers at two or more time points including 25 and 32 days after neural induction. Cells in PSC-MN cultures had processes that stained positive for axonal protein neurofilament and expressed lineage markers of motor neurons that innervate the limb: ISLET1 and HB9.

3.3.5 Multi-electrode array recordings

On day 18 of differentiation, PSC-MNs were dissociated into plates containing multi-electrode arrays (Axion Biosystems). PSC-MNs were matured according to our standard protocol until day 46. On day 32 and day 46 neurons were recorded for 5 minutes in standard media using Axion Biosystems Maestro amplifier.

3.3.6 FLP-In-293 (HEK293-FRT) stable cell line generation

FLP-In-293 cells were obtained from Thermo Fisher Scientific. Cells were grown on Poly-L-Lysine coated plates in DMEM (High Glucose) supplemented with 10% FBS, 1% NEAA, and 1% L-glutamine (Thermo Fisher Scientific). Cells were passaged using TrypLE select (Thermo Fisher Scientific). For stable cell line generation, $1x10^6$ cells were plated into each well of a 6 well plate. After 24 hours, wells were transfected with Lipofectamine 2000 and 3μg of pOG44 + 1μg of plasmid containing the gene of interest (pcdna5/FRT backbone). 48 hours after transfection, cells were split into 10cm dishes and supplemented with 100μg/ml hygromycin. Treatment with hygromycin continued until colonies appeared.

Drug resistant colonies were manually passaged and then expanded. Expression of the gene of interest was confirmed by western blotting.

3.3.7 U-251 MG cell culture and shRNA transfection

The U-251 MG human glioblastoma cell line was obtained as a gift from Frank Funari. Cells were grown in conditions identical to what is described above for fibroblasts. For shRNA mediated hnRNP A2/B1 depletion, U-251 cells were seeded at a density of 100,000 cells per well in 12 well plates. 24 hours after plating, cells were transfected with the pLKO.1 vector containing shRNA constructs targeting hnRNP A2/B1 or GFP (Sigma- Aldrich). Transfection was achieved using Lipofectamine 3000 (Thermo Fisher Scientific) in accordance with the manufacturer's instructions. 2μg of DNA and 3μL of reagent was used per well. Cells were harvested with Trizol (Thermo Fisher Scientific) 48 hours after transfection. hnRNP A2/B1 depletion was verified by western blotting. The sequences and catalog numbers for the shRNA constructs used are as follows. All shRNA constructs were acquired as glycerol stocks (Sigma-Aldrich).

shRNA 59 (CAT#: TRCN0000001059): CCGGCAGAAATACCATACCATCAATCTCGAGATTGATGGTATGGTATTTCTGTTTTT

shRNA 61 (CAT#: TRCN0000001061): CCGGTGACAACTATGGAGGAGGAAACTCGAGTTTCCTCCTCCATAGTTGTCATTTTT

shRNA 82 (CAT#: TRCN0000010582): CCGGAGAAGCTGTTTGTTGGCGGAACTCGAGTTCCGCCAACAAACAGCTTCTTTTTT

shRNA GFP: GCAAGCTGACCCTGAAGTTCAT3

3.4 Antisense oligonucleotide (ASO) based depletion of hnRNP A2/B1

3.4.1 Stereotactic injections of ASOs in mouse

8-week old, female, C57/BL6J mice were anesthetized with isoflurane. Saline containing 500 μg of antisense oligonucleotide targeting Hnrnpa2b1 was delivered by intracerebroventricular injection using a Hamilton syringe. Control animals were injected with saline alone or with an ASO that does not target any known region of the mouse genome. The sequences for the ASOs are as follows: $GT_oA_oC_oAacagcttcttA_oA_oC_oTC$ (Hnrnpa2b1), $CC_oT_oA_oTaggactatccA_oG_oG_oAA$ (Control). ASOs were mixed backbone "gapmers" where capitalized nucleotides contain 2'-O-(2-methoxy)ethyl modifications. The backbone was phosphorothioate DNA except for nucleotides flagged with $_o$ which were phosphodiester DNA. Mice were routinely monitored and sacrificed 28 days post injection. The spinal cords were harvested and flash frozen. RNA and protein were extracted using Trizol (Thermo Fisher Scientific) according to the manufacturer's instructions. Successful knockdown was validated by western blot using sc-32316 (RRID: AB_2279639), sc-53531 (RRID: AB_2248245) (Santa Cruz), or GTX127928 (GeneTex). All procedures were performed in accordance with a protocol approved by the Institutional Animal Care and Use Committee of Isis Pharmaceuticals and the University of California at San Diego.

3.4.2 ASO depletion of hnRNP A2/B1 in human fibroblasts

Patient fibroblasts from control and affected individuals were grown to confluence in triplicate wells. For knockdown experiments 20ng of ASO targeting HNRNPA2B1 or control ASO were transfected using Lipofectamine 2000, in accordance with the manufacturer's instructions (Thermo Fisher Scientific). The sequences for the ASOs are as follows: TTCACatgtcacctgAAACT (HNRNPA2B1-1), GCTTCttaactctacACACG (HNRNPA2B1-2), CTCAGTAACATTGACACCAC (Control). ASOs were phosphorothioate

"gapmers" where capitalized nucleotides contain 2'-O-(2-methoxy)ethyl modifications. Successful knockdown was verified by western blot and qRT-PCR.

3.4.3 ASO depletion of hnRNP A2/B1 in human PSC derived motor neurons

PSC-MNs were differentiated from control individuals and D290V patients as described above. After 25 days 5um ASO against hnRNP A2/B1 or non-targeting ASO (detailed above) was added to the media. For the first 5 days of ASO treatment, cells were also treated with 4μm aphidicolin (Sigma-Aldrich) to eliminate any remaining undifferentiated cells. The media and ASO was replaced every 5 days until 53 days post differentiation. RNA and protein were extracted using TRIzol (Thermo Fisher Scientific) according to the manufacturer's instructions. Successful knockdown was determined by western blotting.

3.5 Western blotting

Unless otherwise noted, protein samples were extracted and solubilized from TRIzol lysates according to the manufacturer's instructions (Thermo Fisher Scientific). Protein concentrations were measured using the Pierce BCA Protein Assay Kit (Thermo Fisher Scientific). For samples solubilized in urea containing buffer (Figure S7A) the Pierce 660nm Protein Assay was used instead (Thermo Fisher Scientific). Proteins were separated on Novex Bis-Tris 4-12% PAGE gels (Thermo Fisher Scientific) and transferred onto nitrocellulose or PVDF membranes. Membranes were blocked for one hour in the Odyssey Blocking Buffer (LiCor) and probed with the appropriate primary antibody (Data S1P). Detection was achieved using species specific LiCor IRDye secondary antibodies and an Odyssey infrared imaging system (LiCor).

3.6 Expression analysis by RNA-seq

3.6.1 Library preparation, sequencing, and analysis

RNA was extracted using TRIzol in accordance with the manufacturer's instructions. RNA quality was determined using the Agilent TapeStation according to the manufacturer's instructions. 1µg of total RNA was used to prepare each library. Library preparation was achieved using a TruSeq stranded total RNA with Ribozero Gold kit (Illumina RS-122-2301). Sequencing was performed on a HISEQ 2500 platform in single end mode with a read length of 100bp. Reads were trimmed to remove adapters and mapped to the genome using STAR with parameters identical to those used for iCLIP analysis. Counts were calculated with featureCounts (Liao et al., 2014) and RPKMs were then computed. Genes with RPKM values lower than 0.1 were not used. Differential expression was measured by calculating two sample T-statistics between ASO treated and control mice. P-values were calculated and then adjusted using a Benjamini-Hochberg FDR <0.01.

3.6.2 Small RNA Sequencing

Mouse spinal cords and human iPSC-MNs were generated and harvested as described in the corresponding sections. Samples were treated with ASOs targeting HNRNPA2B1 or non-target controls in biological triplicate. Libraries were generated using the Illumina TruSeq Small RNA Library Prep Kit using 500ng of total RNA. Libraries were sequenced on the Illumina MiSeq with 50 cycles.

3.6.3 miRNA expression analysis

First, 3' adapters were trimmed from sequencing reads using cutadapt. The data was then mapped to either the human or mouse (hg19 and mm10 respectively; University of California, Santa Cruz [UCSC] [http://genome.ucsc.edu]) genomes using Bowtie software

(version 1.1.1); the following parameters were used:

-k [valid alignments per read], 1; -m [number of possible alignments], 10; -l [seed length], 25; --best [optimal alignments]; --chunkmbs 128

featureCounts was used with the mirBase (http://mirbase.org/) miRNA annotations for human (v20; hg19) and mouse (v21; mm10). Differential miRNA expression was determined using the DESeq2 software (https://bioconductor.org/packages/release/bioc/html/DESeq2.html) (Data S1F and S1G).

3.6.4 Quantitative (qPCR) analysis

500 ng-1 µg of total RNA was reverse transcribed using Superscript III (Thermo Fisher Scientific) with random hexamer primers. cDNA was diluted 10-fold in water and quantified with Power SYBR Green Master Mix (Thermo Fisher Scientific). Detection was carried out on an iQ5 real-time PCR detection system (Bio-Rad). Biological samples were prepared in technical triplicate. Analysis was performed using iQ5 optical system software. Median cT values were calculated from each triplicate set. Genes of interest were normalized by appropriate reference genes (Data S1Q). Relative transcript levels were estimated using the 2-ΔcT method. Biological replicates were averaged to generate mean fold changes. Primer sequences were generated from Primer3 (Untergasser et al., 2012) software or obtained from Integrated DNA Technologies PrimeTime qPCR assays. Wherever possible, primers were designed such that the primer pair flanked an exon-exon junction. Sequences are detailed in Data S1Q.

3.7 Alternative splicing analysis by microarray

3.7.1 Splicing analysis in mouse spinal cord samples and human PSC derived motor neurons (Figure 8)

500 ng of total RNA was used to prepare each microarray sample. Mouse splicing junction mJay or HTA 2.0 (Affymetrix) arrays were prepared and hybridized by the UCSD VA hospital microarray facility according to the manufacturer's instructions. Data analysis was performed as previously described (Huelga et al., 2012). Significant and high quality events were selected using a q-value < 0.05 and an absolute sepscore > 0.5, where sepscore = log2[hnRNP A2/B1 depleted or puromycin stress (Skip/Include)/Control treated (Skip/Include)]. For each set of replicates, the log2 ratio of skipping to inclusion was calculated using robust least squares regression. Differential expression data was also calculated from array data as previously described. Significant events were selected for p-value < 0.05 and log2 fold change > 0.5.

3.7.2 Splicing analysis in human fibroblasts

Human splicing junction HJAY (Affymetrix) microarrays were prepared and hybridized by the UCSD VA hospital microarray facility according to the manufacturer's instructions in technical triplicates. Analysis of AS and differential expression was performed identically to mJay arrays described above. For D290V and VCP mutant patient fibroblast samples, sepscores and q-values were calculated relative to two different fibroblast samples from unaffected individuals. Sepscores and q-values were also calculated between the two control fibroblast samples used. High confidence differential splicing events were filtered by requiring samples to pass the sepscore and q-value cutoff relative to both control samples. Splicing events were further filtered by removing events that were flagged as differentially spliced between the two control samples used.

3.7.3 Splicing analysis in human PSC derived motor neurons (Figure 6)

500 μg of total RNA was used to perform microarray preparation and hybridization. Samples were hybridized in technical triplicates. RNA samples for microarray profiling were prepared using WT Expression Kit (Ambion), hybridized to Affymetrix HTA 2.0 microarrays, and imaged. Signal for all probes was RMA-normalized (Affymetrix Expression Console). Probes quantifying cassette exons (comprising exclusion junction, upstream and downstream inclusion junction, and inclusion exonic probes) were normalized against the average signal for the entire gene (to remove gene expression changes), and Student's t-Test was performed on residuals comparing control versus knockdown in WT and D290V mutant lines separately. Inclusion probes and exclusion probes were analyzed separately, with significant events defined as those with either inclusion or exclusion probe p-value ≤ 0.001. To reduce the confounding effects of genetic variation withing samples, we considered only AS events that were sensitive to hnRNP A2/B1 depletion. Loss of function events were those that were changed in WT samples only. Gain of function events were those that were changed in D290V mutant samples only. Normal function events were those that were changed in all samples.

3.7.4 RT-PCR analysis of splicing changes

1ug of total RNA was reverse transcribed using superscript III (Thermo Fisher Scientific) and random hexamer primers. For RT-PCR experiments, primers were designed in constitutive exons flanking the alternative exon of interest. Primer sequences are detailed in Data S1Q. cDNA was column purified (Qiagen) and quantified. 4 ng of cDNA was subjected to 35 cycles of PCR. The products were analyzed using the Agilent TapeStation. The peaks from the electropherogram were integrated and the normalized included fraction was calculated as:

[(included)/(included+skipped)]ASO/[(included)/(included+skipped)]control

In some cases, PCR products were run on agarose gels, gel extracted and Sanger sequenced to confirm the identity of the observed isoforms. Primer sequences were generated from Primer3 (Untergasser et al., 2012) software.

3.7.5 Alternative Polyadenylation

Alternative polyadenylation (APA) sites were identified from RNA-seq data using the bioinformatics algorithm DaPars (Xia et al., 2014), which uses a regression model to locate endpoints of alternative polyadenylation sites, was used to identify differences in APA events between hnRNP A2/B1 depleted samples and controls. To identify significant APA events, we used the following cutoffs:

FDR < 0.05, $|\Delta PDUI| \geq 0.2$, and $|dPDUI| \geq 0.2$.

APA scatter plots were generated using the R-Studio program with the ggplot2 library. Selected APA changes were validated using qPCR. The primer sequences are detailed in Data S1Q.

3.8 Northern blotting and RNA immunoprecipitation (RIP) northern blotting

For northern blots, RNA from ASO injected mouse spinal cord was used (see above for details). For RIP northern blots, 8 weeks old female C57/BL6J mice were sacrificed and the spinal cords extracted as above. Cords were flash frozen in liquid nitrogen and ground into a fine powder with a mortar and pestle. Ground spinal cords were lysed in lysis buffer (50 mM Tris-HCl, pH 7.4; 150 mM NaCl; 1% NP-40; 0.1% SDS; 0.5% sodium deoxycholate) supplemented with protease Inhibitor (Roche) and murine RNase inhibitor (New England Biolabs). Protein G Dynabeads (Thermo Fisher Scientific) were washed and conjugated with 10μg of antibody against hnRNP A2/ B1 (Genetex) (GTX127928) or normal rabbit

IgG (Thermo Fisher Scientific). Lysates were rotated overnight with conjugated beads at 4°C. The supernatant was removed and beads were washed 8 times with wash buffer (10mM Tris-HCl, pH 7.5; 150 mM NaCl; 0.1% Triton-X 100). The bound RNA was extracted from the beads with Trizol (Thermo Fisher Scientific), quantified and mixed with TBE-Urea (8M) loading buffer. In subsequent steps, RIP northern and standard northern samples were treated identically. RNA was separated by electrophoresis on 9% 19:1 polyacrylamide, 0.6x TBE, 8M Urea at 20 mA/gel for 2 hrs. Gels were transferred in 0.5x TBE to nylon membrane at 25V for 16 hours. Membranes were UV crosslinked, blocked with Ultrahyb Oligo (Life Technologies), and hybridized with 5' end-radiolabeled DNA oligos (see Data S1Q).

3.9 Measurements of alternative isoforms of Dao

3.9.1 RT-PCR of human DAO transcript

Healthy and sporadic ALS (sALS) RNA samples were obtained from the motor cortex of deceased individuals (Courtesy J. Ravits). Astrocyte RNA from cortex, spinal cord, and cerebellum was purchased from Sciencell Research Laboratory. RNA from total brain, total spinal cord, and total cerebellum was purchased from Agilent Technologies. Samples were reverse transcribed and subject to PCR as above. The PCR products were gel extracted and Sanger sequenced with the same primers used to generate the products (Data S1Q).

3.9.2 Constructs

Open reading frames for the mouse Dao long and short isoforms were determined from the UCSC genome browser. A 3xFLAG tag was appended to the 3' end of the sequence. Constructs containing the tagged ORFs were synthesized by Genscript. The 3xFLAG tagged ORFs were cut out with restriction enzymes and subcloned into the multiple cloning site of the pcDNA5/FRT vector. See Data S2A and S2B for sequences.

3.9.3 Tertiary structure prediction

Predicted amino acid sequences for DAO long and short isoforms were obtained from UCSC genome browser.

The sequences were submitted to:

Phyre2 (http://www.sbg.bio.ic.ac.uk/phyre2/) and

SWISS-MODEL (http://swissmodel.expasy.org/interactive.

DAO Isoform 1 (Long Isoform):

MRVAVIGAGVIGLSTALCIHERYHPTQPLHMKIYADRFTPFTTSDVAAGLWQPYLS-
DPSNPQEAEWSQQTFDYLLSCLHSPNAEKMGLALISGYNLFRDEVPDPFWKNAVL-
GFRKLTPSEMDLFPDYGYGWFNTSLLLEGKSYLPWLTERLTERGVKLIHRKVESLE-
EVARGVDVIINCTGVWAGALQADASLQPGRGQIIQVEAPWIKHFILTHDPSLGI-
YNSPYIIPGSKTVTLGGIFQLGNWSGLNSVRDHNTIWKSCCKLEPTLKNARIVGELT-
GFRPVRPQVRLEREWLHFGSSSAEVIHNYGHGGYGLTIHWGCAMEAANLFGK-
ILEEKKLSRLPPSHLDYKDHDGDYKDHDIDYKDDDD

DAO Isoform 2 (Short Isoform):

MRVAVIGAGVIGLSTALCIHERYHPTQPLHMKIYADRFTPFTTSDVAAGLWQPYLS-
DPSNPQEAEWSQQTFDYLLSCLHSPNAEKMGLALISGYNLFRDEVPDPFWKNAVL-
GFRKLTPSEMDLFPDYGYGWFNTSLLLEGKSYLPWLTERLTERGVKLIHRKVESLE-
EVARGVDVIINCTGVWAGALQADASLQPGRGQIIQVEAPWIKHFILTHDPSLGI-
YNSPYIIPGMQELWVNSLASGQSGLRSGDYKDHDGDYKDHDIDYKDDDDK

3.9.4 Proteasome assay

Stable cell lines expressing either the long or short isoform of DAO or control cells expressing no transgene, were plated at 2.5x105 cells/well in a 6-well plate. 72 hours after plating, cells were treated with 4 μM Mg132 proteasome inhibitor (Sigma-Aldrich) for 0, 1, 2, 4, 10, and 24 hours. Cells were harvested in RIPA buffer (50 mM Tris-HCl pH. 7.4, 150 mM NaCl, 0.1% SDS, 0.5% Sodium deoxycholate, 1% NP-40, 1x protease inhibitor (Roche)), incubated at 4°C on a shaker for 30 min, and shredded with a QIAShredder (Qiagen). Harvested cells were stored at -20°C until western blotting.

3.9.5 Cell based activity assay

FLP-In-293 cells expressing either DAO Isoform 1 (long) or DAO Isoform 2 (short) or control cells expressing no transgene were plated at 100,000 cells/well in a 96-well plate overnight. Clones were plated in technical triplicate. The Amplex Red kit (Amplex Red Hydrogen Peroxide/Peroxidase Assay Kit, cat. A-22188, Molecular Probes/Invitrogen) was used to measure H2O2 released into the medium during the oxidation of DAO. Prior to the start of the assay, the media in each well was replaced with 100 μL of HANKS buffer solution (Invitrogen/GIBCO) with 20 mM HEPES for 5-10 min. In the wells containing control cells, H2O2 was added to final concentrations of 0 μM, 1.25 μM, 2.5 μM, 5 μM, 7.5 μM, 10 μM, 15 μM, and 20 μM to create a standard curve. The media in each well was then mixed with 25 μL of a 5x mixture of either assay buffer (50 mM D-Serine, 0.125 units HRP, 50 μM Amplex Red stock solution in HANKS with 20 mM HEPES) or control buffer (assay buffer without D-Serine) and incubated at 37°C for 30 min. The fluorescence signal was measured on an Infinite 200PRO (Tecan) with excitation at 544 nm and emission at 590 nm at 30 min, 60 min, 100 min, and 200 min after the addition of assay or control buffer.

3.9.6 Cell-free activity assay

3XFLAG tagged versions of the long and short isoforms of the mouse Dao protein were expressed in rabbit reticulocyte lysates using the TNT Quick Coupled Reticulocyte Lysate kit (Promega). In a 50-µL reaction, 1 µL of pcDNA5/FRT_mDAO_FLAG (1000 ng/µL) DNA was incubated with 1 µL methionine (1 mM), 41 µL of reticulocyte lysate, and 9 µL water at 30°C for 60 min. Translation product was flash-frozen in dry ice and methanol and then immediately dissolved in 2.5 mM FAD in HANKS buffer (HBSS, calcium, magnesium, no phenol red; Thermo Fisher Scientific) + 10.5 mM HEPES at 4°C for 30 min. The final 100-µL reaction contained the following components: 1 µL reticulocyte lysate (mDAO1_FLAG, mDAO2_FLAG, or T7 Luciferase Control), 4 µM Amplex Red (Thermo Fisher Scientific), 0.6 µL DMSO, 0.1 U/mL HRP (Thermo Fisher Scientific), 50 mM D-serine (Sigma-Aldrich), 500 nM FAD (Sigma-Aldrich), and H2O2 standards, all in HANKS buffer + 10.5 mM HEPES. The H2O2 standards were incubated in a dark room with Amplex Red and HRP in HANKS buffer prior to plating. Resorufin, caused by the oxidation of Amplex Red during mDAO-catalyzed turnover of D-serine, was measured on an Infinite 200PRO (Tecan) during 4-hour kinetic run (5 min time points with agitation) with excitation and emission wavelengths of 563 and 594 nm respectively. The H2O2 concentration was calculated using linear regression on the fluorescence.

3.10 Stress granule assays

3.10.1 Treatment of cells

Motor neurons from control and affected individuals were differentiated and matured as described above. On day 18 the cells were re-plated into glass bottom chamber slides or glass bottom 96 well plates. On day 28 cells were treated with 36 µM puromycin or saline for 24 hours. After 24 hours the cells were fixed and processed for immunofluores-

cence as described below.

3.10.2 Immunofluorescence and imaging

Cells were fixed for 15 minutes in 4% PFA then washed 3 times with PBS + 0.01% Triton-X. Cells were permeablized with PBS+0.1% Triton-X for 45 minutes then blocked for 1 hour in PBS+0.01% Triton-X + 5% normal goat serum. Primary antibodies were incubated overnight at 4°C in PBS+0.01% Triton-X + 5% normal goat serum according to dilutions listed in Data S1P. After incubation the primary antibody was removed and the cells were washed 5 times for 10 minutes in PBS+0.01% Triton-X. Alexa fluor conjugated secondary antibodies were then incubated for 90 minutes at room temperature in PBS+0.01% Triton-X + 5% normal at a dilution of 1:1000 (Thermo Fisher Scientific). Next cells were washed 5 times for 10 minutes in PBS+0.01% Triton-X with the fourth wash containing 10 mg/mL DAPI. Images were acquired on a Zeiss 780 inverted laser scanning confocal microscope using a 20X Plan Apo air objective (Zeiss) or a 63X Plan Apo oil immersion objective (Zeiss). Primary antibodies used are detailed in Data S1P.

3.10.3 Image analysis

Four images were taken for each condition in Figure 7 and Figure S7. In Figures 7D and Figures S7B, images were blinded and then nuclei and G3BP1 and hnRNP A2/B1 foci were counted manually. Bar graphs are expressed as foci / nucleus.

3.10.4 Nuclear / cytoplasmic and Detergent soluble / insoluble fractionation

Nuclear and cytoplasmic fractions were extracted according to (Rio et al., 2010). Cells were rinsed in cold PBS and detached by gentle scraping. Cells were pelleted and resuspended in hypotonic lysis buffer (20 mM Tris HCl pH7.5, 10 mM KCl, 1.5 mM MgCl,

5 mM EGTA, 1 mM EDTA, 1 mM DTT, Protease Inhibitor Cocktail III (EMD Millipore)). The suspension was homogenized with 10 strokes of a dounce homogenizer. The nuclei were pelleted by centrifugation at 1200g and the cytoplasmic fraction was cleared of nuclei and debris by further spins at 1200g. The supernatant containing the cytoplasmic fraction was solubilized by adding 1% NP-40, 0.5 % Na-Deoxycholate, and 0.1% SDS. The nuclei were resuspended in a sucrose buffer (0.32 M sucrose, 3 mM CaCl2, 2 mM MgOAc, 0.1 mM EDTA, 10 mM Tris HCl pH 8, 1 mM DTT, 0.5% NP-40, Protease Inhibitor Cocktail III) and homogenized with 3 strokes of a dounce homogenizer. The nuclear suspension was layered on top of a 2.0 M sucrose cushion (2 M sucrose, 5 mM MgOAc, 0.1 mM EDTA, 10 mM Tris pH 8, 1 mM DTT, Protease Inhibitor Cocktail III) and centrifuged at 20,000g for one hour. Pelleted nuclei were solubilized in RIPA buffer (50 mM Tris HCl pH7.4, 1% NP-40, 0.5% Na-deoxycholate, 0.1% SDS, 150 mM NaCl, 2 mM EDTA, 50 mM NaF, Protease Inhibitor Cocktail III). Cytoplasmic and nuclear fractions solubilized in RIPA were treated with Turbo DNAse (Thermo-Fisher) for 1 hour at 37°C and then sonicated in the Bioruptor (Diagenode) for 10 minutes on high power. The detergent insoluble material was pelleted by centrifugation at 20,000g for one hour and the supernatant was removed (soluble fraction). The detergent insoluble pellets were solubilized in buffer containing (7 M urea, 2 M thiourea, 4% CHAPS, 30 mM Tris HCl pH 8.5, Protease Inhibitor Cocktail III) and sonicated in the Bioruptor (Diagenode) for 10 minutes on high power. All fractions were filtered using a 0.22 μM cellulose acetate spin filter (Costar). Western blotting was performed as above. Antibodies against histone H3 and β-Actin were used to verify the nuclear and cytoplasmic fractions, respectively. See data S1P.

3.11 Long Term Imaging Experiments

3.11.1 Differentiation and Cell Culture

iPSC lines from two ALS patients with hnRNP A2/B1 D290V mutations and two healthy individuals (Miyaoka et al., 2014) were confirmed for normal karyotype. The iPSCs were differentiated into motor neurons using a dual SMAD inhibition protocol as previously described (Burkhardt et al., 2013; Chambers et al., 2009) with modifications from Du et al 2015 (Du et al., 2015). Briefly, the iPSCs were neuralized in IMDM/F12 medium (Thermo Fisher) with SMAD inhibitors: 0.2 μM LDN-193189 (Stemgent) and 10 μM SB431542 (Stemgent). Cultures were split 1:2 after 1 week in medium containing 0.1 μM RA, (Sigma-Aldrich) and 1 μM SAG (Fisher Scientific) and 3 μM CHIR99021, 0.2 μM LDN193189 and 10 μM SB431542. After 1 more week, the cultures were banked frozen in Synthafreeze (Thermo Fisher). All cell lines were then thawed simultaneously to synchronize neuron maturation for imaging experiments. The MN cultures were fed with medium containing Compound E (0.1 μM, Fisher), 2.5 μM DAPT (Fisher), 0.1 μM db-cAMP (Sigma-Aldrich), 200 ng/mL ascorbic acid (Sigma- Aldrich), 10 ng/mL each BDNF and GDNF (Fisher Scientific), together with 0.5 μM all-trans RA and 0.1 μM SAG for an additional 6 days. MN cultures were trypisizined and plated into 96-well plates, lipofected with a plasmid expressing the red fluorescent protein mApple under the neuronal specific promoter Synapsin.

3.11.2 Imaging and analysis.

The iPSC-neurons were imaged starting 2 days after transfection, once every six hours on a custom-built robotic microscopy system comprised of a Nikon T2i widefield fluorescence microscope and 888 Andor camera, and kept in a robotic incubator (Liconic). Individual neurons were tracked using custom algorithms and neuronal survival was analyzed in time-lapse images. Kaplan-Meier survival analysis was used to measure survival

of individual neurons over time. Cumulative risk of death curves were derived from the Kaplan Meier survival curves. Cox proportional hazard analysis was used to measure cumulative hazard ratio of iPSC-MNs from ALS patients compared with healthy individuals and derive P values as previously described (Skibinski and Finkbeiner, 2013).

Chapter 3 is a modified adaptation of the material as it appears in: Protein-RNA networks regulated by normal and ALS-associated mutant HNRNPA2B1 in the nervous system. Fernando J. Martinez, Gabriel A. Pratt, Eric Van Nostrand, Ron Batra, Stephanie C. Huelga, Katannya Kapeli, Mark Fang, Peter Freese, Seung J. Chun, Chelsea Gelboin-Burkhart, Layla Fijany, Harrison Wang, Hong-joo Kim, Rea Lardelli, Shibing Tang, Balaji Sundararaman, John P. Donohue, Jens Lykke-Andersen, Sheng Ding, Shuo-Chien Ling, Frank Bennett, Manuel Ares Jr., Christopher B. Burge, J. Paul Taylor, Frank Rigo, Gene W. Yeo. Neuron. 2016 Nov. The dissertation author was the primary investigator and author of this paper.

APPENDIX

Data S2. Sequences for 3xFLAG tagged Dao open reading frames related to Figure 4 and Figure S4 and supplemental experimental procedures.

(A) mDao_Long_3xFLAG:

GGTACCGCCACCATGCGCGTGGCCGTGATCGGAGCAGGAGTCATTGGGCTCTC-
CACAGCCCTCTGCATTCATGAGCGTTACCACCCAACACAGCCACTGCACAT-
GAAGATCTATGCAGATCGATTCACCCCGTTCACCACGAGCGATGTGGCCGCCG-
GCCTCTGGCAGCCTTATCTCTCTGACCCCAGCAACCCTCAGGAGGCGGAGT-
GGAGCCAGCAAACGTTTGATTACCTGCTGAGCTGCCTCCATTCTCCAAAC-
GCTGAAAAAATGGGCCTGGCCCTAATCTCAGGCTACAACCTCTTCCGAGAT-
GAAGTTCCGGACCCTTTCTGGAAAAACGCAGTTCTGGGATTCCGGAAGCT-
GACCCCCAGTGAGATGGACCTGTTCCCTGATTATGGCTACGGCTGGTTCAATA-
CAAGCCTCCTTCTAGAGGGGAAGAGCTACCTGCCATGGCTAACTGAGAGGTTA-
ACTGAGAGGGGAGTGAAGCTTATCCATCGGAAGGTGGAGTCTCTCGAAGAG-
GTGGCAAGAGGAGTGGATGTGATTATCAACTGCACCGGGGTGTGGGCCGGG-
GCCCTGCAAGCAGATGCCTCCCTGCAGCCAGGCCGGGGCCAGATCATCCAG-
GTGGAGGCCCCTTGGATTAAACACTTCATCCTCACCCATGATCCTAGCCTTG-
GTATCTACAACTCTCCGTACATCATCCCAGGTTCCAAGACAGTTACGCTCGG-
GGGTATATTCCAGCTGGGGAACTGGAGCGGGTTAAACAGCGTCCGTGACCA-
CAATACCATTTGGAAGAGCTGCTGTAAACTGGAGCCCACCCTGAAGAATG-
CAAGAATTGTGGGTGAACTCACTGGCTTCCGGCCAGTCCGGCCTCAGGTCCG-
GCTAGAAAGAGAATGGCTTCATTTTGGATCTTCAAGTGCAGAGGTCATCCA-
CAACTATGGTCATGGAGGTTACGGGCTCACAATCCACTGGGGTTGTGCAAT-
GGAGGCGGCCAACCTCTTCGGGAAAATTCTAGAGGAAAAGAAGTTGTCCAG-
GTTGCCTCCCTCCCACCTCGACTACAAAGACCATGACGGTGATTATAAAGAT-
CATGACATCGATTACAAGGATGACGATGACAAGTGAGCGGCCGC

(B) mDao_Short_3xFLAG:

GGTACCGCCACCATGCGCGTGGCCGTGATCGGAGCAGGAGTCATTGGGCTCTC-
CACAGCCCTCTGCATTCATGAGCGTTACCACCCAACACAGCCACTGCACAT-
GAAGATCTATGCAGATCGATTCACCCCGTTCACCACGAGCGATGTGGCCGCCG-
GCCTCTGGCAGCCTTATCTCTCTGACCCCAGCAACCCTCAGGAGGCGGAGT-
GGAGCCAGCAAACGTTTGATTACCTGCTGAGCTGCCTCCATTCTCCAAAC-
GCTGAAAAAATGGGCCTGGCCCTAATCTCAGGCTACAACCTCTTCCGAGAT-
GAAGTTCCGGACCCTTTCTGGAAAAACGCAGTTCTGGGATTCCGGAAGCT-
GACCCCCAGTGAGATGGACCTGTTCCCTGATTATGGCTACGGCTGGTTCAATA-
CAAGCCTCCTTCTAGAGGGGAAGAGCTACCTGCCATGGCTAACTGAGAGGTTA-
ACTGAGAGGGGAGTGAAGCTTATCCATCGGAAGGTGGAGTCTCTCGAAGAG-
GTGGCAAGAGGAGTGGATGTGATTATCAACTGCACCGGGGTGTGGGCCGGG-

GCCCTGCAAGCAGATGCCTCCCTGCAGCCAGGCCGGGGCCAGATCATCCAG-
GTGGAGGCCCCTTGGATTAAACACTTCATCCTCACCCATGATCCTAGCCTTG-
GTATCTACAACTCTCCGTACATCATCCCAGGTTCCAAGACAGTTACGCTCGG-
GGGTATATTCCAGCTGGGGAACTGGAGCGGGTTAAACAGCGTCCGTGACCA-
CAATACCATTTGGAAGAGCTGCTGTAAACTGGAGCCCACCCTGAAGAATG-
CAAGAATTGTGGGTGAACTCACTGGCTTCCGGCCAGTCCGGCCTCAGGTCCG-
GCTAGAAAGAGAATGGCTTCATTTTGGATCTTCAAGTGCAGAGGTCATCCA-
CAACTATGGTCATGGAGGTTACGGGCTCACAATCCACTGGGGTTGTGCAAT-
GGAGGCGGCCAACCTCTTCGGGAAAATTCTAGAGGAAAAGAAGTTGTCCAG-
GTTGCCTCCCTCCCACCTCGACTACAAAGACCATGACGGTGATTATAAAGAT-
CATGACATCGATTACAAGGATGACGATGACAAGTGAGCGGCCGC

REFERENCES

Ainger, K., Avossa, D., Diana, A.S., Barry, C., Barbarese, E., and Carson, J.H. (1997). Transport and Localization Elements in Myelin Basic Protein mRNA. The Journal of Cell Biology 138, 1077-1087.

Alarcon, C.R., Goodarzi, H., Lee, H., Liu, X., Tavazoie, S., and Tavazoie, S.F. (2015). HNRNPA2B1 Is a Mediator of m(6)A-Dependent Nuclear RNA Processing Events. Cell 162, 1299-1308.

Belzil, V.V., Gendron, T.F., and Petrucelli, L. (2013). RNA-mediated toxicity in neurodegenerative disease. Molecular and Cellular Neurosciences 56, 406-419.

Berson, A., Barbash, S., Shaltiel, G., Goll, Y., Hanin, G., Greenberg, D.S., Ketzef, M., Becker, A.J., Friedman, A., and Soreq, H. (2012). Cholinergic-associated loss of hnRNP-A/B in Alzheimer's disease impairs cortical splicing and cognitive function in mice. EMBO Molecular Medicine 4, 730-742.

Burkhardt, M.F., Martinez, F.J., Wright, S., Ramos, C., Volfson, D., Mason, M., Garnes, J., Dang, V., Lievers, J., Shoukat-Mumtaz, U., Martinez, R., Gai, H., Blake, R., Vaisberg, E., Grskovic, M., Johnson, C., Irion, S., Bright, J., Cooper, B., Nguyen, L., Griswold-Prenner, I., and Javaherian, A. (2013). A cellular model for sporadic ALS using patient-derived induced pluripotent stem cells. Molecular and Cellular Neurosciences 56, 355-364.

Burnet, P.W., Eastwood, S.L., Bristow, G.C., Godlewska, B.R., Sikka, P., Walker, M., and Harrison, P.J. (2008). D-amino acid oxidase activity and expression are increased in schizophrenia. Molecular Psychiatry 13, 658-660.

Chambers, S.M., Fasano, C.A., Papapetrou, E.P., Tomishima, M., Sadelain, M., and Studer, L. (2009). Highly efficient neural conversion of human ES and iPS cells by dual inhibition of SMAD signaling. Nature Biotechnology 27, 275-280.

Cirulli, E.T., Lasseigne, B.N., Petrovski, S., Sapp, P.C., Dion, P.A., Leblond, C.S., Couthouis, J., Lu, Y.F., Wang, Q., Krueger, B.J., Ren, Z., Keebler, J., Han, Y., Levy, S.E., Boone, B.E., Wimbish, J.R., Waite, L.L., Jones, A.L., Carulli, J.P., Day-Williams, A.G., Staropoli, J.F., Xin, W.W., Chesi, A., Raphael, A.R., McKenna-Yasek, D., Cady, J., Vianney de Jong, J.M., Kenna, K.P., Smith, B.N., Topp, S., Miller, J., Gkazi, A., Al-Chalabi, A., van den Berg, L.H., Veldink, J., Silani, V., Ticozzi, N., Shaw, C.E., Baloh, R.H., Appel, S., Simpson, E., Lagier-Tourenne, C., Pulst, S.M., Gibson, S., Trojanowski, J.Q., Elman, L., McCluskey, L., Grossman, M., Shneider, N.A., Chung, W.K., Ravits, J.M., Glass, J.D., Sims, K.B., Van Deerlin, V.M., Maniatis, T., Hayes, S.D., Ordureau, A., Swarup, S., Landers, J., Baas, F., Allen, A.S., Bedlack, R.S., Harper, J.W., Gitler, A.D., Rouleau, G.A., Brown, R., Harms, M.B., Cooper, G.M., Harris, T., Myers, R.M., and Goldstein, D.B. (2015). Exome sequencing in amyotrophic lateral sclerosis identifies risk genes and pathways. Science 347, 1436-1441.

Clower, C.V., Chatterjee, D., Wang, Z., Cantley, L.C., Vander Heiden, M.G., and Krainer, A.R. (2010). The alternative splicing repressors hnRNP A1/A2 and PTB influence pyruvate kinase isoform expression and cell metabolism. Proceedings of the National Academy of Sciences of the United States of America 107, 1894-1899.

Couthouis, J., Hart, M.P., Shorter, J., DeJesus-Hernandez, M., Erion, R., Oristano, R., Liu, A.X., Ramos, D., Jethava, N., Hosangadi, D., Epstein, J., Chiang, A., Diaz, Z., Nakaya, T., Ibrahim, F., Kim, H.J., Solski, J.A., Williams, K.L., Mojsilovic-Petrovic, J., Ingre, C., Boylan, K., Graff-Radford, N.R., Dickson, D.W., Clay-Falcone, D., Elman, L., McCluskey, L., Greene, R., Kalb, R.G., Lee, V.M., Trojanowski, J.Q., Ludolph, A., Robberecht, W., Andersen, P.M., Nicholson, G.A., Blair, I.P., King, O.D., Bonini, N.M., Van Deerlin, V., Rademakers, R., Mourelatos, Z., and Gitler, A.D. (2011). A yeast functional screen predicts new candidate ALS disease genes. Proceedings of the National Academy of Sciences of the United States of America 108, 20881-20890.

Dobin, A., Davis, C.A., Schlesinger, F., Drenkow, J., Zaleski, C., Jha, S., Batut, P., Chaisson, M., and Gingeras, T.R. (2013). STAR: ultrafast universal RNA-seq aligner. Bioinformatics (Oxford, England) 29, 15-21.

Du, Z.W., Chen, H., Liu, H., Lu, J., Qian, K., Huang, C.L., Zhong, X., Fan, F., and Zhang, S.C. (2015). Generation and expansion of highly pure motor neuron progenitors from human pluripotent stem cells. Nature Communications 6, 6626.

Fahling, M., Mrowka, R., Steege, A., Martinka, P., Persson, P.B., and Thiele, B.J. (2006). Heterogeneous nuclear ribonucleoprotein-A2/B1 modulate collagen prolyl 4-hydroxylase, alpha (I) mRNA stability. The Journal of Biological Chemistry 281, 9279-9286.

Gallo, J.M., Jin, P., Thornton, C.A., Lin, H., Robertson, J., D'Souza, I., and Schlaepfer, W.W. (2005). The role of RNA and RNA processing in neurodegeneration. The Journal of neuroscience : The Official Journal of the Society for Neuroscience 25, 10372-10375.

Gao, Y., Tatavarty, V., Korza, G., Levin, M.K., and Carson, J.H. (2008). Multiplexed dendritic targeting of alpha calcium calmodulin-dependent protein kinase II, neurogranin, and activity-regulated cytoskeleton-associated protein RNAs by the A2 pathway. Molecular Biology of the Cell 19, 2311-2327.

Goodarzi, H., Najafabadi, H.S., Oikonomou, P., Greco, T.M., Fish, L., Salavati, R., Cristea, I.M., and Tavazoie, S. (2012). Systematic discovery of structural elements governing stability of mammalian messenger RNAs. Nature 485, 264-268.

Heinz, S., Benner, C., Spann, N., Bertolino, E., Lin, Y.C., Laslo, P., Cheng, J.X., Murre, C., Singh, H., and Glass, C.K. (2010). Simple combinations of lineage-determining transcription factors prime cis-regulatory elements required for macrophage and B cell identities. Molecular Cell 38, 576-589.

Horiike, K., Tojo, H., Arai, R., Nozaki, M., and Maeda, T. (1994). D-amino-acid oxidase is confined to the lower brain stem and cerebellum in rat brain: regional differentiation of astrocytes. Brain Research 652, 297-303.

Huelga, S.C., Vu, A.Q., Arnold, J.D., Liang, T.Y., Liu, P.P., Yan, B.Y., Donohue, J.P., Shiue, L., Hoon, S., Brenner, S., Ares, M., Jr., and Yeo, G.W. (2012). Integrative genome-wide analysis reveals cooperative regulation of alternative splicing by hnRNP proteins. Cell Reports 1, 167-178.

Huppertz, I., Attig, J., D'Ambrogio, A., Easton, L.E., Sibley, C.R., Sugimoto, Y., Tajnik, M., Konig, J., and Ule, J. (2014). iCLIP: protein-RNA interactions at nucleotide resolution. Methods 65, 274-287.

Hutchison, S., LeBel, C., Blanchette, M., and Chabot, B. (2002). Distinct sets of adjacent heterogeneous nuclear ribonucleoprotein (hnRNP) A1/A2 binding sites control 5' splice site selection in the hnRNP A1 mRNA precursor. The Journal of Biological Chemistry 277, 29745-29752.

Iguchi, Y., Katsuno, M., Niwa, J., Takagi, S., Ishigaki, S., Ikenaka, K., Kawai, K., Watanabe, H., Yamanaka, K., Takahashi, R., Misawa, H., Sasaki, S., Tanaka, F., and Sobue, G. (2013). Loss of TDP-43 causes age-dependent progressive motor neuron degeneration. Brain 136, 1371-1382.

Johnson, J.O., Mandrioli, J., Benatar, M., Abramzon, Y., Van Deerlin, V.M., Trojanowski, J.Q., Gibbs, J.R., Brunetti, M., Gronka, S., Wuu, J., Ding, J., McCluskey, L., Martinez-Lage, M., Falcone, D., Hernandez, D.G., Arepalli, S., Chong, S., Schymick, J.C., Rothstein, J., Landi, F., Wang, Y.D., Calvo, A., Mora, G., Sabatelli, M., Monsurro, M.R., Battistini, S., Salvi, F., Spataro, R., Sola, P., Borghero, G., Consortium, I., Galassi, G., Scholz, S.W., Taylor, J.P., Restagno, G., Chio, A., and Traynor, B.J. (2010). Exome sequencing reveals VCP mutations as a cause of familial ALS. Neuron 68, 857-864.

Kabashi, E., Valdmanis, P.N., Dion, P., Spiegelman, D., McConkey, B.J., Vande Velde, C., Bouchard, J.P., Lacomblez, L., Pochigaeva, K., Salachas, F., Pradat, P.F., Camu, W., Meininger, V., Dupre, N., and Rouleau, G.A. (2008). TARDBP mutations in individuals with sporadic and familial amyotrophic lateral sclerosis. Nature Genetics 40, 572-574.

Kapeli, K., Pratt, G.A., Vu, A.Q., Hutt, K.R., Martinez, F.J., Sundararaman, B., Batra, R., Freese, P., Lambert, N.J., Huelga, S.C., Chun, S.J., Liang, T.Y., Chang, J., Donohue, J.P., Shiue, L., Zhang, J., Zhu, H., Cambi, F., Kasarskis, E., Hoon, S., Ares, M., Jr., Burge, C.B., Ravits, J., Rigo, F., and Yeo, G.W. (2016). Distinct and shared functions of ALS-associated proteins TDP-43, FUS and TAF15 revealed by multisystem analyses. Nature Communications 7, 12143.

Kedersha, N., Cho, M.R., Li, W., Yacono, P.W., Chen, S., Gilks, N., Golan, D.E., and Anderson, P. (2000). Dynamic shuttling of TIA-1 accompanies the recruitment of mRNA to mammalian stress granules. The Journal of Cell Biology 151, 1257-1268.

Kim, H.J., Kim, N.C., Wang, Y.D., Scarborough, E.A., Moore, J., Diaz, Z., MacLea, K.S., Freibaum, B., Li, S., Molliex, A., Kanagaraj, A.P., Carter, R., Boylan, K.B., Wojtas, A.M., Rademakers, R., Pinkus, J.L., Greenberg, S.A., Trojanowski, J.Q., Traynor, B.J., Smith, B.N., Topp, S., Gkazi, A.S., Miller, J., Shaw, C.E., Kottlors, M., Kirschner, J., Pestronk, A., Li, Y.R., Ford, A.F., Gitler, A.D., Benatar, M., King, O.D., Kimonis, V.E., Ross, E.D., Weihl, C.C., Shorter, J., and Taylor, J.P. (2013). Mutations in prion-like domains in hnRNPA2B1 and hnRNPA1 cause multisystem proteinopathy and ALS. Nature 495, 467-473.

Kosturko, L.D., Maggipinto, M.J., Korza, G., Lee, J.W., Carson, J.H., and Barbarese, E. (2006). Heterogeneous nuclear ribonucleoprotein (hnRNP) E1 binds to hnRNP A2 and inhibits translation of A2 response element mRNAs. Molecular Biology of the Cell 17, 3521-3533.

Kosuge, Y., Sekikawa-Nishida, K., Negi, H., Ishige, K., and Ito, Y. (2009). Characterization of chronic glutamate-mediated motor neuron toxicity in organotypic spinal cord culture prepared from ALS model mice. Neuroscience Letters 454, 165-169.

Kwon, I., Kato, M., Xiang, S., Wu, L., Theodoropoulos, P., Mirzaei, H., Han, T., Xie, S., Corden, J.L., and McKnight, S.L. (2013). Phosphorylation-regulated binding of RNA polymerase II to fibrous polymers of low-complexity domains. Cell 155, 1049-1060.

Lagier-Tourenne, C., Polymenidou, M., and Cleveland, D.W. (2010). TDP-43 and FUS/TLS: emerging roles in RNA processing and neurodegeneration. Human Molecular Genetics 19, R46-64.

Lagier-Tourenne, C., Polymenidou, M., Hutt, K.R., Vu, A.Q., Baughn, M., Huelga, S.C., Clutario, K.M., Ling, S.C., Liang, T.Y., Mazur, C., Wancewicz, E., Kim, A.S., Watt, A., Freier, S., Hicks, G.G., Donohue, J.P., Shiue, L., Bennett, C.F., Ravits, J., Cleveland, D.W., and Yeo, G.W. (2012). Divergent roles of ALS-linked proteins FUS/TLS and TDP-43 intersect in processing long pre-mRNAs. Nature Neuroscience 15, 1488-1497.

Lalmansingh, A.S., Urekar, C.J., and Reddi, P.P. (2011). TDP-43 is a transcriptional repressor: the testis-specific mouse acrv1 gene is a TDP-43 target in vivo. The Journal of Biological Chemistry 286, 10970-10982.

Lambert, N., Robertson, A., Jangi, M., McGeary, S., Sharp, P.A., and Burge, C.B. (2014). RNA Bind-n-Seq: quantitative assessment of the sequence and structural binding specificity of RNA binding proteins. Molecular Cell 54, 887-900.

Langmead, B., Trapnell, C., Pop, M., and Salzberg, S.L. (2009). Ultrafast and memory-efficient alignment of short DNA sequences to the human genome. Genome Biology 10, R25.

Liao, Y., Smyth, G.K., and Shi, W. (2014). featureCounts: an efficient general purpose program for assigning sequence reads to genomic features. Bioinformatics (Oxford, England) 30, 923-930.

Ling, S.C., Polymenidou, M., and Cleveland, D.W. (2013). Converging mechanisms in ALS and FTD: disrupted RNA and protein homeostasis. Neuron 79, 416-438.

Liu-Yesucevitz, L., Bilgutay, A., Zhang, Y.J., Vanderweyde, T., Citro, A., Mehta, T., Zaarur, N., McKee, A., Bowser, R., Sherman, M., Petrucelli, L., and Wolozin, B. (2010). Tar DNA binding protein-43 (TDP-43) associates with stress granules: analysis of cultured cells and pathological brain tissue. PloS One 5, e13250.

Lobsiger, C.S., Boillee, S., and Cleveland, D.W. (2007). Toxicity from different SOD1 mutants dysregulates the complement system and the neuronal regenerative response in ALS motor neurons. Proceedings of the National Academy of Sciences of the United States of America 104, 7319-7326.

Lovci, M.T., Ghanem, D., Marr, H., Arnold, J., Gee, S., Parra, M., Liang, T.Y., Stark, T.J., Gehman, L.T., Hoon, S., Massirer, K.B., Pratt, G.A., Black, D.L., Gray, J.W., Conboy, J.G., and Yeo, G.W. (2013). Rbfox proteins regulate alternative mRNA splicing through evolutionarily conserved RNA bridges. Nature Structural & Molecular Biology 20, 1434-1442.

Mackenzie, I.R., Bigio, E.H., Ince, P.G., Geser, F., Neumann, M., Cairns, N.J., Kwong, L.K., Forman, M.S., Ravits, J., Stewart, H., Eisen, A., McClusky, L., Kretzschmar, H.A., Monoranu, C.M., Highley, J.R., Kirby, J., Siddique, T., Shaw, P.J., Lee, V.M., and Trojanowski, J.Q. (2007). Pathological TDP-43 distinguishes sporadic amyotrophic lateral sclerosis from amyotrophic lateral sclerosis with SOD1 mutations. Annals of Neurology 61, 427-434.

McGlincy, N.J., Tan, L.Y., Paul, N., Zavolan, M., Lilley, K.S., and Smith, C.W. (2010). Expression proteomics of UPF1 knockdown in HeLa cells reveals autoregulation of hnRNP A2/B1 mediated by alternative splicing resulting in nonsense-mediated mRNA decay. BMC Genomics 11, 565.

Mitchell, J., Paul, P., Chen, H.J., Morris, A., Payling, M., Falchi, M., Habgood, J., Panoutsou, S., Winkler, S., Tisato, V., Hajitou, A., Smith, B., Vance, C., Shaw, C., Mazarakis, N.D., and de Belleroche, J. (2010). Familial amyotrophic lateral sclerosis is associated with a mutation in D-amino acid oxidase. Proceedings of the National Academy of Sciences of the United States of America 107, 7556-7561.

Miyaoka, Y., Chan, A.H., Judge, L.M., Yoo, J., Huang, M., Nguyen, T.D., Lizarraga, P.P., So, P.L., and Conklin, B.R. (2014). Isolation of single-base genome-edited human iPS cells without antibiotic selection. Nature Methods 11, 291-293.

Modic, M., Ule, J., and Sibley, C.R. (2013). CLIPing the brain: studies of protein-RNA interactions important for neurodegenerative disorders. Molecular and Cellular Neurosciences 56, 429-435.

Mohagheghi, F., Prudencio, M., Stuani, C., Cook, C., Jansen-West, K., Dickson, D.W., Petrucelli, L., and Buratti, E. (2016). TDP-43 functions within a network of hnRNP proteins to inhibit the production of a truncated human SORT1 receptor. Human Molecular Genetics 25, 534-545.

Molliex, A., Temirov, J., Lee, J., Coughlin, M., Kanagaraj, A.P., Kim, H.J., Mittag, T., and Taylor, J.P. (2015). Phase separation by low complexity domains promotes stress granule assembly and drives pathological fibrillization. Cell 163, 123-133.

Neumann, M., Sampathu, D.M., Kwong, L.K., Truax, A.C., Micsenyi, M.C., Chou, T.T., Bruce, J., Schuck, T., Grossman, M., Clark, C.M., McCluskey, L.F., Miller, B.L., Masliah, E., Mackenzie, I.R., Feldman, H., Feiden, W., Kretzschmar, H.A., Trojanowski, J.Q., and Lee, V.M. (2006). Ubiquitinated TDP-43 in frontotemporal lobar degeneration and amyotrophic lateral sclerosis. Science 314, 130-133.

Nussbacher, J.K., Batra, R., Lagier-Tourenne, C., and Yeo, G.W. (2015). RNA-binding proteins in neurodegeneration: Seq and you shall receive. Trends in neurosciences 38, 226-236.
Pasinelli, P., and Brown, R.H. (2006). Molecular biology of amyotrophic lateral sclerosis: insights from genetics. Nature Reviews Neuroscience 7, 710-723.

Paul, P., and de Belleroche, J. (2014). The role of D-serine and glycine as co-agonists of NMDA receptors in motor neuron degeneration and amyotrophic lateral sclerosis (ALS). Frontiers in Synaptic Neuroscience 6, 10.

Paul, P., Murphy, T., Oseni, Z., Sivalokanathan, S., and de Belleroche, J.S. (2014). Pathogenic effects of amyotrophic lateral sclerosis-linked mutation in D-amino acid oxidase are mediated by D-serine. Neurobiology of Aging 35, 876-885.

Polymenidou, M., Lagier-Tourenne, C., Hutt, K.R., Bennett, C.F., Cleveland, D.W., and Yeo, G.W. (2012). Misregulated RNA processing in amyotrophic lateral sclerosis. Brain Research 1462, 3-15.

Polymenidou, M., Lagier-Tourenne, C., Hutt, K.R., Huelga, S.C., Moran, J., Liang, T.Y., Ling, S.C., Sun, E., Wancewicz, E., Mazur, C., Kordasiewicz, H., Sedaghat, Y., Donohue, J.P., Shiue, L., Bennett, C.F., Yeo, G.W., and Cleveland, D.W. (2011). Long pre-mRNA depletion and RNA missplicing contribute to neuronal vulnerability from loss of TDP-43. Nature Neuroscience 14, 459-468.

Raju, C.S., Fukuda, N., Lopez-Iglesias, C., Goritz, C., Visa, N., and Percipalle, P. (2011). In neurons, activity-dependent association of dendritically transported mRNA transcripts with the transacting factor CBF-A is mediated by A2RE/RTS elements. Molecular Biology of the Cell 22, 1864-1877.

Ray, D., Kazan, H., Cook, K.B., Weirauch, M.T., Najafabadi, H.S., Li, X., Gueroussov, S., Albu, M., Zheng, H., Yang, A., Na, H., Irimia, M., Matzat, L.H., Dale, R.K., Smith, S.A., Yarosh, C.A., Kelly, S.M., Nabet, B., Mecenas, D., Li, W., Laishram, R.S., Qiao, M., Lipshitz, H.D., Piano, F., Corbett, A.H., Carstens, R.P., Frey, B.J., Anderson, R.A., Lynch, K.W., Penalva, L.O., Lei, E.P., Fraser, A.G., Blencowe, B.J., Morris, Q.D., and Hughes, T.R. (2013). A compendium of RNA-binding motifs for decoding gene regulation. Nature 499, 172-177.

Rio, D.C., Ares, M., Jr., Hannon, G.J., and Nilsen, T.W. (2010). Preparation of cytoplasmic and nuclear RNA from tissue culture cells. Cold Spring Harbor Protocols 2010, pdb.prot5441.

Rogelj, B., Easton, L.E., Bogu, G.K., Stanton, L.W., Rot, G., Curk, T., Zupan, B., Sugimoto, Y., Modic, M., Haberman, N., Tollervey, J., Fujii, R., Takumi, T., Shaw, C.E., and Ule, J. (2012). Widespread binding of FUS along nascent RNA regulates alternative splicing in the brain. Scientific Reports 2, 603.

Sasabe, J., Chiba, T., Yamada, M., Okamoto, K., Nishimoto, I., Matsuoka, M., and Aiso, S. (2007). D-serine is a key determinant of glutamate toxicity in amyotrophic lateral sclerosis. EMBO Journal 26, 4149-4159.

Sasabe, J., Miyoshi, Y., Suzuki, M., Mita, M., Konno, R., Matsuoka, M., Hamase, K., and Aiso, S. (2012). D-amino acid oxidase controls motoneuron degeneration through D-serine. Proceedings of the National Academy of Sciences of the United States of America 109, 627-632.

Scekic-Zahirovic, J., Sendscheid, O., El Oussini, H., Jambeau, M., Sun, Y., Mersmann, S., Wagner, M., Dieterle, S., Sinniger, J., Dirrig-Grosch, S., Drenner, K., Birling, M.C., Qiu, J., Zhou, Y., Li, H., Fu, X.D., Rouaux, C., Shelkovnikova, T., Witting, A., Ludolph, A.C., Kiefer, F., Storkebaum, E., Lagier-Tourenne, C., and Dupuis, L. (2016). Toxic gain of function from mutant FUS protein is crucial to trigger cell autonomous motor neuron loss. EMBO Journal 35, 1077-1097.

Schwartz, J.C., Ebmeier, C.C., Podell, E.R., Heimiller, J., Taatjes, D.J., and Cech, T.R. (2012). FUS binds the CTD of RNA polymerase II and regulates its phosphorylation at Ser2. Genes & Development 26, 2690-2695.

Shan, J., Munro, T.P., Barbarese, E., Carson, J.H., and Smith, R. (2003). A molecular mechanism for mRNA trafficking in neuronal dendrites. The Journal of neuroscience : The Official Journal of the Society for Neuroscience 23, 8859-8866.

Siomi, M.C., Eder, P.S., Kataoka, N., Wan, L., Liu, Q., and Dreyfuss, G. (1997). Transportin-mediated nuclear import of heterogeneous nuclear RNP proteins. The Journal of Cell Biology 138, 1181-1192.

Skibinski, G., and Finkbeiner, S. (2013). Longitudinal measures of proteostasis in live neurons: features that determine fate in models of neurodegenerative disease. FEBS Letters 587, 1139-1146.

Sofola, O.A., Jin, P., Qin, Y., Duan, R., Liu, H., de Haro, M., Nelson, D.L., and Botas, J. (2007). RNA-binding proteins hnRNP A2/B1 and CUGBP1 suppress fragile X CGG premutation repeat-induced neurodegeneration in a Drosophila model of FXTAS. Neuron 55, 565-571.

Sreedharan, J., Blair, I.P., Tripathi, V.B., Hu, X., Vance, C., Rogelj, B., Ackerley, S., Durnall, J.C., Williams, K.L., Buratti, E., Baralle, F., de Belleroche, J., Mitchell, J.D., Leigh, P.N., Al-Chalabi, A., Miller, C.C., Nicholson, G., and Shaw, C.E. (2008). TDP-43 mutations in familial and sporadic amyotrophic lateral sclerosis. Science 319, 1668-1672.

Sun, S., Ling, S.C., Qiu, J., Albuquerque, C.P., Zhou, Y., Tokunaga, S., Li, H., Qiu, H., Bui, A., Yeo, G.W., Huang, E.J., Eggan, K., Zhou, H., Fu, X.D., Lagier-Tourenne, C., and Cleveland, D.W. (2015). ALS-causative mutations in FUS/TLS confer gain and loss of function by altered association with SMN and U1-snRNP. Nature Communications 6, 6171.

Thompson, M., Marecki, J.C., Marinesco, S., Labrie, V., Roder, J.C., Barger, S.W., and Crow, J.P. (2012). Paradoxical roles of serine racemase and D-serine in the G93A mSOD1 mouse model of amyotrophic lateral sclerosis. Journal of Neurochemistry 120, 598-610.

Tollervey, J.R., Curk, T., Rogelj, B., Briese, M., Cereda, M., Kayikci, M., Konig, J., Hortobagyi, T., Nishimura, A.L., Zupunski, V., Patani, R., Chandran, S., Rot, G., Zupan, B., Shaw, C.E., and Ule, J. (2011). Characterizing the RNA targets and position-dependent splicing regulation by TDP-43. Nature Neuroscience 14, 452-458.

Udan-Johns, M., Bengoechea, R., Bell, S., Shao, J., Diamond, M.I., True, H.L., Weihl, C.C., and Baloh, R.H. (2014). Prion-like nuclear aggregation of TDP-43 during heat shock is regulated by HSP40/70 chaperones. Human Molecular Genetics 23, 157-170.

Untergasser, A., Cutcutache, I., Koressaar, T., Ye, J., Faircloth, B.C., Remm, M., and Rozen, S.G. (2012). Primer3--new capabilities and interfaces. Nucleic Acids Research 40, e115.

Van Deerlin, V.M., Leverenz, J.B., Bekris, L.M., Bird, T.D., Yuan, W., Elman, L.B., Clay, D., Wood, E.M., Chen-Plotkin, A.S., Martinez-Lage, M., Steinbart, E., McCluskey, L., Grossman, M., Neumann, M., Wu, I.L., Yang, W.S., Kalb, R., Galasko, D.R., Montine, T.J., Trojanowski, J.Q., Lee, V.M., Schellenberg, G.D., and Yu, C.E. (2008). TARDBP mutations in amyotrophic lateral sclerosis with TDP-43 neuropathology: a genetic and histopathological analysis. Lancet Neurology 7, 409-416.

Van Nostrand, E.L., Pratt, G.A., Shishkin, A.A., Gelboin-Burkhart, C., Fang, M.Y., Sundararaman, B., Blue, S.M., Nguyen, T.B., Surka, C., Elkins, K., Stanton, R., Rigo, F., Guttman, M., and Yeo, G.W. (2016). Robust transcriptome-wide discovery of RNA-binding protein binding sites with enhanced CLIP (eCLIP). Nature Methods 13, 508-514.

Vance, C., Rogelj, B., Hortobagyi, T., De Vos, K.J., Nishimura, A.L., Sreedharan, J., Hu, X., Smith, B., Ruddy, D., Wright, P., Ganesalingam, J., Williams, K.L., Tripathi, V., Al-Saraj, S., Al-Chalabi, A., Leigh, P.N., Blair, I.P., Nicholson, G., de Belleroche, J., Gallo, J.M., Miller, C.C., and Shaw, C.E. (2009). Mutations in FUS, an RNA processing protein, cause familial amyotrophic lateral sclerosis type 6. Science 323, 1208-1211.

Watts, G.D., Wymer, J., Kovach, M.J., Mehta, S.G., Mumm, S., Darvish, D., Pestronk, A., Whyte, M.P., and Kimonis, V.E. (2004). Inclusion body myopathy associated with Paget disease of bone and frontotemporal dementia is caused by mutant valosin-containing protein. Nature Genetics 36, 377-381.

Wu, L.S., Cheng, W.C., and Shen, C.K. (2012). Targeted depletion of TDP-43 expression in the spinal cord motor neurons leads to the development of amyotrophic lateral sclerosis-like phenotypes in mice. The Journal of Biological Chemistry 287, 27335-27344.

Xia, Z., Donehower, L.A., Cooper, T.A., Neilson, J.R., Wheeler, D.A., Wagner, E.J., and Li, W. (2014). Dynamic analyses of alternative polyadenylation from RNA-seq reveal a 3'-UTR landscape across seven tumour types. Nature Communications 5, 5274.

Xiang, S., Kato, M., Wu, L.C., Lin, Y., Ding, M., Zhang, Y., Yu, Y., and McKnight, S.L. (2015). The LC Domain of hnRNPA2 Adopts Similar Conformations in Hydrogel Polymers, Liquid-like Droplets, and Nuclei. Cell 163, 829-839.

Yang, C., Wang, H., Qiao, T., Yang, B., Aliaga, L., Qiu, L., Tan, W., Salameh, J., McKenna-Yasek, D.M., Smith, T., Peng, L., Moore, M.J., Brown, R.H., Jr., Cai, H., and Xu, Z. (2014). Partial loss of TDP-43 function causes phenotypes of amyotrophic lateral sclerosis. Proceedings of the National Academy of Sciences of the United States of America 111, E1121-1129.

Yang, H.C., Liu, C.M., Liu, Y.L., Chen, C.W., Chang, C.C., Fann, C.S., Chiou, J.J., Yang, U.C., Chen, C.H., Faraone, S.V., Tsuang, M.T., and Hwu, H.G. (2013). The DAO gene is associated with schizophrenia and interacts with other genes in the Taiwan Han Chinese population. PloS One 8, e60099.

Zhang, Y., Chen, K., Sloan, S.A., Bennett, M.L., Scholze, A.R., O'Keeffe, S., Phatnani, H.P., Guarnieri, P., Caneda, C., Ruderisch, N., Deng, S., Liddelow, S.A., Zhang, C., Daneman, R., Maniatis, T., Barres, B.A., and Wu, J.Q. (2014). An RNA-sequencing transcriptome and splicing database of glia, neurons, and vascular cells of the cerebral cortex. Journal of Neuroscience 34, 11929-11947.

Zisoulis, D.G., Lovci, M.T., Wilbert, M.L., Hutt, K.R., Liang, T.Y., Pasquinelli, A.E., and Yeo, G.W. (2010). Comprehensive discovery of endogenous Argonaute binding sites in Caenorhabditis elegans. Nature Structural & Molecular Biology 17, 173-179.